

JAERI-M

5888

ANNUAL REPORT OF JAERI THERMONUCLEAR  
FUSION LABORATORY

(for the period of April 1, 1973  
to March 31, 1974)

October 1974

Thermonuclear Fusion Laboratory

この報告書は、日本原子力研究所が JAERI-M レポートとして、不定期に刊行している研究報告書です。入手、複製などのお問い合わせは、日本原子力研究所技術情報部（茨城県那珂郡東海村）あて、お申しこしください。

JAERI-M reports, issued irregularly, describe the results of research works carried out in JAERI. Inquiries about the availability of reports and their reproduction should be addressed to Division of Technical Information, Japan Atomic Energy Research Institute, Tokai-mura, Naka-gun, Ibaraki-ken, Japan.

Annual Report of Thermonuclear Fusion Laboratory

(for the period of April 1, 1973 to March 31, 1974)

Thermonuclear Fusion Laboratory, Tokai, JAERI

(Received October 11, 1974)

Activities in Thermonuclear Fusion Laboratory for the period April 1973 - March 1974 are described.

- (1) At the end of June 1973, the JFT-1 was shut down after four years of successful operation.
- (2) A preliminary experiment with a dynamic limiter and experiments with an improved diagnostic system were carried out with the JFT-2, which started operation in the preceding year. Power-up of the generator for the toroidal coil for the JFT-2 phase-II experiment was started.
- (3) Construction of the JFT-2a (a tokamak of teardrop cross-section with an axisymmetric divertor) continued.
- (4) Further heating of tokamak plasma with neutral beam injection, the energy loss by impurities in plasma and stability of plasma were studied theoretically.
- (5) A concept of the JT-60 (a tokamak confining a plasma of nearly reactor conditions) was developed and its design was started.
- (6) Design study of a fusion reactor was carried out in order to clarify the problems on fusion reactor development.

## 核融合研究室年報（昭和48年度）

日本原子力研究所東海研究所核融合研究室

（1974年10月11日受理）

核融合研究室における昭和48年度の研究進行状況をまとめたものである。その概要は次のとおりである。

- (1) 4年間に亘るJFT-1を用いての研究は48年6月末で終了した。(2) JFT-2では前年度に引きつづき、さらに計測を充実した実験、および可動リミターの予備実験が行なわれ、これと並んでPhase II計画のためのトロイダル磁場用電源増設工事が進められた。(3) JFT-2a（ダイバータ付涙滴断面トカマク）の建設が進められた。
- (4) 理論的研究の面では中性粒子入射によるプラズマ加熱、プラズマ中の不純物によるエネルギー損失、プラズマの安定性の解析などが進められた。(5) JT-60（臨界炉心プラズマ試験装置）の基本概念が検討され、プラズマ特性解析と装置の設計が進められた。
- (6) 核融合炉の概念を明らかにし、開発上の問題点を摘出するための炉の設計研究が行なわれた。

## CONTENTS

PREFACE .....	1
I. TOROIDAL CONFINEMENT EXPERIMENTS .....	3
1. JFT-1 .....	3
1.1 Introduction .....	3
1.2 Experimental Studies .....	3
1) Support-induced plasma loss .....	3
2. JFT-2 .....	4
2.1 Introduction .....	4
2.2 Experimental Studies .....	5
1) Dynamic limiter experiment .....	5
2) Particle and energy balances in JFT-2 Tokamak .....	7
3) Soft X-ray measurement .....	7
4) Measurement of the effective plasma radius and the electrical conductivity distribution .....	8
5) Permeation of vertical magnetic field through a thin shell...	9
2.3 Numerical Analysis .....	10
1) Numerical simulation of the tokamak plasma with a movable boundary .....	10
2) Estimation of the plasma characteristic quantities from the electromagnetic signals obtained in tokamak experiments .....	11
2.4 Neutral Beam Injection Heating .....	12
3. JFT-2a .....	23
3.1 Introduction .....	23
3.2 Main Components of the Device .....	24
1) Shell .....	24
2) Limiter .....	25
3) Divertor .....	25
4) Gas supply system .....	25
5) Pre-ionization system .....	26
6) Vacuum system .....	26

7) Toroidal magnetic field .....	27
8) Vertical magnetic field .....	27
9) Power supply system .....	27
10) Gas pressure measurement .....	27
11) Magnetic measurement .....	28
12) Electrostatic measurement .....	28
3.3 Numerical Analysis .....	28
1) Equilibrium of JFT-2a plasmas .....	28
2) Numerical simulation of JFT-2a plasmas .....	29
3) Shaping of a plasma cross section by external current carrying conductors .....	30
4. Diagnostics .....	40
4.1 Introduction .....	40
4.2 Measurements .....	40
1) Microwave interferometric measurements .....	40
2) Spectroscopic measurements .....	42
3) Thomson scattering measurements .....	43
4) Charged-exchanged particle measurements .....	45
4.3 Developments .....	46
1) Loss flux measurements by bolometric method .....	46
2) Measurements of current distribution by means of high- energy particles .....	46
3) Doppler broadening measurements in vacuum ultra-violet regions .....	47
4) Data processing system and its preliminary study .....	48
5. Operation and Technical Development .....	63
5.1 Introduction .....	63
5.2 JFT-2 .....	63
1) Remodeling of JFT-2 .....	63
2) Operation and mainlenance .....	64
5.3 JFT-2a (DIVA) .....	64
II. DESIGN STUDY OF JT-60 .....	66

III. THEORY .....	67
1. Introduction .....	67
2. MHD Stability and Equilibrium .....	67
1) MHD stability of belt-pinch-type plasmas .....	67
2) Nonlinear effect on the $m=1$ internal kink mode .....	67
3) Feedback stabilization of high $m$ kink mode .....	69
4) Kink instability of a pinch in a slotted casing .....	69
5) An analysis of bifurcated helical equilibria of a pinch .....	70
6) A computer code for the charged particle motion in toroidal magnetic fields .....	73
3. Impurity Ions in a Tokamak Plasma .....	75
1) The Pfirsch-Schluter diffusion in a multicomponent plasma ...	75
2) Impurity drift instability by trapped ions .....	75
3) Impurity problems in tokamak devices .....	75
4. Heating of a Tokamak Plasma .....	77
1) Efficiency of neutral injection heating in tokamak devices ..	77
2) Numerical calculation of the dispersion equation near the lower hybrid frequency .....	78
5. Study of a Gas-Insulated Plasma .....	79
IV. REACTOR DESIGN STUDY .....	87
1. Introduction .....	87
2. Conceptual Design of a Gas Cooled Tokamak Reactor .....	87
3. Design Related Studies .....	88
1) On the optimization of a tokamak fusion reactor .....	88
2) Start-up and shutdown of a D-T tokamak reactor .....	89
3) Fuel supply by neutral gas surrounding core plasma .....	90
4) Tritium breeding in ceramic lithium-compound blanket .....	90
5) Nuclear heating calculation in fusion reactor blanket .....	91
6) Toroidal field magnet .....	91
APPENDICES .....	101
1. Publication List .....	101
2. Budget and Personnel .....	106

## PREFACE

At the end of June 1973, JFT-1 was shut down after successful operation of four years since 1969. On the other hand, new plans were started, such as construction of JFT-2a and a new generators for JFT-2, and design study of fusion reactor.

A brief summary of activities in this period\*, from April, 1973 to March, 1974 is as follows.

A laser scattering apparatus and a VUV spectrometer are consolidated to the diagnostic system, which make us possible to cross-check the data of JFT-2 plasma. Some typical parameters of JFT-2 are 500eV and 200eV in the electron and the ion temperature, respectively,  $2 \times 10^{13} \text{ cm}^{-3}$  in the density and 10 ms in the energy confinement time at a plasma current of 80 kA. A preliminary experiment with "dynamic limiter" (rapid removal of the limiter after production of hot plasma) was done towards the end of this fiscal year. Contrary to our expectation, the plasma seemed to expand with the fast moving limiter.

A dc-power supply of 21 MW peak for the JFT-2 phase-II experiment was ordered to Hitachi Co. In the phase-II, toroidal field will be increased to 18 kG from 10 kG in the present phase-I. Installation of the new power supply and reinforcement of coil supports will begin in April and be finished in October, 1974.

A group of operation and technical development was newly organized in May. The operation of JFT-2 was very satisfactory with no unexpected shutdown longer than a week during this period.

Dr. Kazawa (Hitachi Co.), Dr. Itoh et al. (JAERI) were awarded a prize on construction and phase-I experiment of JFT-2 by Atomic Energy Society of Japan.

Construction of JFT-2a, a tokamak with tear-drop cross-section with an axisymmetric divertor was begun in July, 1973 and scheduled to finish in August, 1974.

Further heating of tokamak plasma with neutral beam injection was studied with emphasis on heating efficiency with injection angle and energy. Also, spacial distribution of impurities and radiation loss was calculated.



The result shows radiation loss or necessary heating power to maintain the temperature as a function of impurity contents and plasma temperature. It indicates that severe impurity suppression is necessary in tokamak of 10 keV regime.

A design of a fusion reactor was begun by a newly organized group in close cooperation with fission reactor engineering people at Tokai. The design of tokamak reactor of 2,000 MW(t) with He cooled  $\text{Li}_2\text{O}$  blanket was completed as a first approximation and proceeded to the second. The design is a unique one, in which fertile material for tritium production is Li ceramic, such as  $\text{Li}_2\text{O}$ . It is to be noted that a reactor type of solid fertile material with gas cooling has a very good "affinity" with the core plasma.

Another design activity was on a tokamak containing a plasma of nearly reactor condition.

The present JAERI's CTR is in accordance with the plan of Special Integrated Research of Atomic Energy on CTR, from FY 1969 to 1974. The Japanese AEC founded Nuclear Fusion Research and Development Committee to formulate the CTR plan after 1975. We cooperated with the Committee in setting up the plan, which includes R&D on 1 to 10 keV tokamak plasma, reactor engineering, and related technology.

(S. Mori)

\* The preceding annual reports are JAERI-M 4564, 5029 and 5564.

## I. TOROIDAL CONFINEMENT EXPERIMENTS

## 1. JFT-1

T. Nagashima, H. Ohtsuka,  
T. Shiina and S. Tamura

## 1.1 Introduction

The JFT-1 toroidal hexapole experiment was terminated in the first quarter of 1973. During the period, only an experiment to study the support-induced plasma loss was made. A brief summary of the experiment is described in the next section.

(S. Tamura)

## 1.2 Experimental studies

1) Support-induced plasma loss<sup>1)</sup>

To investigate the effect of hoop supports on the plasma loss process, a model support was introduced into the plasma and the subsequent changes in the plasma potential and the density were measured. The experiment was carried out mainly with helium plasma produced by microwave discharge with density,  $n \sim 10^{11} \text{ cm}^{-3}$ , and electron temperature,  $T_e \sim 2 \text{ eV}$ .

Besides the charge separation electric fields resulting from the average grad B drifts of ions and electrons, an additional azimuthal electric field which exists in the vicinity of the support was found to explain the observed enhancement of the plasma loss to the hoop and the wall (support-induced convection). The observed enhancement of the plasma loss due to the model support was at most a factor of 2. This indicates that the plasma loss due to the actual hoop supports by way of a plasma convection may not be sufficient to explain the observed anomaly in the plasma loss in JFT-1.

(H. Ohtsuka, S. Tamura, T. Nagashima and T. Shiina)

## Reference

- 1) H. Ohtsuka, et al.: JAERI-M 5649 (February, 1974).

## 2. JFT-2

N. Fujisawa, S. Itoh\*, M. Maeno,  
S. Matsuda, T. Sugawara\*\*, N. Suzuki,  
T. Takeda, and K. Toi

## 2.1 Introduction

During the first half of the past year, there was a major shutdown to accomplish the following: (a) install a observation box for a ruby laser Thomson scattering measurement; (b) improve a vacuum vessel. The dimensions of the JFT-2 device are shown in Table 1, and Figs. 1 and 2. The axis of the fan-shaped toroidal field coils is shifted outwards by 10 cm from the aluminum shell axis in order to minimize the non-uniformity of the field at the outer surface of the plasma. The distance between the plasma periphery and the wall is fairly larger than other tokamak devices.

Our main emphasis has been on understanding tokamak plasma confinement, especially the dynamic limiter experiments which will be discussed in the next subsection. We have also emphasized studies of particle and energy balances.

Experiments in the increased toroidal field (18 kG) will be started at the end of 1974. Neutral beam injection heating experiments are planned in 1976.

(S. Itoh and N. Fujisawa)

---

\* Present address: Institute of Plasma Physics, Nagoya University,  
Nagoya, Japan.

\*\* On leave from Research and Development Center, Tokyo Shibaura Electric  
Co., Ltd., Kawasaki, Japan.

## 2.2 Experimental Studies

### 1) Dynamic limiter experiments in JFT-2 Tokamak<sup>†</sup>

In an ordinary tokamak device a solid limiter is equipped to define a plasma cross-section. It is, however, presumed that the material limiter may not be used in a tokamak-type fusion reactor because the material limiter in contact with a high temperature plasma is an intense source of impurity atoms and removal of heat deposited on the limiter presents a very serious problem. Therefore, it is very important to investigate, experimentally, how the plasma behaviour changes when the material limiter is removed and to know whether a material limiter is indispensable or not for the equilibrium and stability of a tokamak plasma. Until now, however, free boundary plasmas which are not in contact with a material limiter are obtained only in compression heating experiments such as ATC<sup>1)</sup> and TUMAN<sup>2)</sup>. The main objective of these experiments is the heating of the tokamak plasma and consequently the result of the investigation of the effect of the separation of the plasma from the material limiter is not reported. Moreover, it is not most plausible that the compression technique is used for the separation of the plasma from the material limiter in a future tokamak. One of the alterations to the compression of the plasma is fast retraction of the material limiter after the plasma formation. In JFT-2<sup>3)</sup> the plasma behaviour can be investigated by retracting a "dynamic limiter"<sup>4)</sup> at any time during the discharge.

The dynamic limiter is composed of two molybdenum plates which are set parallel to each other inside the vacuum chamber of JFT-2 and can be driven upwards and downwards pneumatically (Fig. 3). The variable range of the distance ( $L_d$ ) between the two plates is from 250 mm to 500 mm and the dynamic limiter set at an arbitrary position within this range can be retracted outside the fixed limiter (a 500 mm  $\phi$  aperture limiter). The average and maximum speeds of the dynamic limiter are 5 m/sec and 9 m/sec, respectively. The retraction velocity of the dynamic limiter is designed to be much higher than that of the expansion of the plasma boundary for the case where the neoclassical transport theory holds.

The experiments were carried out for two modes of operation concerning the dynamic limiter, the fixed and dynamic modes. In the fixed mode operation two cases with different positions of the dynamic limiter were studied, that is, the case for the "closed" position ( $L_d=250$  mm) and the

case for the "open" position ( $L_d=500$  mm). In the dynamic mode operation the dynamic limiter was triggered to move 60 msec after the initiation of a discharge. The experimental conditions are as follows; the toroidal magnetic field is 10 kG, the vertical magnetic field is 50 G and the filling pressure is  $2 \times 10^{-4}$  Torr  $H_2$ . The plasma parameters just before the triggering time are estimated as: the mean conductivity electron temperature is about 200 eV for an assumed effective charge of unity, and ion temperature measured by the charge-exchanged neutral particle analyzer is about 200 eV. Figures 4 and 5 show the typical waveforms of the loop voltage and the plasma current and the shift of the plasma axis ( $\Delta_h$ ) along the major radius for the above-mentioned three cases.

The results of the measurement of the effective plasma radius obtained by the plasma conductivity distribution measurement (response of the plasma ring to high frequency electric field)<sup>5)</sup> and observation of the time variation of the light intensity are summarized in Fig. 6, where it is remarked that the electron temperature at the effective radius is estimated to be 20-100 eV from the skin depth of the superposed high frequency electric field. From this figure it is known that the plasma boundary expands together with the dynamic limiter and the radius of the plasma decreases in the later stage of the discharge. The apparent shrinkage of the plasma radius in the later stage is, however, explained by the fact that the plasma ring moves inwards (Fig. 5) and the peripheral region of the plasma is scraped off by the inner side of the limiter. The count of the fast neutral atoms measured by the charge-exchanged neutral particle analyzer and the ion temperature decrease very much when the dynamic limiter is moving compared with the case for the "closed" operation. Electromagnetic fluctuations were measured by the magnetic probes set on the inner surface of the conducting shell. The signals from the probes are filtered to a single harmonic component and the toroidal and poloidal mode numbers are obtained in conjunction with the other plasma parameters. We have not, however, found any evidence that the stability of the tokamak plasma is considerably affected by the fast retraction of the dynamic limiter.

In conclusion it has been experimentally investigated whether a stable equilibrium of a tokamak plasma separated from outside solid materials are attainable or not. Strictly speaking, contrary to our expectation a free boundary plasma separated from a solid material was

not attained, because the experimentally obtained expansion velocity of the plasma boundary was same as or larger than the retraction velocity of the dynamic limiter. The decrease of the count of the fast neutral atoms suggests, however, as one of possibilities that the interaction between the plasma and the limiter was reduced by the fast retraction of the dynamic limiter because it may be possible that the fast neutral atoms are produced by the charge exchange process of the hot ions with the cold atoms which are released from the limiter by bombardment of hot plasma particles.

(S. Itoh, T. Sugawara, N. Suzuki, T. Takeda  
and K. Toi)

S. Itoh, T. Sugawara, N. Suzuki, T. Takeda and K. Toi : Nucl.  
Fusion 14 (1974) 581

T. Sugawara, S. Itoh, N. Suzuki, T. Takeda and K. Toi : Nucl.  
Fusion 14 (1974) 451.

## 2) Particle and energy balance

Particle and energy balances in the JFT-2 device have been measured under the following conditions. The filling pressure is  $3.3 \times 10^{-4}$  Torr in hydrogen, toroidal ohmic heating current 75~80 kA, the aperture limiter radius 25 cm, and the toroidal confining field 9 kG.

Electron temperature measured by Thomson scattering of a ruby laser pulse is 300 - 500 eV at the center. Electron temperature, obtained from a soft X-ray measurement, is in agreement with that obtained from Thomson scattering. Proton temperature, measured by charge exchanged neutrals, reaches a peak value of 200 eV. Radial profiles of electron temperature and density are more strongly peaked than those reported for other tokamak devices. Particle confinement time measured by the  $H_{\alpha}$  line is about 10 ms, and energy confinement time is less than 10 ms.

(N. Fujisawa, M. Maeno and N. Suzuki)

## 3) Soft X-ray measurement

In order to measure the energy spectrum of soft X-ray radiation a Si(Li) semiconductor detector system and a multichannel pulse height analyser system have been prepared. Main specifications of this system are as follows. The thickness of Be window in front of the detector is

8  $\mu$ , the Si(Li) detector is 6 mm $^{\phi}$   $\times$  3 mm $^t$ , the energy resolution is 180 eV in FWHM at 5 keV and maximum counting rate is 30 kcps. A test run of this system was performed in such discharges where hard X-ray radiations are a little.

The results are shown in Figs. 7(a) and 7(b). The data are averaged over 20 ms and are summed up over 10 shots of discharges. Taking account of the absorption of Be window, central electron temperatures are determined from the energy spectrum. These temperatures are in good agreement with the temperature obtained from the laser scattering measurement. A residual problem is that of the counting rate. The maximum counting rate of present system is limited to 30 kcps, therefore the time resolution and the statistical error of measurements are not sufficient. A improvement of the counting rate is the next subject.

(N. Suzuki)

#### 4) Measurement of the effective plasma radius and the electrical conductivity distribution

By measuring the A.C. impedance of a plasma, the effective plasma radius which defines the high electrical conductivity region and the radial distribution of the electrical conductivity can be obtained<sup>5)</sup>. The A.C. impedance is estimated from the response of the plasma to the small oscillatory voltage superimposed on the main loop voltage.

The effective plasma radius obtained by the measurement is useful for investigating the time behaviour of the hot region of the tokamak plasma. Moreover, the radial distribution of the effective charge of the plasma can be derived from that of the electrical conductivity through the comparison with the distribution of the electron temperature obtained by the laser scattering.

In JFT-2 the oscillatory voltage is excited by the electrical circuit composed of the capacitors, inductor and the switching circuit which is inserted in the primary circuit of the current transformer.

Figure 3 shows the time variation of the effective plasma radius in the dynamic limiter experiment. This result is derived from the inductance of the plasma for the oscillatory voltage with the frequency of about 1 kHz on the assumption that the superimposed oscillatory field vanishes inside the effective radius. The distribution of the electrical conductivity is determined by the magnitude and dependence of the inductance on the

frequency of the oscillatory field. The method based on the non-linear optimization has been adopted to derive the distribution from the above informations as follows. The plasma is assumed to be composed of  $N$  cylindrical shells (thickness:  $t_n$ ) with constant electrical conductivity ( $\sigma_n$ ;  $n=1,2,\dots,N$ ). The distribution of the electrical conductivity is obtained by minimizing the following objective function ( $F$ ) with respect to  $N$  variables ( $\sigma_0, t_n$ ;  $n=1,2,\dots,N-1$ )

$$F = \sum_{m=1}^M w_m [L_i(\sigma_0, t_n; n=1,2,\dots,N-1; f_m) - L_i^{\text{exp}}(f_m)]^2 \quad (M > N) \quad (1)$$

where  $w_m$ ,  $L_i(\sigma_0, t_n; n=1,2,\dots,N-1, f_m)$  and  $L_i^{\text{exp}}(f_m)$  are the weighting coefficient, the inductance calculated by using the above model and the one obtained in the experiment for the  $m$ -th frequency ( $f_m$ ), respectively. The calculated inductance  $L_i$  is expressed as follows,

$$L_i = \mu_0 R_0 \operatorname{Re} \left[ \frac{I_0(j^{\frac{1}{2}} \omega^{\frac{1}{2}} p_n) + C_n K_0(j^{\frac{1}{2}} \omega^{\frac{1}{2}} p_n)}{j^{\frac{1}{2}} \omega^{\frac{1}{2}} p_n \{I_0'(j^{\frac{1}{2}} \omega^{\frac{1}{2}} p_n) + C_n K_0'(j^{\frac{1}{2}} \omega^{\frac{1}{2}} p_n)\}} \right] \quad (2)$$

where  $p_n = \sqrt{\mu_0 a^2 \sigma_n}$ ,  $\omega_m = 2\pi f_m$ , and  $a$  and  $R_0$  are the minor and major radii of a plasma. The parameter  $C_n$  is determined from the continuity condition of the electric and magnetic fields at the boundary of each shell and is function of  $\sigma_n$  ( $n=1, 2, \dots, N$ ),  $f_m$  and so on. In the numerical calculation, the modified Bessel functions of the complex argument ( $I_0$ ,  $K_0$ ,  $I_0'$  and  $K_0'$ ) are expressed by the kelvin functions. The test run has been carried out to examine the applicability of the above procedure, where the experimental dependence of the inductance on the frequency ( $L_i^{\text{exp}}(f_m)$ ) is simulated by using the theoretical relation for the case of the parabolic distribution of the electrical conductivity. The result is presented in Fig. 8 and the applicability of the procedure has been demonstrated. At present, the analysis of the data in JFT-2 is in progress.

(K. Toi, T. Takeda and S. Itoh)

##### 5) Permeation of vertical magnetic field through a thin shell

The vertical magnetic field generated by the eddy current in a shell was previously measured for the short time scale compared with the skin time. The effects of resistivity and transverse cuts of a shell are studied



analytically and experimentally. By expanding the eddy current into Fourier series along the toroidal axis, the permeation equation is derived as

$$\left(\frac{d}{dt} + \frac{1}{\tau_n}\right) B_V^n = k_n \frac{d}{dt} \frac{B_b}{b} \left\{ 1 + \frac{b^2}{2R} \left( \ln \frac{8R}{b} - 1 \right) + \frac{a^2}{2R} \left( \beta_\theta + \frac{11-1}{2} \right) \right\}$$

$$\tau_n = \mu_0 b \sigma_* \frac{x_n^2}{x_n^2 + 1} \left| I_1'(x_n) K_1'(x_n) \right|$$

$$k_n = \left\{ \frac{2}{(2n+1)\pi} \right\}^2 / I_1'(x_n)$$

for the vertical field due to the shifted current with respect to the shell, where  $\sigma_*$  is an area conductivity,  $B_b = \mu_0 I / 2\pi b$ ,  $x_n = (n + \frac{1}{2})Nb/R$ , and  $N$  the section number. The penetration of the leakage magnetic field from the iron core of a transformer is described as well as an above equation. In the experiment the 1/5 model device is used and the plasma current is simulated by the current carrying loop of copper. Since the values of  $k_n$  decrease rapidly with  $n$  for the device parameter, the vertical field is generated mainly by the fundamental mode of the eddy current. The measured values of  $k_0$  and  $\tau_0$  are in agreement with the calculated values.

(T. Sugawara)

### 2.3 Numerical Analysis

#### 1) Numerical simulation of the tokamak plasma with a movable boundary

A numerical simulation of the tokamak plasma with the magnetohydrodynamic fluid model is described. The code has the following two applications: interpretation of the experiment of a tokamak plasma with a dynamic limiter, and comparison of the experimental with the theoretical results obtained with various transport theories. For the former application position of the boundary in the code is movable<sup>6)</sup>. For the latter main part of the code can be written automatically by using a code written in a formula manipulation language (IBM-FORMAC)<sup>7)</sup>.

The dynamic limiter which is installed in JFT-2 tokamak is a quickly retractable limiter. It can be triggered to move at any time during the discharge. It is driven to move by a pair of air cylinders and the maximum

velocity of the limiter is about 10 m/sec. The main purpose of the experiment of the dynamic limiter is to investigate whether the equilibrium and the stability of the plasma is sustained when the plasma is insulated from the external solid material (fixed) limiter or not. The transport phenomena such as particle diffusion will be also investigated experimentally using the dynamic limiter. These experiments are, however, very difficult to analyse because available diagnostic methods are not sufficient to get a spatial distribution of the plasma parameters. Therefore we analyze the experimental data by comparing them with the results of the numerical simulation. The following example of the results of the simulation shows qualitatively the effect of the neutral particles on the behaviour of the profile of the electron density after the dynamic limiter is retracted, where the experimentally obtained waveform of the plasma current is given as input data and simplified neoclassical transport coefficients are adopted. In the case (a) the neutral particle influx is kept to be  $3 \times 10^{20} \text{ m}^{-3} \text{ sec}^{-1}$  throughout the discharge, whereas the case (b) shows the results for the condition that the influx is reduced to  $1 \times 10^{20} \text{ m}^{-3} \text{ sec}^{-1}$  when the dynamic limiter is retracted (at  $t = 60 \text{ msec}$ ).

Detailed analyses of the experiments with both the dynamic limiter and normal fixed limiter are now in progress using the simulation code.

(T. Takeda and S. Itoh)

## 2) Estimation of the plasma characteristic quantities from the electromagnetic signals obtained in tokamak experiments\*

In tokamak experiments the plasma characteristic quantities such as the mean conductivity temperature and the energy confinement time are often estimated by using the electromagnetic measurements from reason that the measurements are comparatively easy and are convenient to obtain the time variations of these quantities.

The method of processing the data obtained by the measurements has been investigated. In order to process the data, it is necessary to treat carefully the set of equations with differentiations, because inaccuracies and fluctuations of the data due to sampling and quantization errors are magnified in the course of the differentiations. These errors mainly result from the analogue-to-digital conversion of the observed data. Therefore,

---

\* K. Toi and T. Takeda: Nuclear Instrum and Methods 118 (1974) 299-305.

the smoothing of the digitized data is required in the numerical analysis of the data. Figure 10 shows an example of the observed waveforms of the one-turn voltage at the measuring loop and the total secondary current in JFT-2 and time variations of the mean conductivity temperature and energy confinement time without smoothing. The method of least squares is adopted as the smoothing method. The degree of smoothing (smoothing parameter) must be evaluated carefully so that the reasonable results should be obtained. As a practical procedure, the following criteria are considered for checking the degree of smoothing: 1) the differences between the raw and smoothed data are within the corresponding reading errors; 2) the resulting curve obtained from analysis of the smoothed data is smooth enough under physical considerations. If the fluctuations with smaller wavelength than the maximum energy confinement time, which is estimated roughly from the first run of the analysis, are removed, the smoothing parameter which satisfies both criteria can be found for analysis of the data obtained in tokamak experiments.

In Figs. 11, 12 and 13 the time variations of the mean conductivity temperature, the quantities required in estimation of the energy confinement time (i.e., the total kinetic energy  $W$ , its time derivative  $\dot{W}$  and the input power of a plasma  $Q_{in}$ ) and the energy confinement time are shown, which are derived from the above-mentioned analysis for the data of Fig. 10. It is concluded that this method is suitable for numerical data processing of the electromagnetic signals obtained in tokamak experiments. It is expected that this procedure will be useful for the analysis of the data by an automatic data processing system.

(K. Toi and T. Takeda)

## 2.4 Neutral Beam Injection Heating

A preliminary consideration has been made on the neutral beam injection heating of the JFT-2 plasma. Perpendicular injection system composed of a couple of 6A 25 keV beams is adopted instead of the tangential injection system mainly because it is difficult to install the latter without disturbing the magnetic field uniformity. The purpose of the experiment is to investigate the physical and/or engineering problems

subject to perpendicular injection of fast neutral atoms.

Ion temperature rise owing to injection heating is estimated based on the scaling laws so far obtained from the JFT-2 experiments and is expected nearly 15 % of the initial ion temperature for a  $3 \times 10^{13} \text{ cm}^{-3}$ ,  $T_i \sim 350 \text{ eV}$ ,  $T_e \sim 1 \text{ keV}$  plasma in the high field version of the toroidal magnetic field (18 kG). Since the scaling law for the ion temperature increase indicates a strong dependence on the plasma density, a higher ion temperature would be attainable in the low density operation. Injection experiments will start sometime in 1976.

(S. Matsuda and T. Sugawara)

#### References

- 1) H.P. Furth, in Proc. of the Third Intern. Symposium on Toroidal Plasma Confinement (Garching, March 1973) B9-1.
- 2) A.I. Anisimov, et al., in Plasma Physics and Controlled Nuclear Fusion Research (Proc. 4th Int. Conf. Madison, 1971) 3, IAEA, Vienna (1971) 543.
- 3) S. Itoh et al., in Proc. of the Fifth European Conf. on Controlled Fusion and Plasma Physics (Grenoble, Aug. 1972) Vol 2, (1972) 231.
- 4) S. Itoh et al., in Proc. of the Third Intern. Symposium on Toroidal Plasma Confinement (Garching, March 1973) B4.
- 5) D.P. Ivanov, S.S. Krasilnikov, State Publishing House of Literature of Atomic Science and Technology, State Committee for the Utilization of Atomic Energy, Moscow, 1963. translation: AEC-tr-6518 (US Atomic Energy Commission, 1964) 266.
- 6) S. Matsuda; JAERI-M 5035 (1972) in Japanese.
- 7) B. Rosen and M. Okabayashi ; Nucl. Fusion 13 (1973) 3.

Table 1 Dimensions of JFT-2

Major Radius	(cm)	90
Minor Radius	(cm)	
Vacuum Chamber		30
(Liner)		
Shell		36
Thickness	(cm)	
Liner		0.06
Shell		3
Fixed Limiter		
Radius of	L (cm)	25
	M	20
	S	16.3
Dynamic Limiter		
Minimum Distance	(cm)	25
Maximum Distance	(cm)	51
Maximum Speed	(m/sec)	9
Maximum Toroidal		
Magnetic Field	(kG)	10
Maximum Vertical		
Magnetic Field	(G)	
DC		200
Pulsed		-200
Flux of the Iron Core (V.sec)		
(without Bias)		0.58

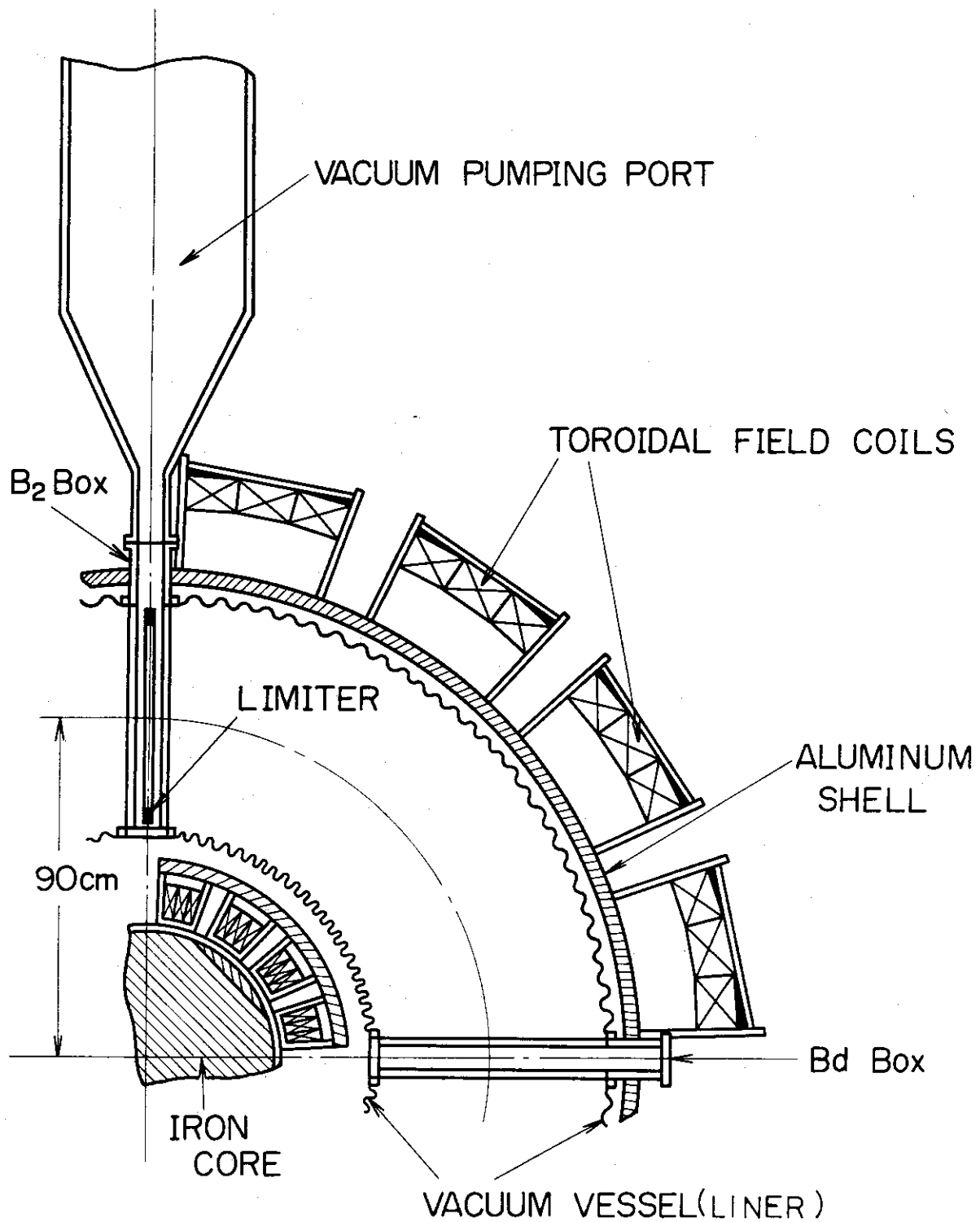


Fig. 1 Plan section of one quadrant of JFT-2

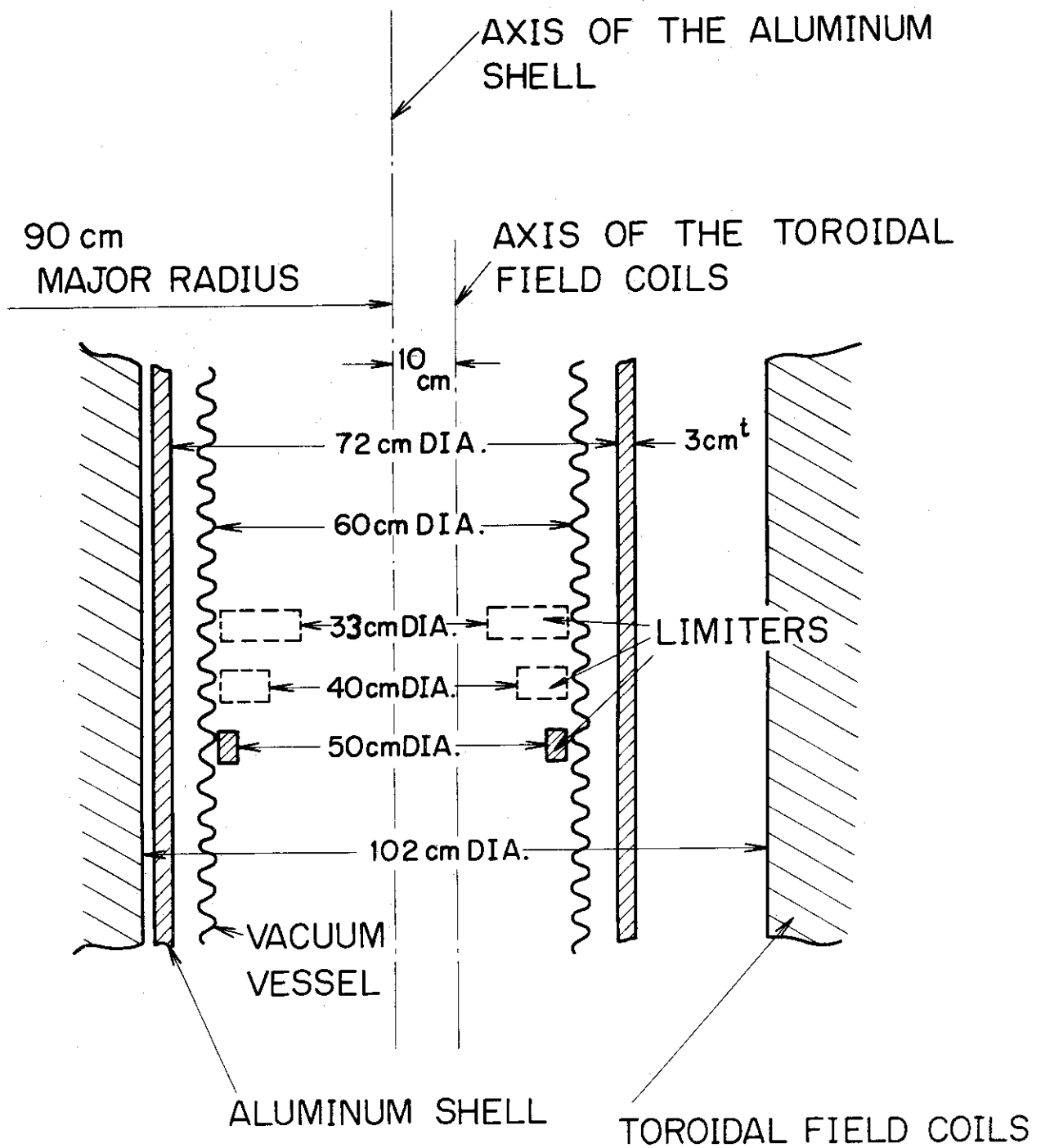


Fig. 2 Minor dimensions for JFT-2

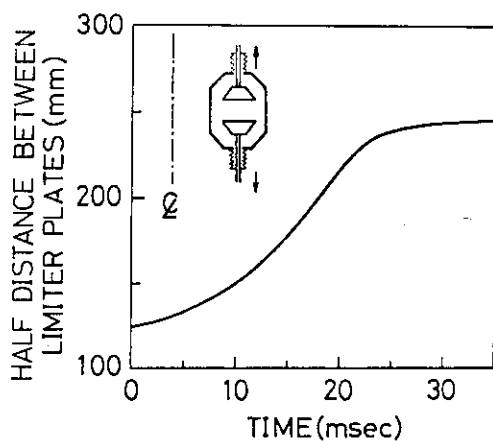


Fig. 3 Half distance between limiter plates after the dynamic limiter has been triggered to expand, and the schematic diagram of the dynamic limiter where the sign  $\cdot$  denotes the axis of the tokamak device.

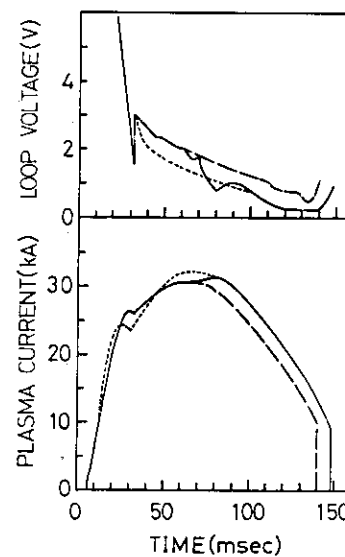


Fig. 4 Loop voltage and plasma current for three discharges: for the dynamic mode operation (solid line), and for the fixed mode operation in closed (broken line) and open (dotted line) position.

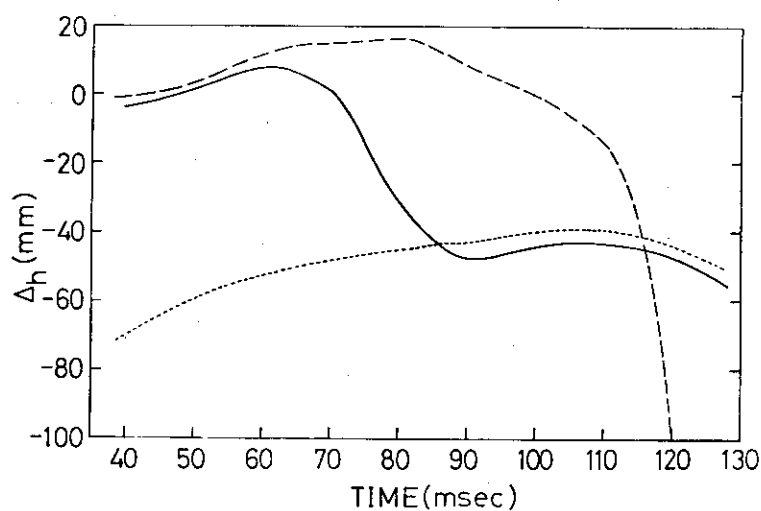


Fig. 5 Horizontal shift ( $\Delta_h$ ) of the plasma column for the discharges shown in Fig. 4.



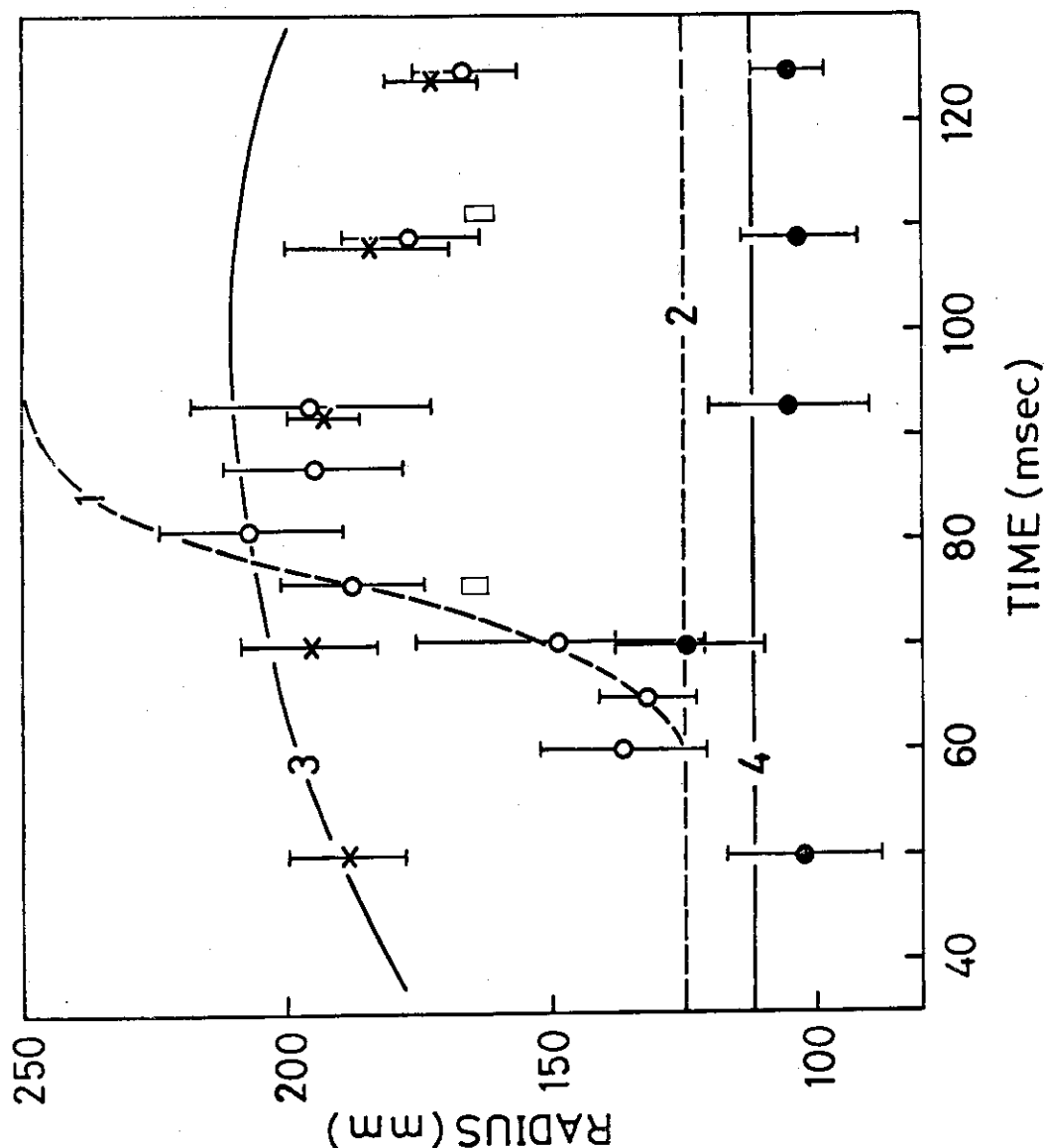


Fig. 6 Effective plasma radius determined with the plasma conductivity distribution measurement system; for the dynamic mode operation (open dot), and for the fixed mode operation in the closed (solid dot) and open (cross) position. The radius derived from the time behaviour of the light intensity is designated by squares. The broken lines (1 and 2) designate the half distance between limiter plates for the dynamic and fixed mode operation, respectively. The lines (3 and 4) show the radius of the plasma column scraped off owing to the shift of the plasma column for the open and the closed position, respectively. The difference of the observed effective radius from the line (3) in the later phase of the discharge may be explained by the peaking of the profile of the electron temperature.

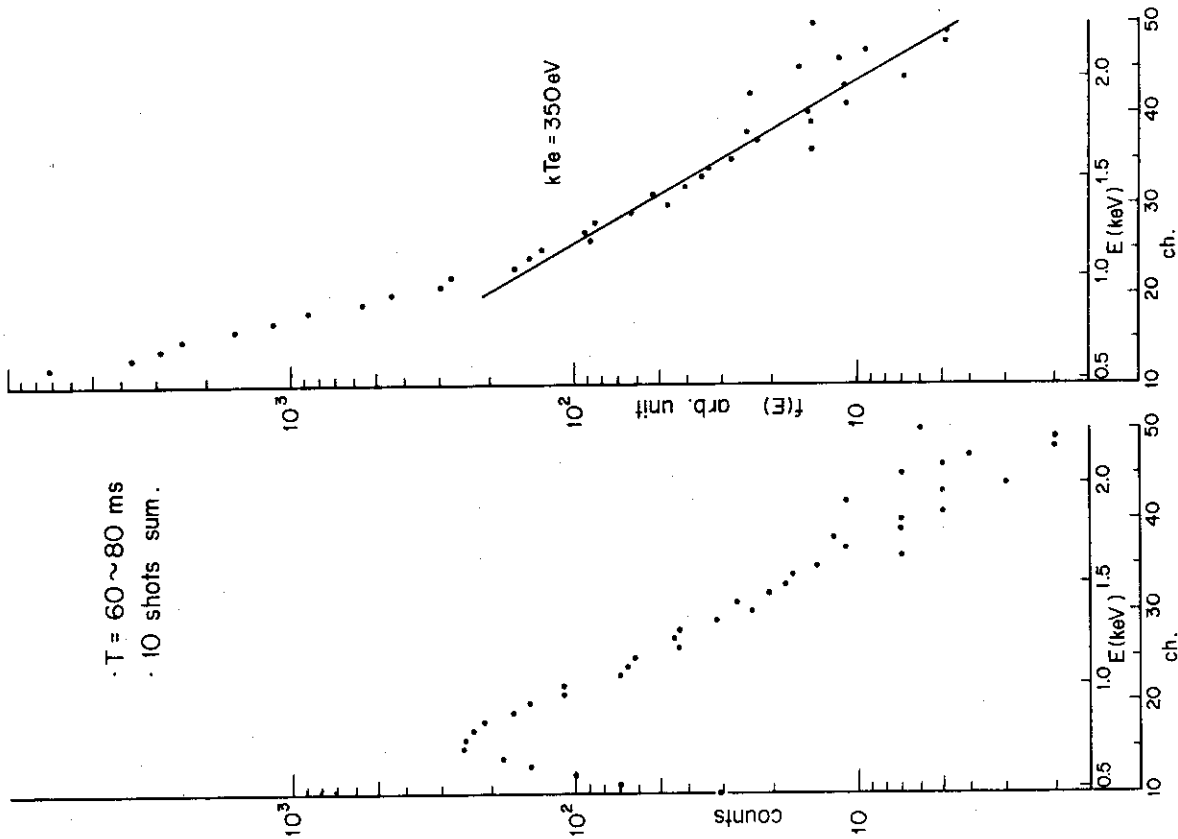


Fig. 7(a) Data obtained by 256 ch. P.H.A.

$E = 44.8 \text{ ch.} + 31 \text{ (eV)}$

(b) A energy spectrum obtained by correction of the absorption of Be window. In view of a central electron temperature the higher component is taken.

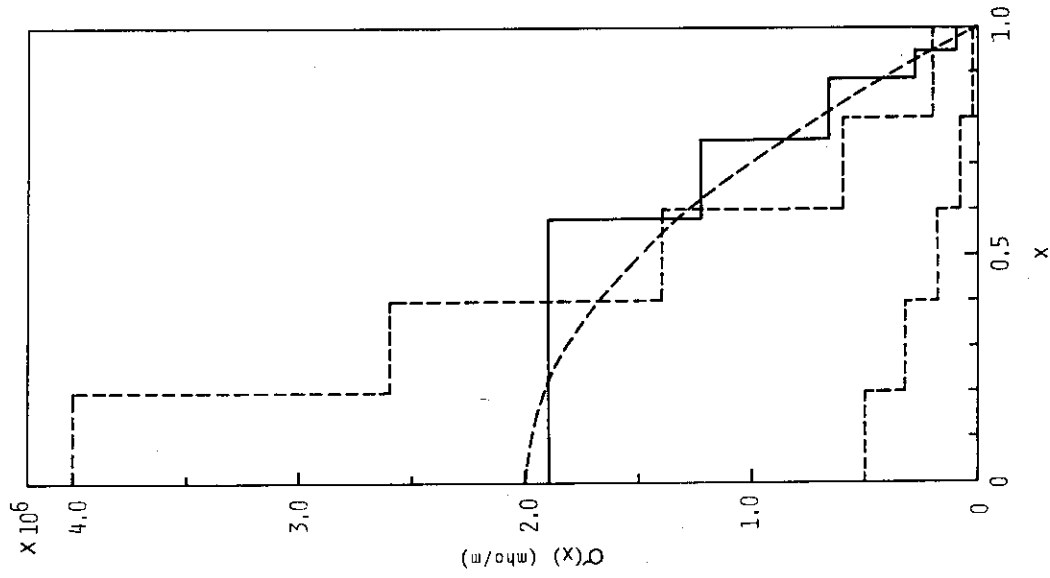


Fig. 8 The result of the test run for the case of five cylindrical shells. The stepped distributions (broken lines) show the initial guesses for the non-linear optimization. The parabolic distribution (broken curve) shows the curve to be fitted. The solid line is the converged distribution obtained by the above method.

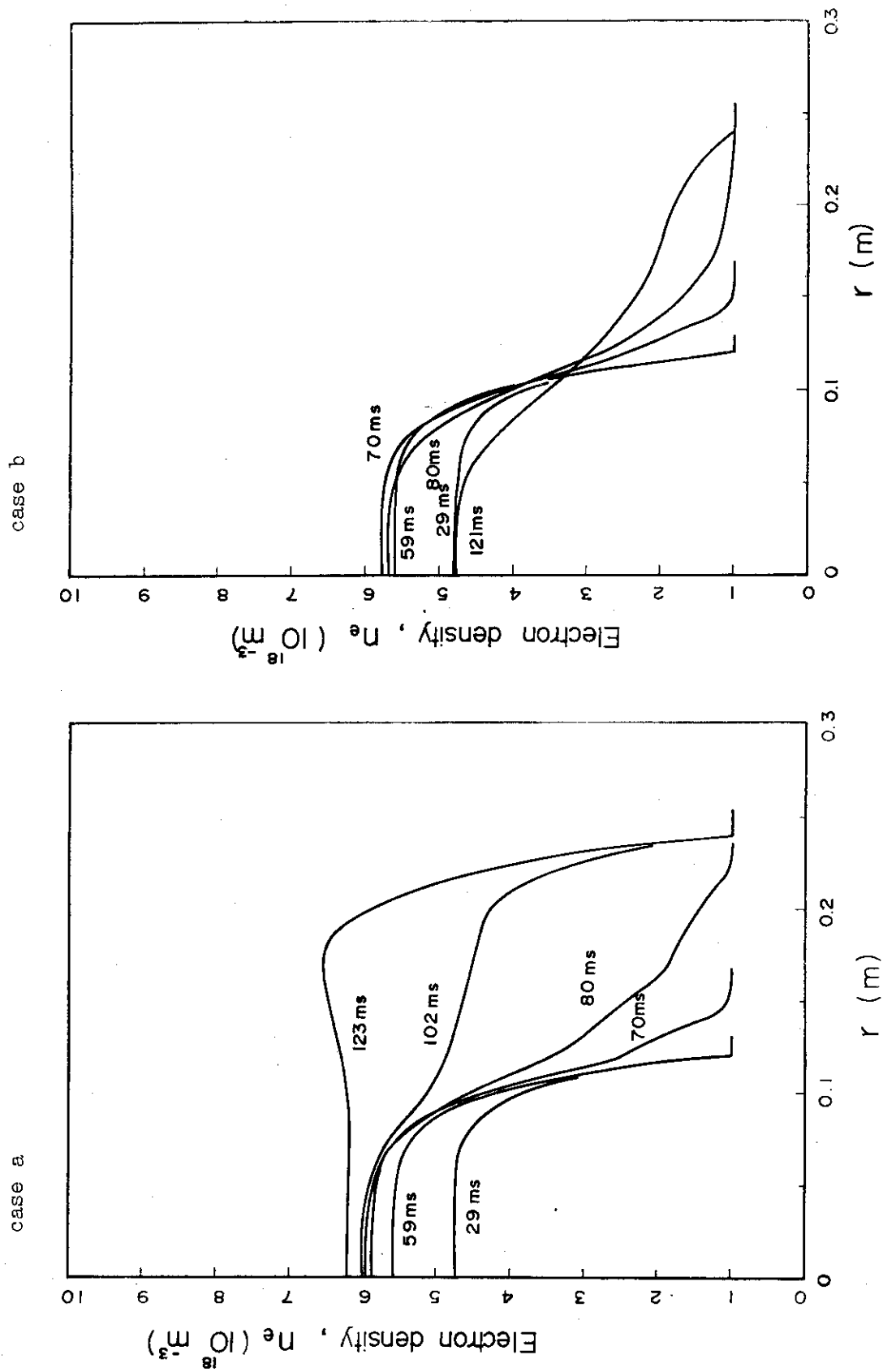


Fig. 9 The profiles of electron density for the neutral particle influx of  $3 \times 10^{20} \text{ m}^{-3} \text{ sec}^{-1}$  (case a) and  $1 \times 10^{20} \text{ m}^{-3} \text{ sec}^{-1}$  (case b) after the dynamic limiter is retracted (at  $t = 60 \text{ msec}$ ).

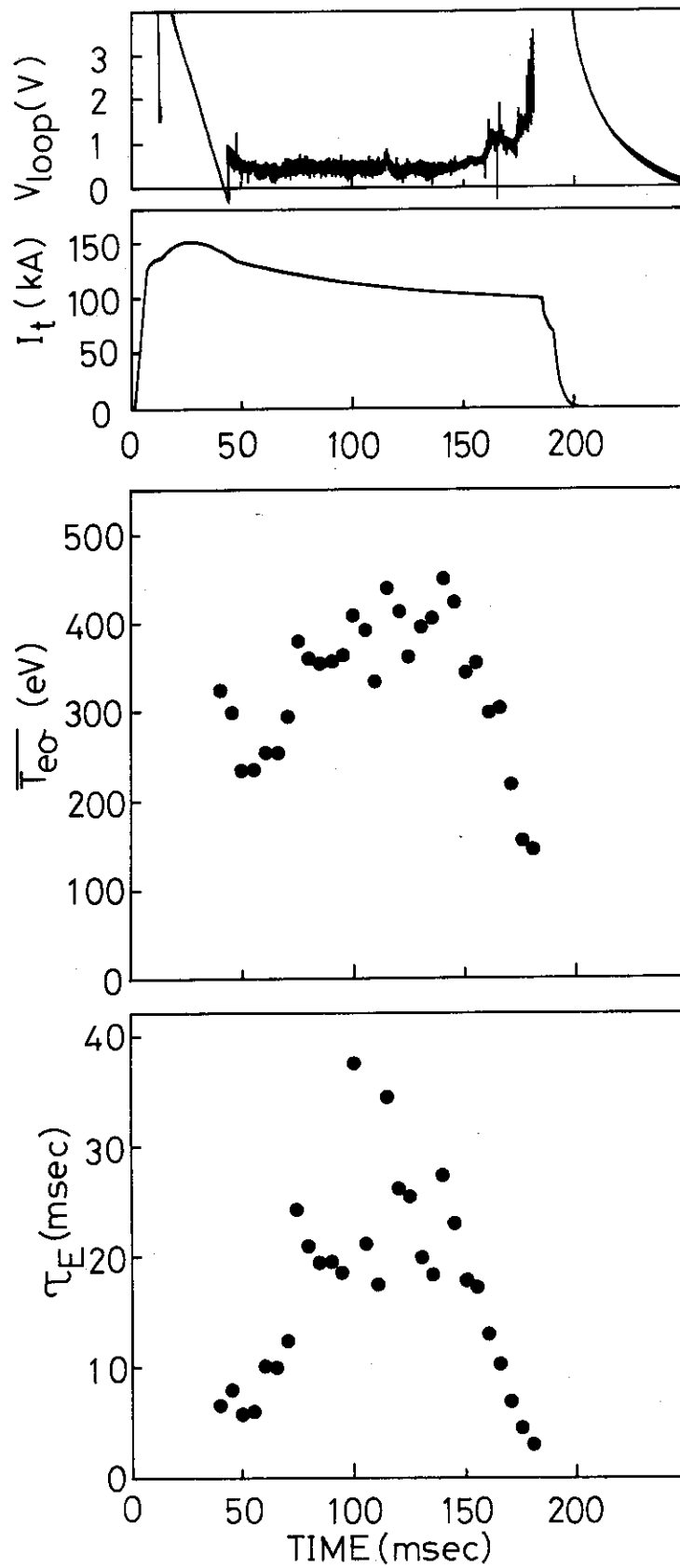


Fig. 10 The observed waveforms of the one-turn voltage at the measuring loop and the secondary current, and time variations of the mean conductivity temperature ( $\overline{T_e}$ ) and the energy confinement time ( $\tau_E$ ) obtained without smoothing of the observed data.

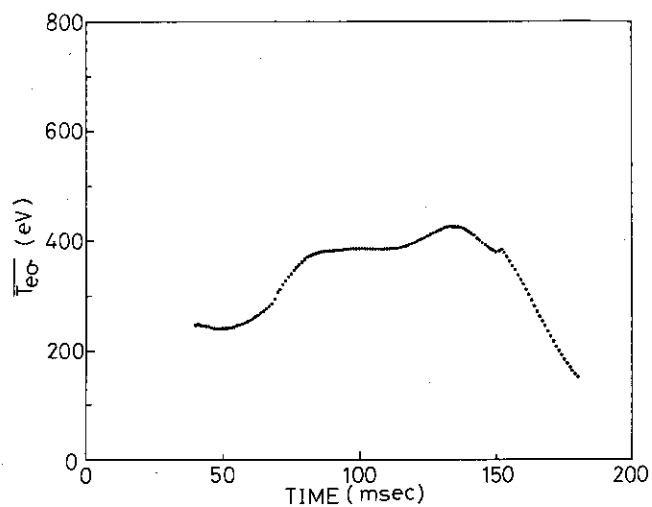


Fig. 11 Time variation of the mean conductivity temperature obtained by the appropriate smoothing.

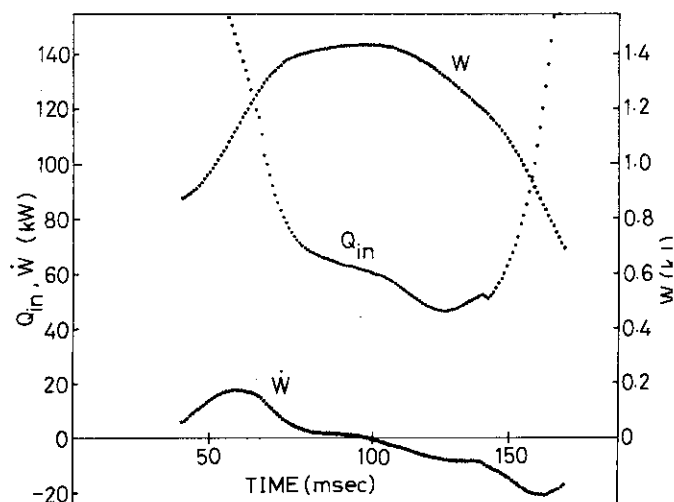


Fig. 12 Time variations of the total kinetic energy ( $W$ ), its time derivation ( $\dot{W}$ ) and the input power of a plasma ( $Q_{in}$ ).

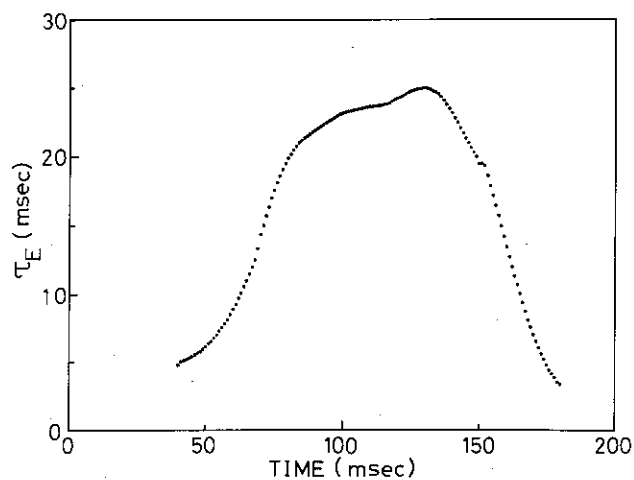


Fig. 13 Time variation of the energy confinement time.

### 3. JFT-2a

A. Kitsunozaki, H. Maeda, M. Nagami,  
T. Nagashima, H. Ohtsuka,  
Y. Shimomura, T. Tokutake and M. Yoshikawa

#### 3.1 Introduction

JFT-2a is a Tokamak device with a teardrop-like cross section capable of operating on an axisymmetric divertor designed in 1972. The engineering design and the construction of the device were started in 1973 and it will be put into operation in August 1974.

The construction of the device has already been completed at the present reporting period. Basic machine parameters are shown in Table 1 and, the cross-sectional and the plan view of the device are shown in Figs. 1, 2 and Fig. 3 respectively. The photograph of the device is also shown in Fig. 4 and Fig. 5.

The objectives of the present experimental program on the device are described below.

#### (1) Plasma confinement in a Tokamak with a teardrop-like cross section

A variety of cross-sectional shapes for Tokamaks have been proposed in the past. A teardrop-like cross section has been chosen for the device. It can provide larger magnetic shear and well than other cross-sectional shapes of the same average aspect ratio, depending on the plasma parameters. Consequently, the current density limit required to stabilize local instability is higher than for the other cross-sectional shapes in cases of a flat current distribution, and of a parabolic distribution at low beta. Furthermore the teardrop-like cross section appears to be better suited than the others for the installation of an axisymmetric divertor.

#### (2) Plasma production and confinement in a magnetic surface with separatrixes

It is necessary for a Tokamak with a divertor to produce and confine a plasma in a magnetic surface with separatrixes. The plasma production and confinement are to be studied and the plasma behaviour at the

separatrix magnetic surfaces is also to be studied.

### (3) Effect of a divertor on the plasma confinement

The contamination of confined plasmas by impurities released at the wall has an adverse effect on the energy balance and magnetohydrodynamic stability of the plasmas.

A divertor offers a possibility of lowering impurity content by guiding the plasma ions to the burial chamber and consequently reducing the bombardment of the wall by plasma ions.

An experimental study is made on the operation of an axisymmetric divertor. Plasma equilibrium in the required plasma configuration, longitudinal and transverse particle and energy transport on the divertor magnetic surfaces, and basic operational characteristics of the divertor is to be studied experimentally.

An experimental study will initially be made on the production and the confinement in the separatrix magnetic surfaces. Experimental studies on the effect of a divertor and the teardrop-like cross section on the plasma confinement will follow and be finished within March 1977.

A summary is given below on the main components of the device (3.2) and on the numerical studies (3.3).

Some diagnostic methods are being prepared for JFT-2a. They include 4mm. microwave interferometer measurement, visible spectroscopy and X-ray measurement. Other diagnostic methods, ruby laser scattering, neutral particle energy analysis and VUV spectroscopy prepared for JFT-2, are being prepared to be applied to JFT-2a. Some descriptions of these diagnostic methods are shown in section 4 and others are shown in the previous annual report.

(Y. Shimomura and M. Yoshikawa)

## 3.2 Main Components of the Device

### 1) Shell

The shell enclosing the plasma is made of copper of 2-3 cm. in thickness and contained within a vacuum chamber. The quarter part of the shell is shown in Fig. 4.

Part of the shell, the movable shell, can be moved vertically. For plasma confinement without the divertor in operation, the movable shell is placed at the "closed" position as shown in Fig. 2. The operation of the divertor is studied by moving the movable shell vertically to the "open" position.

The surface of the shell is ion-plated with gold of 10-20  $\mu$  in thickness. The gold surface was studied and reported in the previous annual report. The cross sectional shape of the inner surface of the shell was reported in Ref. 3).

(H. Maeda, A. Kitsunozaki)

## 2) Limiter

Three molybdenum pieces clad in gold of 1mm. in thickness. They are manually retractable for experiments with the divertor in operation.

(H. Maeda)

## 3) Divertor

Brief description of the disjunctable divertor hoop is as follows; major radius 0.37m, minor radius 16mm, maximum m.m.f. 60 kAT, air cooled, attached with divertor plates of 99.9% titanium (Fig. 2).

Titanium evaporation was studied experimentally and an optimum operation mode was determined. Other miscellaneous problems which would arise in the evaporation were studied by a preparatory experiment.

A computer simulation which investigates particle transport in the divertor configuration is now under study.

(H. Ohtsuka)

## 4) Gas supply system

Plasmas are produced by two ways of gas supply method. The one is continuous gas supply throughout every current pulse and the other is pulsed gas admission into the shell just before discharge. Continuous gas admission of 0.1 Torr·l/sec into the vacuum chamber results in  $2 \cdot 10^{-4}$  Torr of filling pressure. Pulsed gas of about 200  $\mu$ sec time duration is applied by four fast acting gas valve. The plenum volume of a FAV is 0.2 cc and filling pressure of 60 Torr in four FAVs give  $2 \cdot 10^{-4}$  Torr of pressure when the admitted gas spreads in the shell, and purity of the gas



is over 99.9 per cent. Power of FAVs is supplied by a capacitor bank ( $40 \mu\text{F}$ , 3 kV).

(M. Nagami, T. Tokutake)

#### 5) Pre-ionization system

For the initial ionization of the gas in the device microwave discharge at the electron cyclotron resonance frequency and breakdown due to the energetic electrons emitted from a electron gun are available.

The electron cyclotron frequency is found to be 28 GHz, where the toroidal magnetic field is 10 kG. For heating we use a travelling tube operating at 28 GHz and with the maximum power 1 kW and the microwave pulse length 2 msec. The energy is fed into the chamber by means of a rectangular waveguide with a little attenuation.

Electrons emitted from the filament are accelerated by the biasing electric fields applied to the filament and drifted into the minor axis of the torus due to a toroidal magnetic field. For the filament we use 0.5-mm-diam. tungsten wire with an effective emitting length of 2 cm located along the toroidal magnetic field. The heating time of the filament is from 2 to 90 sec. The voltage and the width of the accelerating pulse are 0.1-3 keV and 0.1-2 msec, respectively. The operation of the electron gun is determined from the contamination rate of the gold coated shells by the evaporated tungsten atoms from the filament.

The electron density of the preionized plasmas by these two methods is expected to be  $10^9$ - $10^{10} \text{ cm}^{-3}$  in a hydrogen discharge.

(T. Nagashima)

#### 6) Vacuum system

The vacuum chamber is made of stainless steel and consists of two toroidal sections. Surrounding the plasma, the surfaces of the copper shells of four toroidal sections are covered with gold of 10 to 20  $\mu$  in thickness by ion plating method. The gold coated shells minimize chemical- and electron- induced adsorption and prevent impurities coming into the plasma under wall bombardment.

The main pumping circuit consists of one primary rotary pump, two turbo-molecular pumps in parallel. The measured pumping speed is about 560 l/s at pressure of  $5 \cdot 10^{-6}$  Torr ( $\text{N}_2$ ). The vacuum chamber is bakable at temperature of 110°C.

(T. Tokutake, H. Maeda)

## 7) Toroidal magnetic field

Toroidal magnetic field of 10 kG at the maximum is produced with 16 coils each having 26 turns. Deviation of the field intensity in the plasma region is less than 3 % and the spatial ripples of magnetic field lines are less than 1 mm. Stray field due to the current feeder cable is compensated by two parallel turns of return windings whose positions are independently adjustable. The time constant of the toroidal coil is 0.68 sec. The coils are cooled by water through copper hollow conductors. The current is supplied by SCR controlled rectifier of 4700 kVA and the current ripple is less than 0.1 %.

(T. Tokutake)

## 8) Vertical magnetic field

Vertical magnetic field of 120 G at the maximum is used to control the position of plasma column. Stability factor of the produced field for circular cross section plasmas  $n = R/B_v \cdot dB_v/dR$  is -0.2 -0.4. The current for the vertical field coil of 40 kAT is supplied by a motor - dc generator couple.

(T. Tokutake)

## 9) Power supply system

Current for the primary winding of the main core is supplied by a capacitor bank of 90 kJ. Current for the divertor hoop coil is supplied through a transformer coupled with the primary current in order to make the hoop coil current proportional to the plasma current. The ratio of the divertor hoop current to the plasma current is adjustable from 0.2 to 0.9 with taps.

(T. Tokutake)

## 10) Gas pressure measurement

Density measurements on the neutral gas are made by means of a fast ionization gauge specially constructed for work under the conditions of quasistationary discharge in a strong magnetic field.

Discrimination of the pressure signal from the background noise is accomplished by modulating the current of ionizing electrons. Owing to the small size of the slit of the aperture, the gas impedance of the

manometer entrance aperture is negligibly increased by its presence. The calculated value of the gas-kinetic time constant of the instrument do not exceed 0.5 msec in the range of pressures  $10^{-6}$  to  $10^{-3}$  Torr.

(T. Nagashima)

#### 11) Magnetic measurement

The basic parameters of the plasma column are measured with Rogowski coils, a one-turn-voltage coil and magnetic probes. Each magnetic probe is installed in a casing of stainless steel and set in a channel just inside the shell. Distortion of waveform caused by casing and cable is avoided with compensation circuit.

(A. Kitsunezaki)

#### 12) Electrostatic measurement

One of the fundamental techniques for measuring the properties of plasmas near the divertor hoop is electrostatic probes. In spite of the difficulties which arise when probes are used in a strong magnetic field, the method is an important one because it has one advantage over all other diagnostic techniques: it can make local measurements.

In order to measure the properties of plasmas near the divertor floating double probes are used with the probe tip of cylindrical molybdenum rod and the insulator of beryllium oxide. The probe tips are movable 6 cm vertically along the major axis.

(T. Nagashima)

### 3.3 Numerical Analysis

#### 1) Equilibrium of JFT-2a plasmas

Equilibria of toroidal plasmas with non-circular cross section are analysed using special form of equilibrium solutions. Another calculation method to analyse plasma equilibria is developed which employs three-stage iteration scheme using the ADI method. The plasma equilibria both for cases of closed shell and for cases of open shell and an external current carrying ring are obtained with the iteration method. The plasma current density distribution is either flat ( $j_\phi = a \cdot R + b/R$ ) or parabolic

( $j_\phi = (a \cdot R + b/R) \cdot \psi$ ). The calculation results are used to analyse the data obtained with magnetic probes.

(A. Kitsunezaki)

## 2) Numerical simulation of JFT-2a plasmas

One of a feature of JFT-2a plasmas that differ from ordinary Tokamak is that the flux of neutral and impurity particles penetrating into the plasma is decreased by the system of magnetic limiter, titanium divertor, gold-plated shell and pulsed gas injection just before discharge. At this point of view, we have investigated in an one dimensional two fluids Tokamak simulation code including neutral and impurity particles effects.

Four equations of particle diffusion, electron and ion thermal diffusion and field diffusion are solved with the Crank-Nicolson's finite difference method.

Cold neutral penetrating into the plasma and created fast neutrals are calculated as follows. According to Dnestrovskii's<sup>12)</sup> method, we consider the problem in plane geometry, and fast neutral created by charge exchange with an ion have an energy equal to the ion temperature at the space point and equiprobable forward and backward velocity directions. Thus (m+1)th charge exchange neutral at  $r = x$  is obtained from m-th neutral as

$$N_{m+1}(x) = \int_0^a K(x,r) N_m(r) dr$$

, where  $a$  is the plasma minor radius. We calculated first and second fast neutrals. Oxygen impurity behaviour is also calculated in simple method. According to multicharge diffusion theory,<sup>13)</sup> we obtain a distribution of total number of oxygen impurity particles as

$$\sum_z O_z(r+\Delta r) = \sum_z O_z(r) \left[ \frac{n(r+\Delta r)}{n(r)} \right]^z$$

, and ionization stage is calculated by Corcna equilibrium model, where  $O_z$  is density of oxygen and  $z$  is charge number. Current supply circuit is also calculated and one of the results is shown in Fig. 8. In this case pseudoclassical transport coefficient<sup>14)</sup> appropriate to particle and electron thermal diffusion, and neoclassical transport coefficient<sup>15)</sup>

appropriate to ion thermal diffusion, and the iteration converges usually in about five iterations.

(M. Nagami)

### 3) Shaping of a plasma cross section by external current carrying conductors

Equilibrium configurations have analytically been obtained for a straight plasma column with a surface current in the magnetic field produced by external current-carrying conductors (Fig. 10). The method of analysis is similar to that used by Namiot to derive equilibrium configurations of a plasma column placed between parallel conducting plates.

Equilibrium configurations have been studied numerically of a straight plasma column with various current density profiles in the magnetic field produced by external current-carrying conductors (Fig. 11). The intensity of external currents to keep a shape of the plasma cross-section is larger when the plasma current concentrates on the magnetic axis than when it diffuses over the plasma cross-section. It is thus necessary to control the currents of external conductors in order to keep a suitable shape of the plasma cross-section when the plasma current density profiles varies with time.

(H. Maeda, Y. Shimomura)

### References

- 1) A. Kitsunezaki, H. Maeda, Y. Shimomura and M. Yoshikawa: in Proceedings of Third International Symposium on Toroidal Plasma Confinement, Garching, March 26-30, 1973, Paper G2.
- 2) M. Yoshikawa, Y. Shimomura, H. Maeda and A. Kitsunezaki: in Proceedings of Sixth European Conference on Controlled Fusion and Plasma Physics, Moscow, July 30- August 4, 1973, Vol. I, p. 173.
- 3) A. Kitsunezaki, Y. Shimomura, H. Maeda, M. Yoshikawa, JAERI-M-5612 (1974) (in Japanese)
- 4) A. Kitsunezaki, H. Maeda, Y. Shimomura: to be published in Nuclear Fusion.

- 5) T. Ohkawa: Kakuyugo-kenkyu 22, 99 (1968).
- 6) L.S. Solov'ev: Soviet Phys. JETP 26, 400 (1968).
- 7) S. Komiya, T. Narusawa and C. Hayashi: J. Vac. Sci. Tech. 9, 302 (1972).
- 8) M. Mizuno, et al. : Report on technical development and evaluation on gold evaporation method, ULVAC Corporation, 1972 (in Japanese).
- 9) S. Komiya, M. Mizuno, T. Narusawa, H. Maeda, M. Yoshikawa: in Proceedings of 6th International Vacuum Congress, Kyoto, March 25 29, (1974).
- 10) H. Maeda, Y. Shimomura, A. Kitsunozaki, M. Yoshikawa : JAERI-M-5462 (1973) (in Japanese)
- 11) Y. Shimomura, H. Maeda, A. Kitsunozaki, M. Yoshikawa, JAERI-M-5621 (1974) (in Japanese)
- 12) Y.N. Dnestrovskii, et al. Atomn. Energ. 32 301 (1972).
- 13) T. Tuda, M. Tanaka : JAERI-M-5376 (1973) (in Japanese)  
J.W. Connor Plasma Phys 15 765 (1973)
- 14) S. Yoshikawa Phys. Rev. Letters 25 353 (1970)
- 15) F.L. Hinton, et al. Phys. Rev. Letters 29 698 (1972)

Table 1 Basic parameters of JFT-2a

Flux of iron core		0.3V.sec
Toroidal magnetic flux density		10 kG
Vertical flux density		120 G
Shell	inner radius	105 x 140 mm
	major radius	600 mm
	thickness	20 mm
Main condenser energy		90 kJ
Plasma	major radius	600 mm
	average aspect ratio	5.5

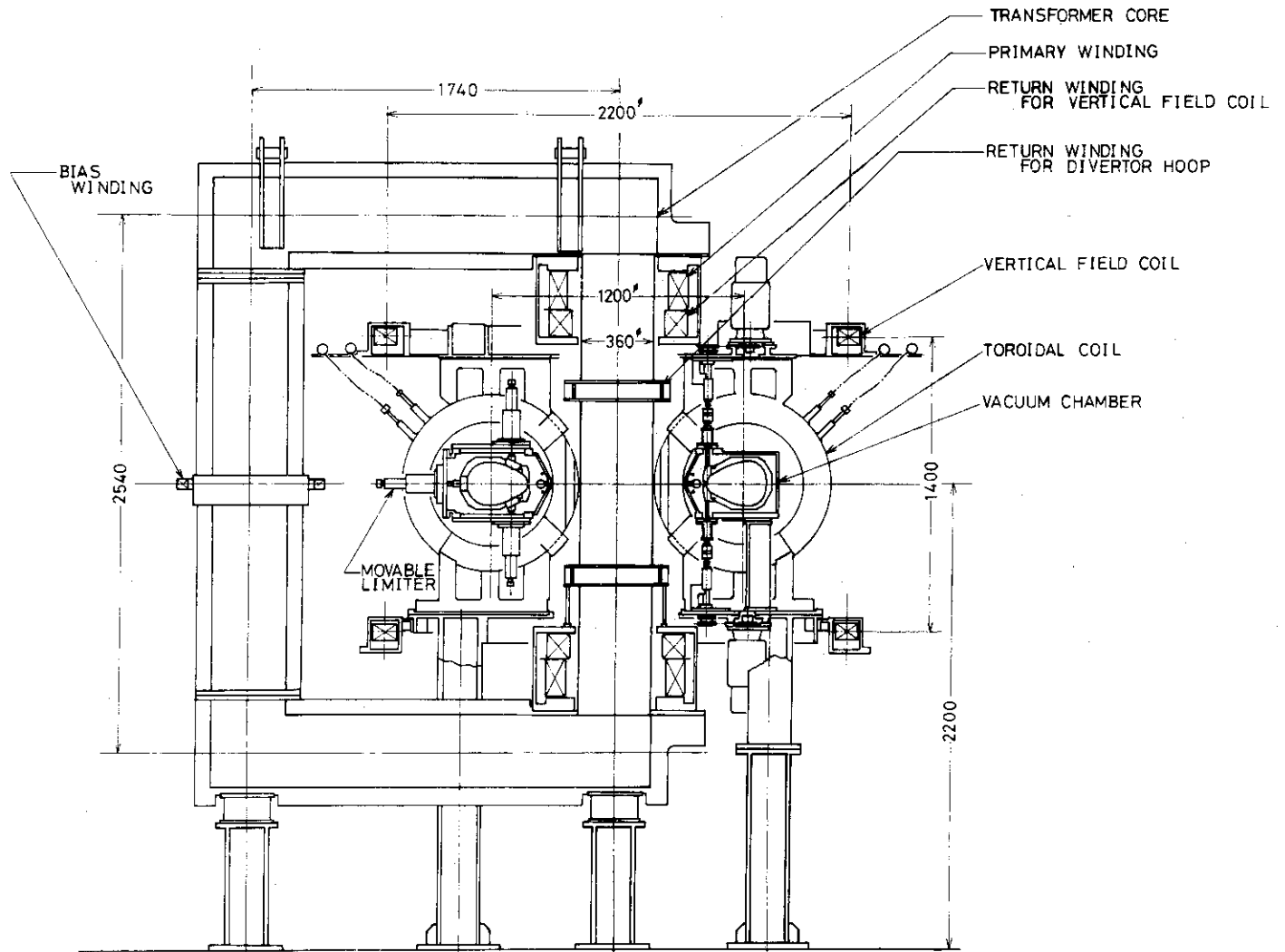


Fig. 1 Cross-section of JFT-2a



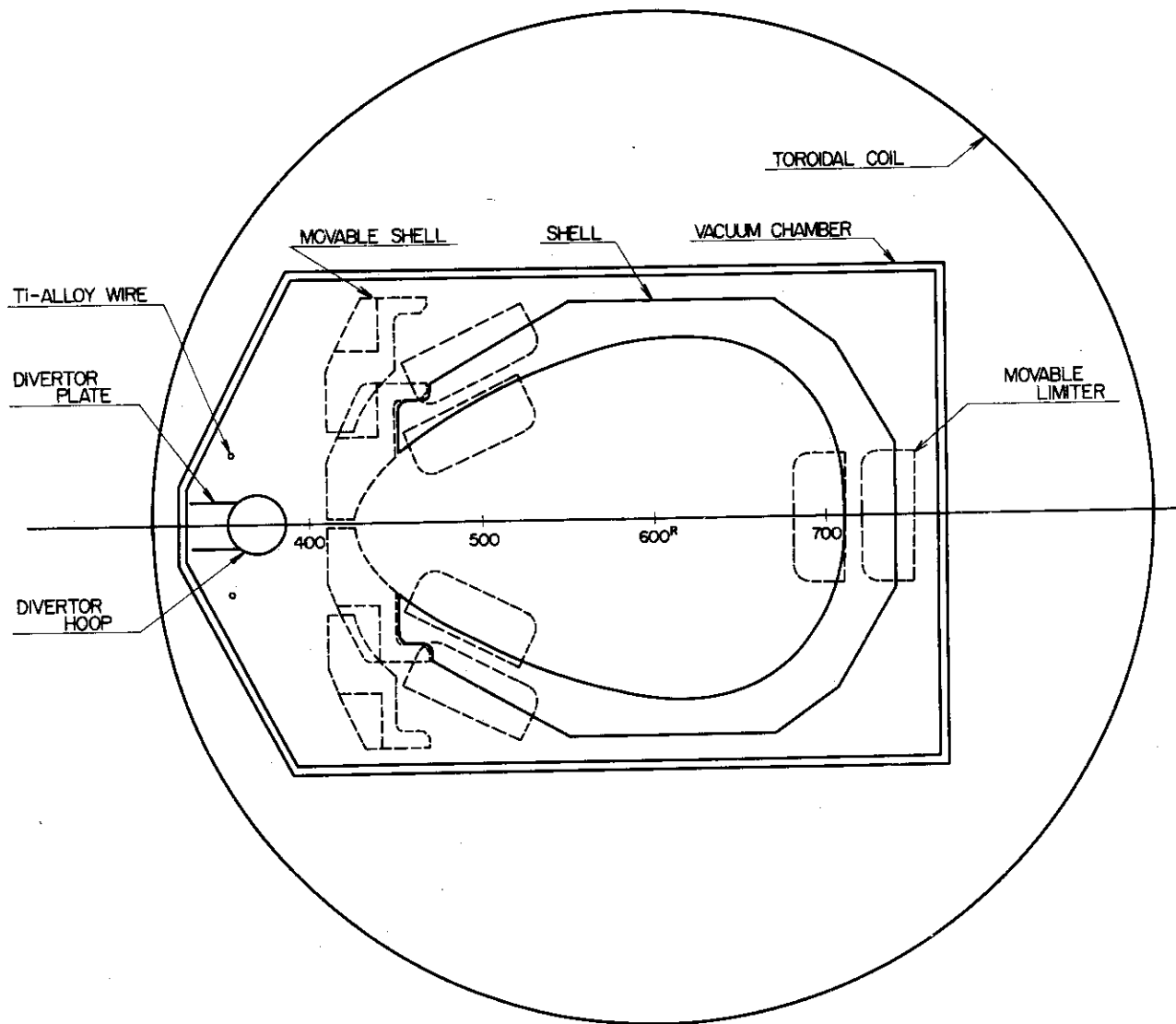


Fig. 2 Cross section of the vacuum chamber

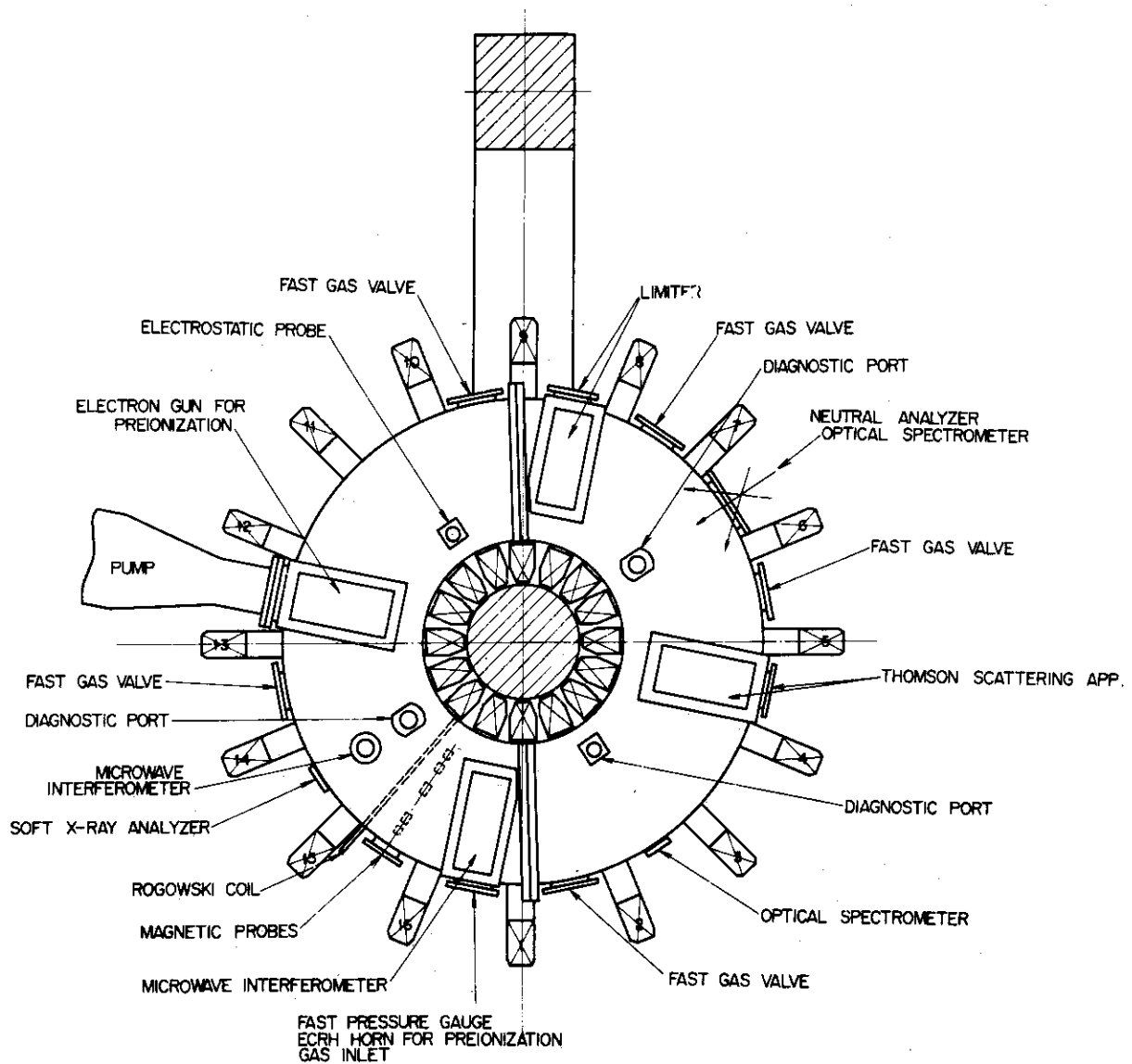


Fig. 3 Plan view of JFT-2a

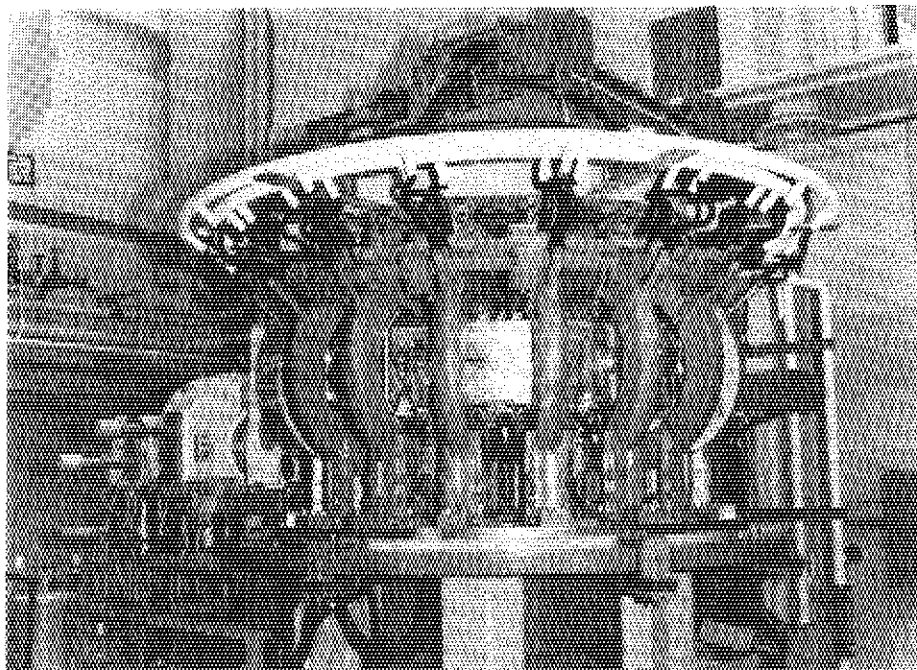


Fig. 4 Photograph of JFT-2a

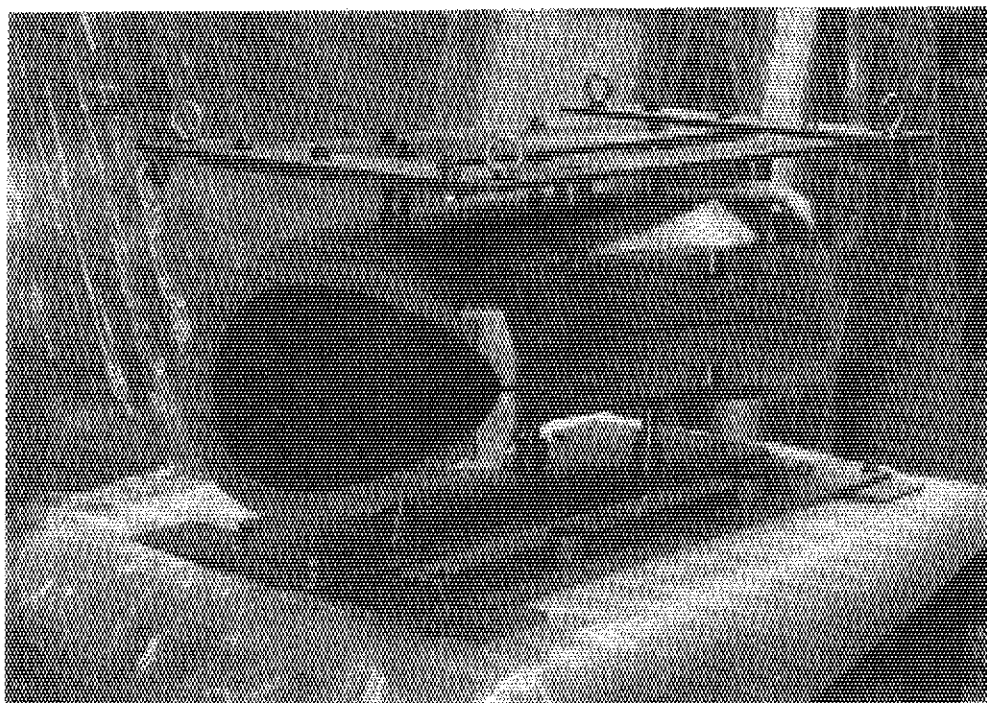


Fig. 5 Photograph of shell

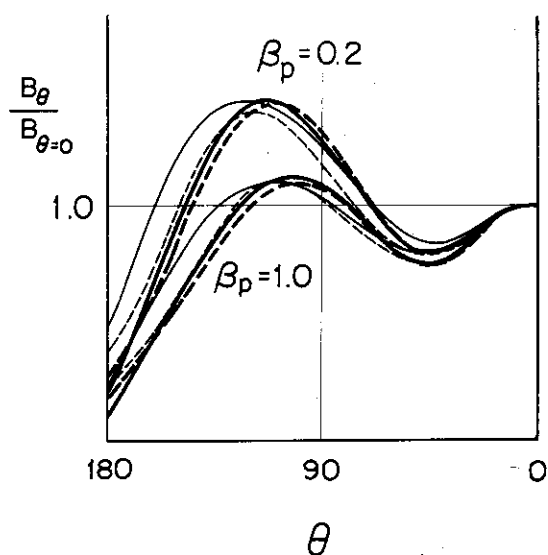


Fig. 6 Magnetic field distribution along the shell surface

fat lines	parabolic current distribution
thin lines	flat current distribution
solid lines	plasma-shell gap is 10 mm
broken lines	plasma-shell gap is 20 mm

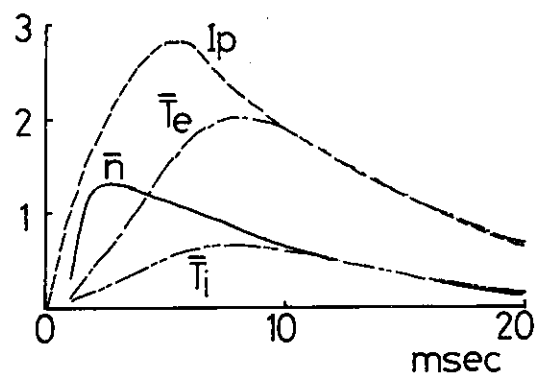


Fig. 8

Profiles are given in case of charging voltage of 3 kV for plasma current  $I_p (\times 10^4 \text{ A})$ , average density  $\bar{n} (\times 10^{13} \text{ cm}^{-3})$ , and average temperature  $\bar{T}_e, \bar{T}_i (\times 10^2 \text{ eV})$ .

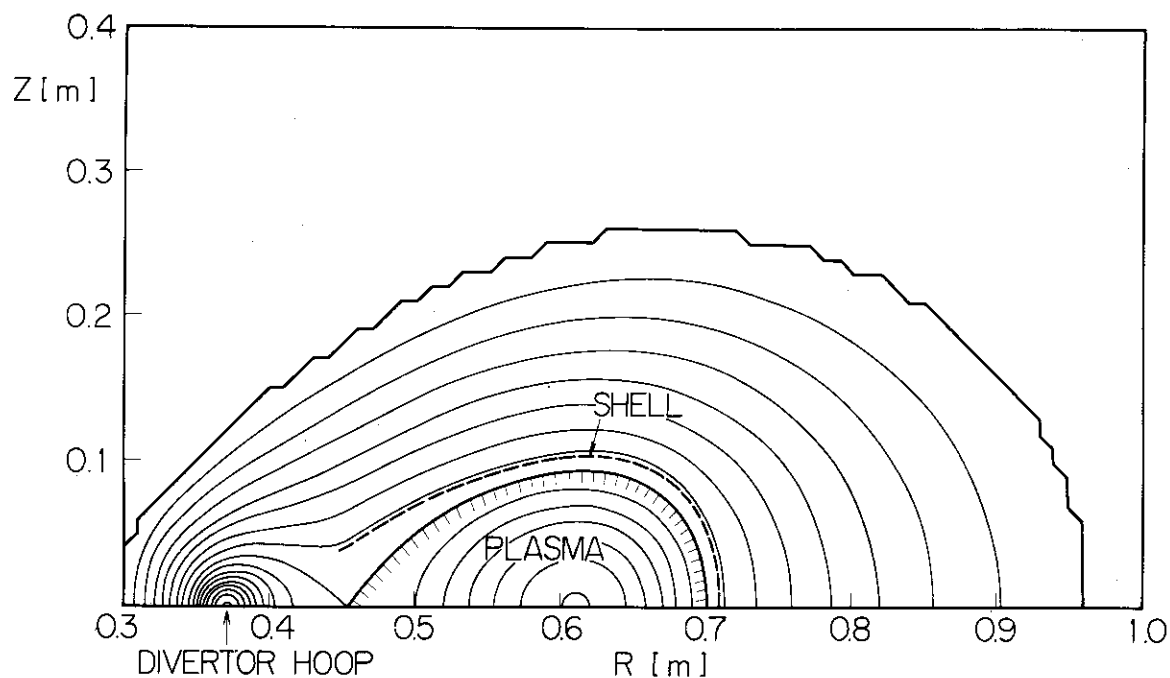


Fig. 7 Plasma equilibrium in an open shell and a divertor hoop

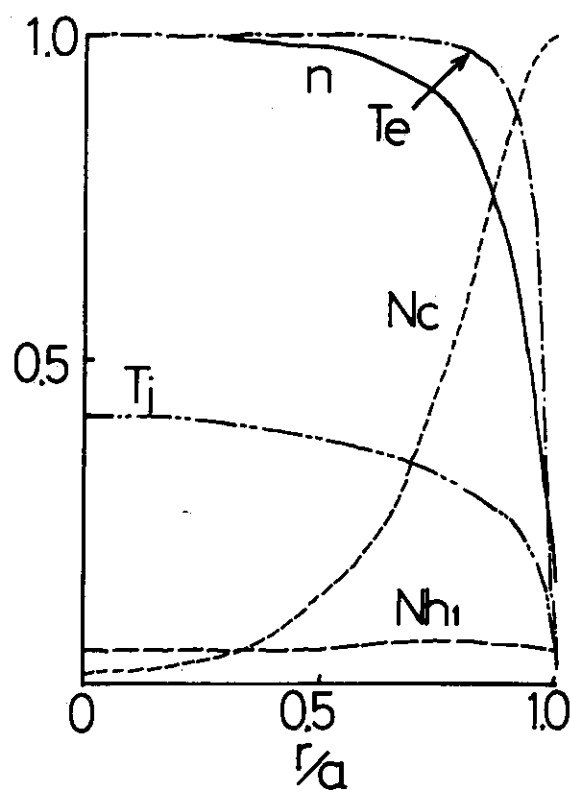


Fig. 9 Profiles are given at 6 msec for density  $n$ , temperatures  $T_e$ ,  $T_i$ , cold neutral density  $N_c$ , and first hot neutral density  $N_{h1}$ . Maximum :  $n = 1.23 \times 10^{13} \text{ cm}^{-3}$ ,  $T = 196 \text{ eV}$   
 $N = 2.69 \times 10^9 \text{ cm}^{-3}$ .

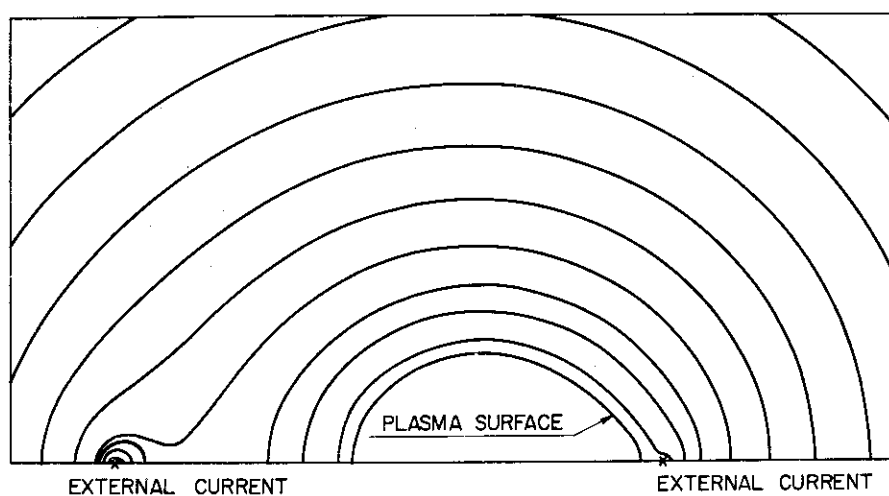


Fig. 10 Example of equilibrium configuration in case of skin current :  $I_D = 0.08 I_P$ ,  $I_D' = 0.2 I_P$

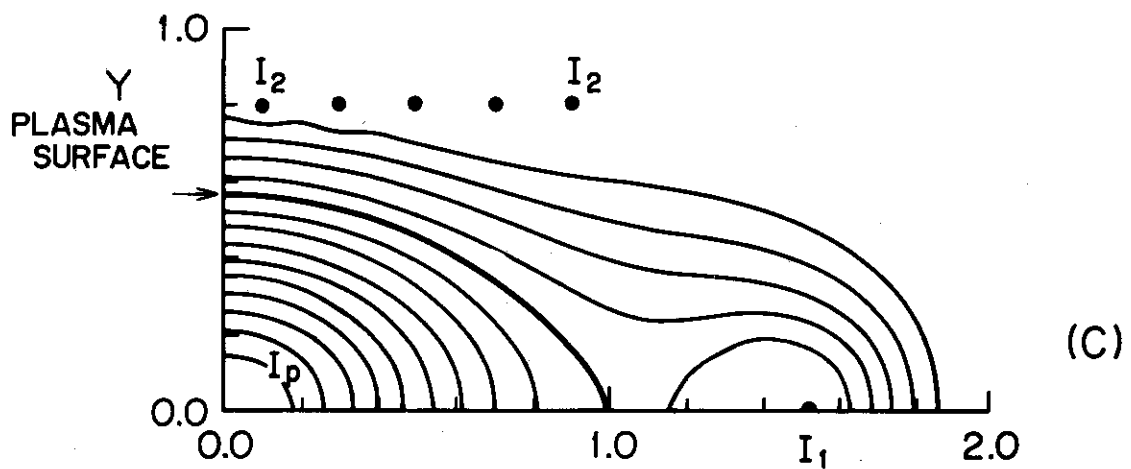
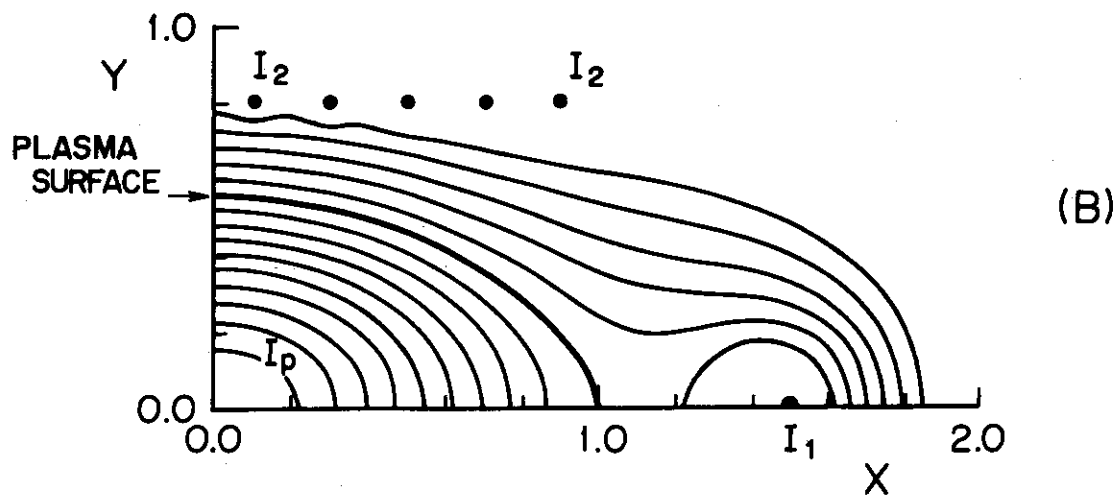
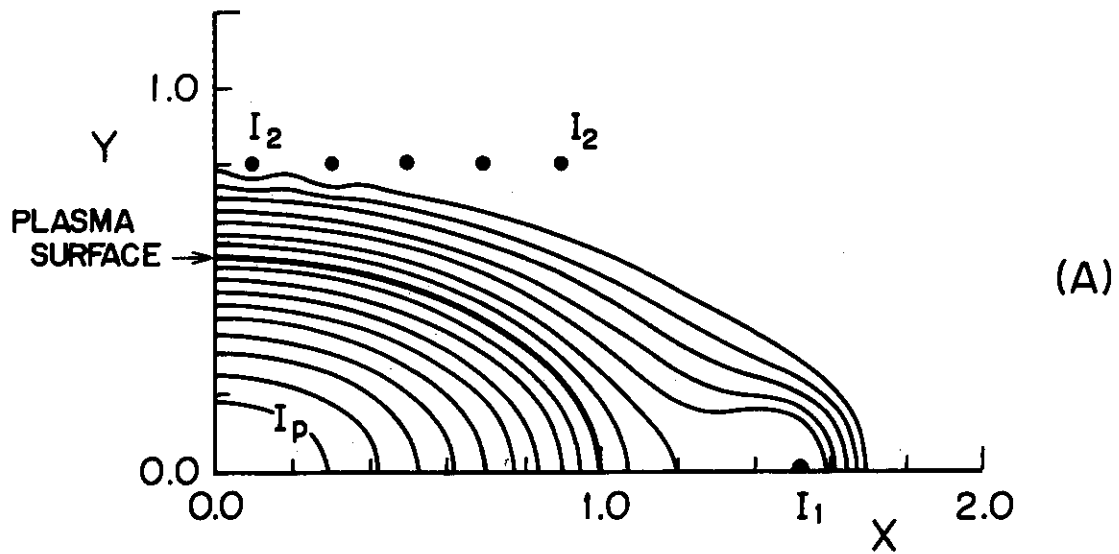


Fig. 11 Examples of equilibrium configurations.

(A) ....  $J_z = \alpha$ ,  $I_1 = 0.2 I_p$  and  $I_2 = -0.02 I_p$

(B) ....  $J_z = \beta (1 - \psi/\psi_s)$ ,  $I_1 = 0.3 I_p$  and  $I_2 = -0.03 I_p$

(C) ....  $J_z = \gamma (\exp(-2\psi/\psi_s) - \exp(-2))$ ,  $I_1 = 0.35 I_p$   
and  $I_1 = -0.035 I_p$

## 4. Diagnostics

A. Funahashi, S. Kasai, T. Kawakami, T. Matoba, T. Shoji

### 4.1 Introduction

The purposes of the diagnostic study are to diagnose and measure high-temperature plasmas up to the fusion state. The investigations of this group are classified into

- (a) measurements of the fundamental quantities of produced-plasmas, and presenting information to confirm the performances of fusion-research machines,
- (b) designs of new diagnostic apparatus, corresponding to an extension of plasma parameters or the construction of new fusion machines, and
- (c) developments of advanced diagnostic method, for example, for measurements of current distributions, impurity quantities and fluctuations and for data processing systems.

In this reporting period, many efforts are devoted to diagnostics of JFT-2 plasmas and to measuring fundamental quantities such as electron and neutral atom densities, temperatures, impurities, ionization rates and particle and energy confinement times. Some developmental and design works are also made for data processing systems, the  $\alpha$ -particle method, doppler measurements in a VUV region and so on. The instruments of these diagnoses are now being manufactured in several companies.

Lastly, we are now preparing some diagnostic instruments for JFT-2a plasmas, such as multichannel 4mm-wave interferometers, a visible spectrometer for doppler temperatures, and data processing systems. Some improvements in Thomson scattering apparatus (cf 4. 2. 3) are also designed to be able to apply to the JFT-2a apparatus.

(A. Funahashi)

### 4.2 Measurements

#### 1) Microwave interferometric measurements

The millimeter microwave interferometric measurements are useful for electron densities less than  $10^{14} \text{ cm}^{-3}$  and are often used in low-beta

toroidal plasmas. We have furnished the 2-mm and 4-mm interferometers for Tokamak plasmas. The wave sources are a carcinotron tube (5W) and a OKI KA-701 klystron (400 mW) respectively.

In this reporting period, electron densities in JFT-2 Tokamak plasmas are measured with the 4-mm wave interferometer at the opposite position of a limiter. The 4-mm waves penetrate vertically into plasmas through quartz lenses to improve spatial resolutions. These lenses are also used for vacuum seals of the measuring ports, and mechanical shutters are attached into the lenses in order to prevent them from being opaque by sputtering of wall materials. There are eight pairs of the ports with intervals of 6 cm. The transmitting and receiving horns of the interferometer are moved horizontally at port positions to determine density profiles.

The measurements are performed for the wide ranges of plasma current and filling pressure. The following description is devoted to one typical experimental condition, which shows good reproducibility of plasmas, of maximum plasma current 70 kA, filling pressure of hydrogen  $3.6 \times 10^{-4}$  Torr, limiter radius 25 cm, plasma duration 190 msec, and toroidal field 10 kG.

The time-variation of electron density  $\bar{n}_e$  is shown in Fig. 1 measured averaged along the wave-path by 6 cm inside from the liner center. In this figure the time-variation of plasma current is also shown. Similar measurements are made for the other wave-paths. Figure 2 shows density profiles at different times, which are determined from the averaged values along the eight vertical wave-paths by using the inversion method. The abscissa X in the figure is the horizontal position in the equator plane, where plus and minus signs denote the inside and outside of the torus respectively. At 60 msec a symmetric profile is realized, and the profile is nearly a parabolic distribution as shown in Fig. 2(B). Figure 3 shows the time-variation of the density profiles during the discharge period. The horizontal displacement  $\delta$  of the maximum-density point from the liner center is also shown in this figure. Figure 4 shows comparisons between these  $\delta$ -values and the horizontal displacement  $\Delta H$  of plasma current column determined from the signals of two magnetic probes on the shell. These two values are in good agreement except during the initial discharge period. Comparisons are shown in Fig. 5 of time-variations of plasma currents  $I_p$ , peak density  $n_{e,MAX}$ , and total density per unit length N.



It is shown from this figure that these peak and total densities are nearly proportional to the plasma current.

(A. Funahashi, S. Kasai and N. Fujisawa)

## 2) Spectroscopic measurements

Recently it was pointed out that impurities in high temperature plasmas make an important role with respect to particle confinements as well as radiation losses. Thus spectroscopic measurements become more worth-while especially in a vacuum ultraviolet (VUV) region. In addition visible spectroscopic technics are often used to determine neutral atom densities and ionization rates in Tokamak plasmas.

The time histories of intensities of impurity spectral lines radiated from JFT-2 plasmas and those spatial distributions are investigated over the wavelength range of 500 -- 2300 Å. In these measurements, a 50 cm VUV normal incidence monochrometer is used (c.f. Fig. 6). In the visible region, absolute intensities of  $H_\alpha$  and  $H_\beta$  lines are measured with a 25 cm and 100 cm visible monochrometers calibrated by using a tungsten-ribbon standard lamp. These measurements are made under the following experimental conditions; the filling pressure of the hydrogen gas  $P_F$  is  $(3.0 -- 3.3) \times 10^{-4}$  Torr, the toroidal magnetic field  $B_t$  is 9 -- 10 KG, the plasma current is 75 -- 80 KA, the plasma duration time is 100 -- 130 msec and the diameter of the molybdenum limiter is 50 cm.

The changes of intensities of carbon, oxygen and nitrogen ions which are in various ionized states are shown in Fig. 7. These spectral line intensities are normalized by their maximum intensities. From this figure, it is found that as the plasma current and electron temperature are increasing the spectral lines due to highly ionized ions appear in sequence. The spatial distribution of the intensity of CV (2270.9 Å) line has a shell type profile at 23 msec after the breakdown of the plasma. On the other hand, the OVII (1623.3 Å) line has a distribution whose maximum intensity is near the center of the plasma at this time and a shell type profile at 33 msec.

From the measurements of  $H_\alpha$  and  $H_\beta$  absolute intensities and electron densities with a 4-mm microwave interferometer, the charged particle confinement times of the JFT-2 plasma under the above-mentioned experimental conditions are shown to be about 5 -- 10 msec. And the concentrations of

the neutral hydrogen atoms  $\bar{n}_0$ , which are averaged over the light path along the plasma center, are about  $(2 - 5) \times 10^9 \text{ cm}^{-3}$  as shown in Fig. 8.

(S. Kasai, T. Matoba, A. Funahashi)

### 3) Thomson scattering measurements

A measuring apparatus of electron temperature and density by the Thomson scattering method was brought to completion in March 1973. The photograph and the optical arrangement of this apparatus are shown in Fig. 9 and 10, respectively. An observation port which is included in the discharge chamber of JFT-2 is shown in Fig. 11. Chief specifications of this apparatus are as follows.<sup>1)</sup>

#### (1) Q-switched ruby laser

laser power		500 MW,
pulse duration	MAX	20 nsec,
beam divergence	MAX	5 mrad.

#### (2) Optical system

focusing system of laser light		
horizontal scanning		360 mm,
focal spot size		3--10mm,
focusing system of scattered light		
vertical scanning		475 mm,
spectrometer Czerny-Turner mount	F: 6.5,	f = 1 m,
grating :		1200 lines/mm.

#### (3) Observation port

laser dump and viewing dump	glass filter.
-----------------------------	---------------

#### (4) Photodetector system

number of channels	12,
photomultiplier	RCA C31026,
wavelength range	70 Å/ch.

#### (5) Sequenced pulse delay system

delay time between channels	50 nsec,
gate width	slow gate (PM) 3 μsec,
	fast gate (circuit) 50 nsec.

A stray light intensity was the first to be measured. Its results are shown in Fig. 12. Central wave lengths detected with photomultipliers PM 1 and PM 12 are  $6943 \text{ \AA}$  which is the wave length of ruby laser light and  $6179 \text{ \AA}$ , respectively. We express an orthogonal co-ordinate system with the horizontal direction as the  $\rho$  (or  $X$ ) co-ordinate axis and the vertical direction as the  $Z$  co-ordinate axis, and the origin is the liner center. Intensities of Rayleigh scattered light at 1 atm. are shown with the arrow labelled as 'AIR'. The reason why stray light intensity increases at horizontal position above 12 cm is that glasses of viewing dump are short in breadth. But this intensity levels of stray light do not obstruct the measurement of tokamak plasma.

This apparatus had been used for measuring electron temperature in JFT-2 from September 1973 to April 1974. Typical signals obtained from preliminary experiment are shown in Fig. 13. It becomes evident that signal to noise ratio,  $S/N$ , exceed the allowed value. In Fig. 14, intensities of individual channel signals in a logarithmic scale are plotted as a function of the square of the wave length shift for the typical discharges. A least-mean-square fit gives an electron temperature which is tabulated in the insert. Error bars illustrate the amount of scatter in measured values. Time dependences of electron temperature and density are shown in Fig. 15. The electron temperature takes a maximum value of about 250 eV at about 40 msec and then is rapidly reduced to about 100 eV. Electron density and maximum temperature are compared in Fig. 16 with the peak plasma current. The square of current value is proportional to electron temperature at current below 80 kA but electron temperature is nearly constant at current above 80 kA. On the other hand electron density is nearly constant in the range of experiments. Electron temperature profiles in the horizontal and vertical planes at 40 msec are illustrated in Fig. 17. The temperature profiles are approximately parabolic following a relation

$$T_e = T_e(0) \cdot [1 - (r/b)^2]^2$$

where  $b$  is the liner radius. These profiles may not be changed from 30 msec till 100 msec. The mechanical shutter which has protected the window from sputtering has not been used in experiments because of some troubles. Therefore, the radial profiles of electron density are not accurate enough.

Another problem is that sensitivity changes of photomultipliers during discharge. We have made correction at every measurement. This problem may be solved with addition of magnetic shield.

(T. Matoba and A. Funahashi)

#### 4) Charge-exchanged particle measurements

In order to eliminate the effect of an X-ray background from the discharge, an ion detector of a single-channel neutral particle analyzer was improved. The channel type electron multiplier (ceratron) was used as a new ion detector instead of the Daly type detector.<sup>2)</sup> Operating characteristics of the ceratron were measured with a proton beam of about 1 keV. Good characteristics were obtained for a neutral particle analyzer, and the X-ray background decreased remarkably. The counting efficiency of a ceratron for detecting the X-rays was less than 2 % at 103 keV. The improved analyzer was used for the neutral particle measurement in JFT-2 and has operated satisfactorily since October 1973.

The neutral particle measurements in JFT-2 were then resumed at the position of B-3 observation box. In the measurements, the time dependence and the spatial distribution of ion temperature were examined in detail, because of the improved accuracy of measurement. From the measurement, the ion temperature was found to be in good agreement with the scaling law proposed by Artsimovich et al.<sup>3)</sup> Typical radial profiles of the ion temperature are shown in Fig. 18.

In December the same year, neutral particle measurements were made during the dynamic limiter experiment in JFT-2. In this measurement, large number of the fast neutral particles were observed to be emitted from the plasma with the "closed" condition of the dynamic limiter, but the fast neutral particles rapidly decreased after the operation of the dynamic limiter was triggered. Behaviour of the ion temperature during the operation of the dynamic limiter was also similar to that of the neutral particles; i.e. the ion temperature decreased. Typical time-variation of the ion temperature is shown in Fig. 19.

In the course of dynamic limiter experiment, the particle measurement was made in the shadow of the limiter. Unexpectedly, a large number of energetic neutrals emitted from the shadow of the limiter was observed. Intensity of the neutral flux was about as high as those from the center of the plasma. The necessity is thus indicated for investigation of the

interaction between a plasma and a limiter.

In the meantime, a ten-channel particle analyzer has been investigated, to obtain rapid, high-accuracy measurement of the results. By March 1974, the parallel plate type electrostatic analyzer and some channels of the electronic-circuits were constructed. The electrostatic analyzer is shown in Fig. 20. The whole system will be completed by the end of 1974.

(H. Shirakata\*, K. Takahashi\*, S. Yano\*,\*\*)

#### 4.3 Developments

##### 1) Loss flux measurements by bolometric method

The bolometric method may be simpler than any other method in direct measurements of thermal loss flux from plasma. In U.S.S.R., the thermister bolometer of high speed response type (the time constant is about few  $\mu\text{sec}$  and the sensitivity nearly equals  $10^{-5} \text{ J/cm}^2$ ) had been developed<sup>4,5)</sup>, but useful results have not been reported in tokamak plasmas.

In our laboratory, the trial manufacture of three thin layer bolometers has been planned. Its performances are aimed specifically at high sensitivity and medium speed response. The specifications are as follows:

materials ;	Al ( $\sim 25 \mu\text{m}$ ) : $\text{Al}_2\text{O}_3$ ( $\sim 5 \mu\text{m}$ ) : Ge ( $1 \sim 2 \mu\text{m}$ )
structures ;	shown in Fig. 21. a) is a differential type and b) is a integral type.
sensitivity ;	$\sim 10^{-6} \text{ J/cm}^2$
rise time ;	under 1 msec
resistivity ;	above 100 k .

A Ge thermister involves two problems to be solved in case of applications to tokamak plasmas. One is the induction noise from plasma and the other is the change of sensitivity caused by strong magnetic fields. These problems are expected to be experimentally solved in each case.

(T. Matoba and H. Shirakata)\*

##### 2) Measurements of current distribution by means of high-energy particles

The principle of this method is that a current distribution can be determined from the orbit analysis in Tokamak configurations of high-energy,

---

\* Ionized Gas Laboratory, Division of Physics

\*\* Present address: Kobe University of Mercantile Marine, Kobe.

charged, rather light particles such as  $\alpha$ -particles emitted from a radio-isotope  $^{210}\text{Po}$ .<sup>6)</sup> In this reporting period, the details are designed of the experimental arrangements to measure for the JFT-2 apparatus, according to the  $\alpha$ -particle orbit analysis shown in ref. 7.

The arrangements consist of a vacuum vessel, an  $\alpha$ -source and a detector and their moving systems, and a gate valve and an auxiliary pumping system. An  $\alpha$ -source is located at a position of 33 cm or 38 cm horizontally away from the liner center. The emitting angle of the  $\alpha$ -particle can be varied by tilting the source holder in both the toroidal and poloidal directions. The tilting angles are designed to be from  $+5^\circ$  to  $-5^\circ$  in the toroidal direction and from  $5^\circ$  to  $90^\circ$  in the poloidal direction. A position sensitive detector is adopted to measure toroidal displacements of the  $\alpha$ -particle. The detector is moved to vary its vertical position and can be tilted in the poloidal direction from 0 to  $60^\circ$  on its position.

(K. Inoue and A. Funahashi)

### 3) Doppler broadening measurements in vacuum ultraviolet regions

In the measurements of the ion temperatures in high-temperature plasmas, two different methods have been often adopted. The one is a measurement of the charge-exchange neutrals and the other is a measurement of the Doppler broadenings of spectral lines. We are now preparing a VUV monochrometer to measure the Doppler width of various impurity spectral lines (longer than  $1220 \text{ \AA}$ ) radiated from high temperature plasmas.

The typical specifications are the following. The optical system is 1m Czerny-Turner type. It has a plane grating with 1200 G/mm, blazed at  $1 \mu\text{m}$  and coated with  $\text{MgF}_2$ . A wavelength resolution is  $0.1 \text{ \AA}$  for first order lights. This value is chosen to be able to measure Doppler broadenings of higher order lights (e.g. 6-th or 7-th order lights) of CIV ( $1548.2 \text{ \AA}$ ) or OVII ( $1623.3 \text{ \AA}$ ) etc. We use optical lens systems in front of the entrance slit of this monochrometer, and these consist of collimating and field lenses whose materials are  $\text{CaF}_2$ . Then the measurable spectral lines are limited to above  $1220 \text{ \AA}$ . Pumping systems consist of 4"-oil diffusion, mechanical booster and oil rotary pumps. The pressure in the vacuum chamber of this monochrometer is designed to be about  $1 \times 10^{-5}$  Torr.

We estimated the ratio of signal to noise (S/N) for measurements of Doppler broadenings of spectral lines of impurities, and determined the specifications of a monochrometer to be able to make measurements of  $S/N > 1$ .

We wish to thank Dr. K. Mori of the Institute of Physical and Chemical Research for his helpful suggestions in preparing a VUV monochrometer.

(S. Kasai, A. Funahashi)

#### 4) Data processing system and its preliminary study

With more precision and large-scaling of torus experiments, the online "data processing system" much larger than the "data acquisition system" has been designed and constructed and its preliminary experiments were performed.

The data processing system is composed corresponding to characteristics of torus experiments. To keep the independence of the acquisition of data, the analysis and the indication of results, the multi-CPU system are adopted and each port has the input controller of itself. To cover the wider ranges of the level and the frequency of input signals the sampling times may be variable by monitor signals. Noises are removed by the filters with the characteristic frequency of signals. Many experimental conditions and external parameters are also monitored.

The block diagram of the system is shown in Fig. 22. The input processing parts have 75 input channels. These parts include the followings, that is, (a) 10 ch. (with sampling time of 50-4000  $\mu$ S) for the electro-magnetic probe measurement, (b) 10 ch. (50-4000  $\mu$ S) and 10 ch. (1 mS) for the correlational measurement and the spectroscopic doppler measurement, (c) 2 ch. (2  $\mu$ S) for the analysis of high frequency signals, (d) 8 ch. (20-4000  $\mu$ S) and 2 ch. (1 mS) for the microwave interferometric measurement, (e) 2 ch. (1 mS) for the spectroscopic measurement, (f) 2 ch. (5  $\mu$ S) for the soft and hard X-ray measurement, (g) 2 ch. (1 mS) for the medium X-ray measurement, (h) 2 ch. (50  $\mu$ S) for the  $\alpha$ -particle measurement and also (i) 25 ch. (the sampling hold of the pulse of half-value width, 20 nS) for the laser scattering measurement. Experimental data are converted to digital signals from analog signals in the input controller part and stored in CPU-1 (OKITAC-4500 C with memories of 12 kW), CPU-2 (12 kW) and CPU-3 (16 kW) and then sent into Magnetic Tape and Disk Memory. The data stored in the Disk Memory are analysed in the CPU-0 (OKITAC-4500C with memories of 28 kW) and indicated on the Graphic Display through the CPU-3 and on the synchroscope through the analog output port. The choice of data to be acquired, analysed and indicated are made by each corresponding

switch on the operational panel. The scales of graph on the Graphic Display are chosen automatically or manually by the digital switches of the graphic panell. The signal of the monitor and the toroidal current are acquired on the time of the preparatory pulse earlier in three second than the main pulse and experimental data start to be collected on the time of the master pulse, the interval of which is 3-8 minutes. The external aspect of the system is shown in Fig. 23.

Also the preliminary experiment was done for the data processing of the electromagnetic probe signals. Especially the following method appears to be much suitable for the measurement of the plasma energy by the electromagnetic probe without the use of the gated integral circuit and the smoothing method. The systematic noise is stored in the memories at the blank shot operation and the random noise of signal is removed by the filter with the characteristic frequency that is about 0.5-1 kHz corresponding to the rise up time of the plasma current. The electromagnetic probe signals are directly acquired in the original form that is the differential wave form and are integrated by the numerical processing, so that the divergent error at the differential operation is removed away and the quantumised error becomes much small and the calculation time is also short. The data processing system will be completed in the next reporting period.

(T. Shoji, T. Kawakami, A. Funahashi and T. Takeda)

## References

- 1) T. Matoba, A. Funahashi and K. Ando, JAERI-M 5515, (1974)
- 2) N.R. Daly, Rev. Sci. Instr. 31 (1960) 264.
- 3) L.A. Artsimovich, et al., JETP Letters 11 (1970) 304.
- 4) L.L. Gorelik, Soviet Phys. - Tech. Phys., 9, 386 (1964)
- 5) L.L. Gorelik and V.V. Sinitsyn, Soviet Phys. - Tech. Phys., 9 393 (1964)
- 6) S. Kawasaki and K. Inoue : Nucl. Fusion 12 387 (1972),  
S. Kawasaki, K. Inoue and T. Takeda : JAERI-M 4531 (July 1971).
- 7) S. Kawasaki, K. Inoue and T. Takeda : JAERI-M 5146 (Feb. 1973).



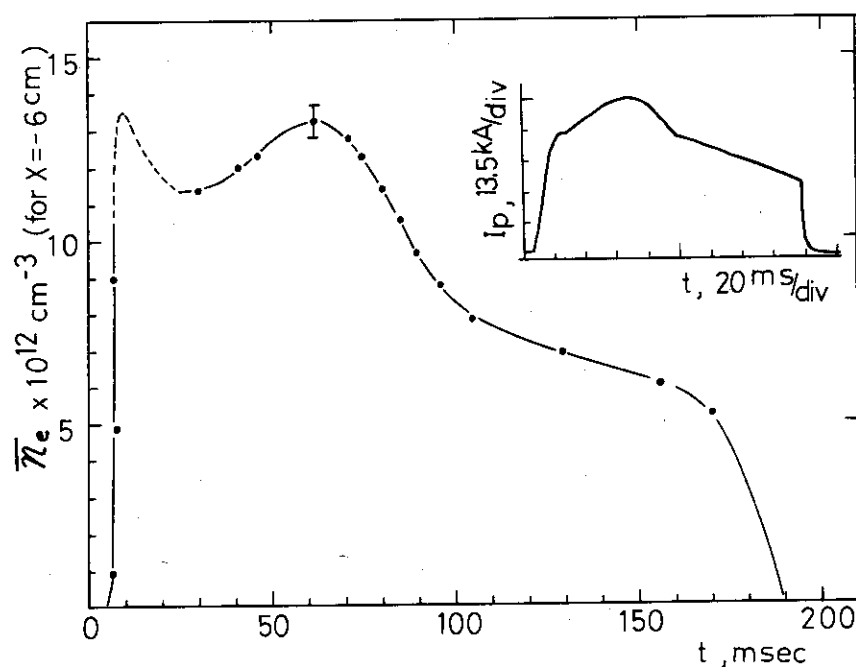


Fig. 1 Time-variation of electron density  $\bar{n}_e$  in JFT-2, measured averaged along the wave-path by 6 cm inside from the liner center.

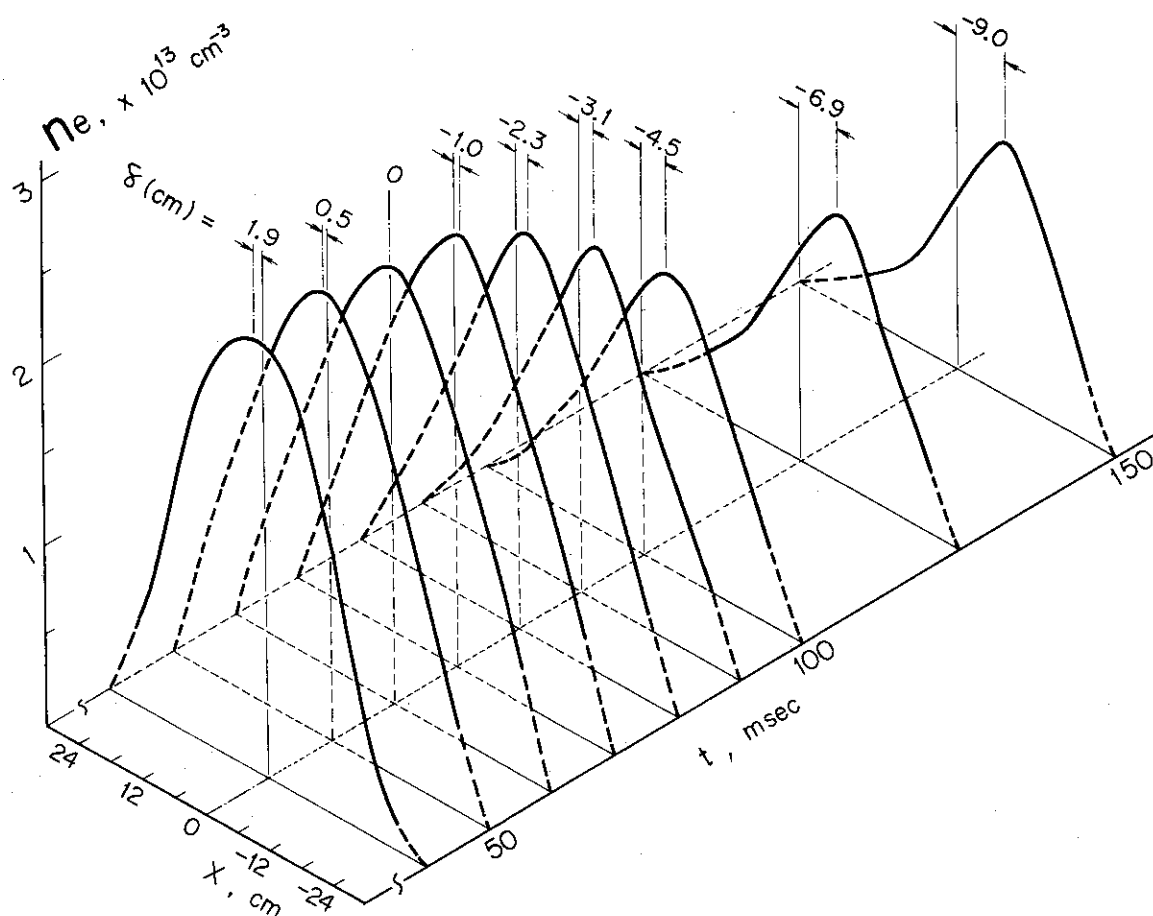


Fig. 3 Time-variation of density profiles in JFT-2.

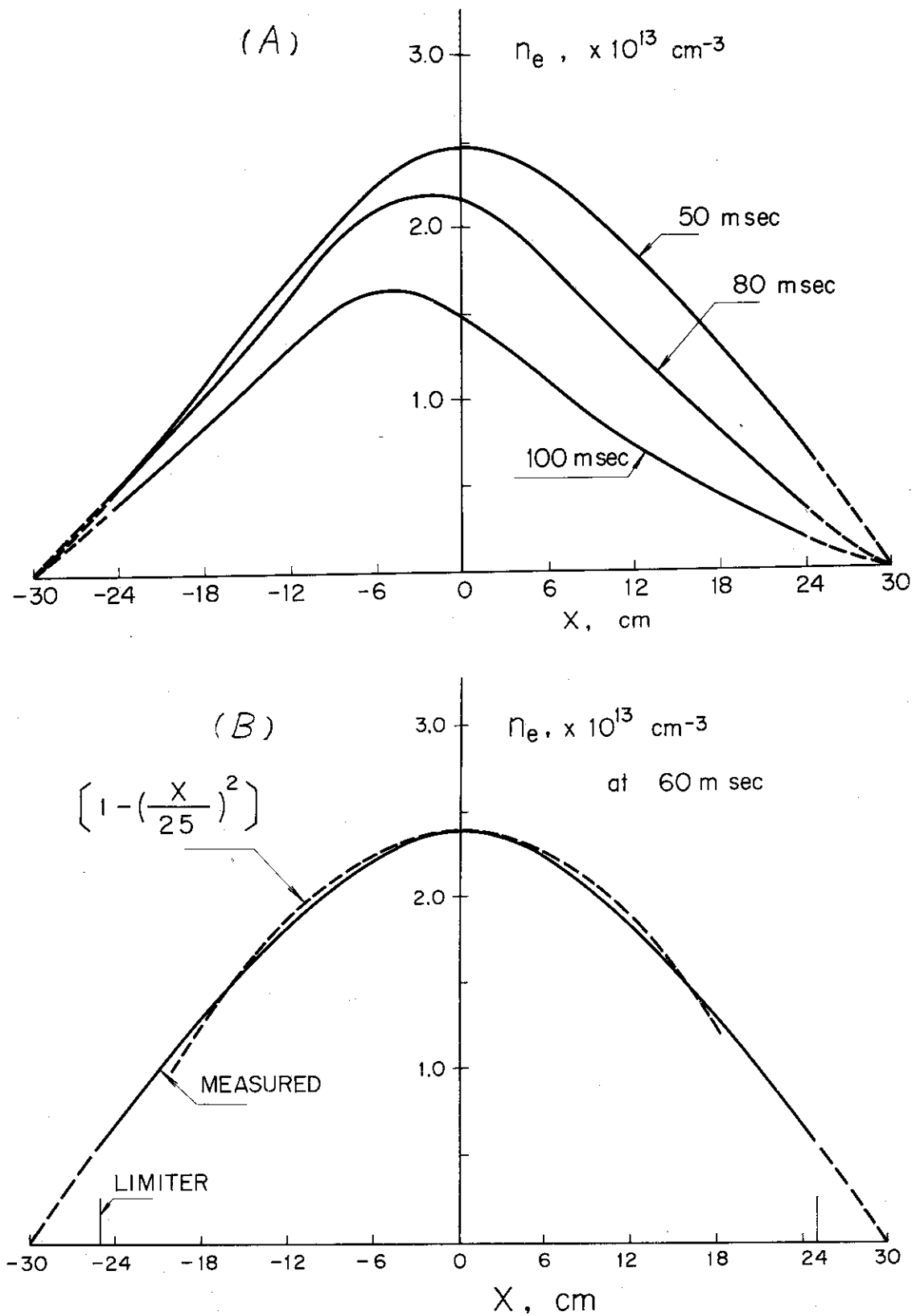


Fig. 2 Density profiles at different times. Solid curves are experimental distributions. A dotted curve shows a parabolic distribution  $n_e(r) = n_e(0) \cdot (1 - (X/25)^2)$ .

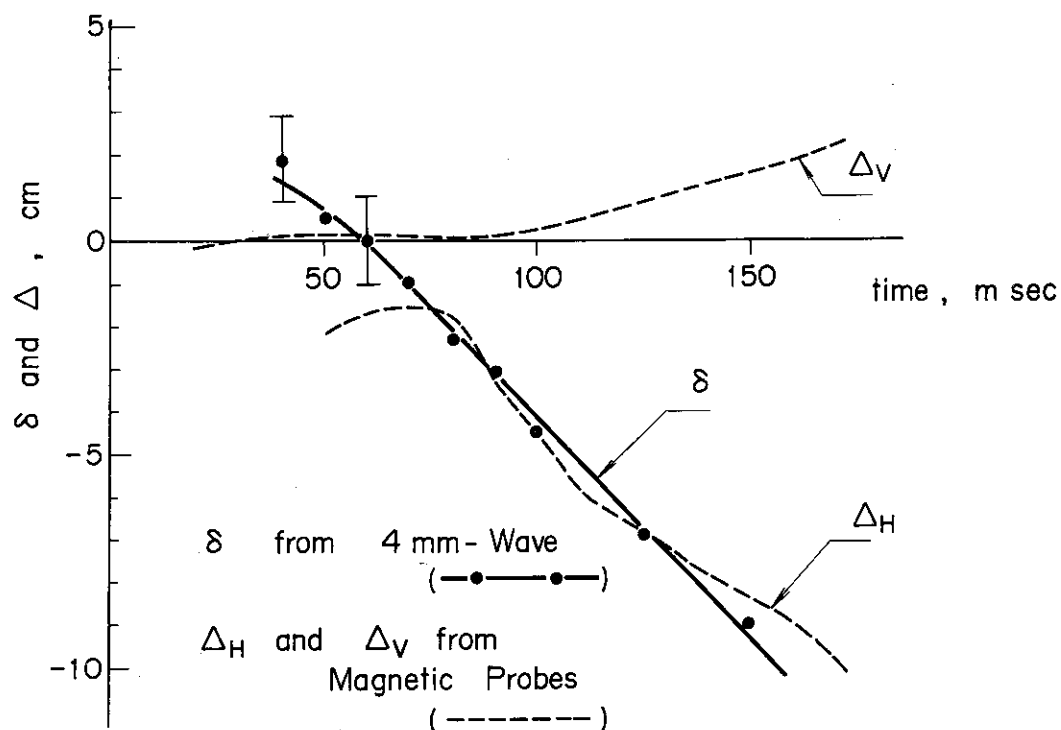


Fig. 4 Comparisons between the horizontal displacements of maximum density point  $\delta$  and plasma current column  $\Delta H$ .

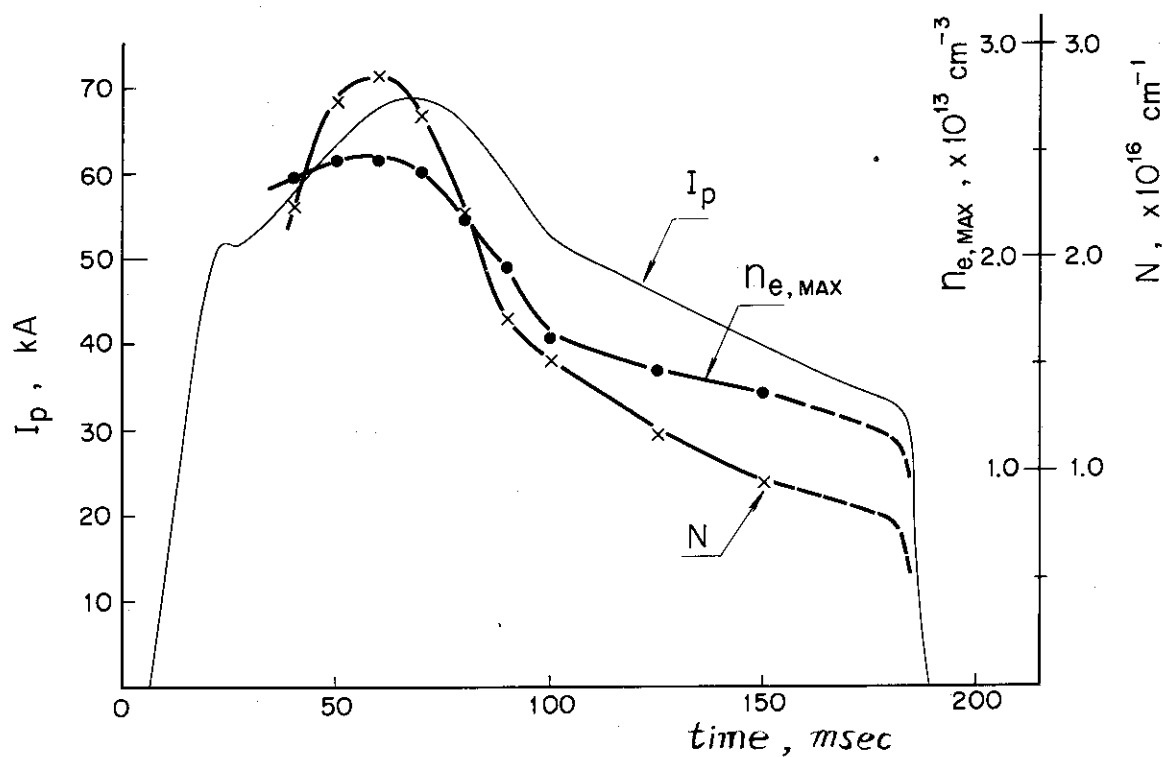


Fig. 5 Comparisons of plasma current  $I_p$ , peak density  $n_{e,MAX}$  and total density  $N$ .

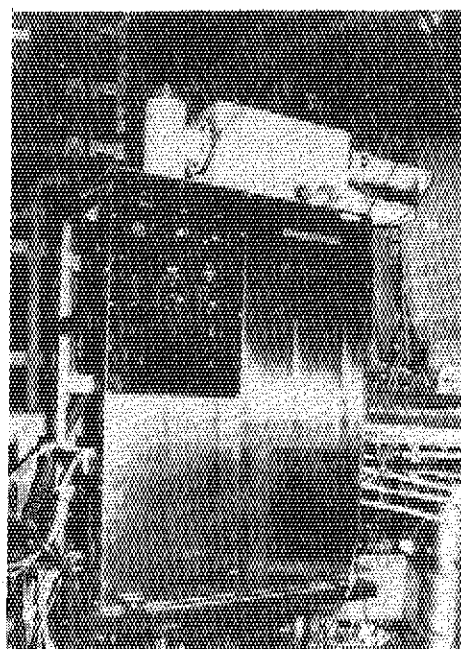


Fig. 6 Side view of a 50 cm VUV monochromator connecting with JFT-2 apparatus.

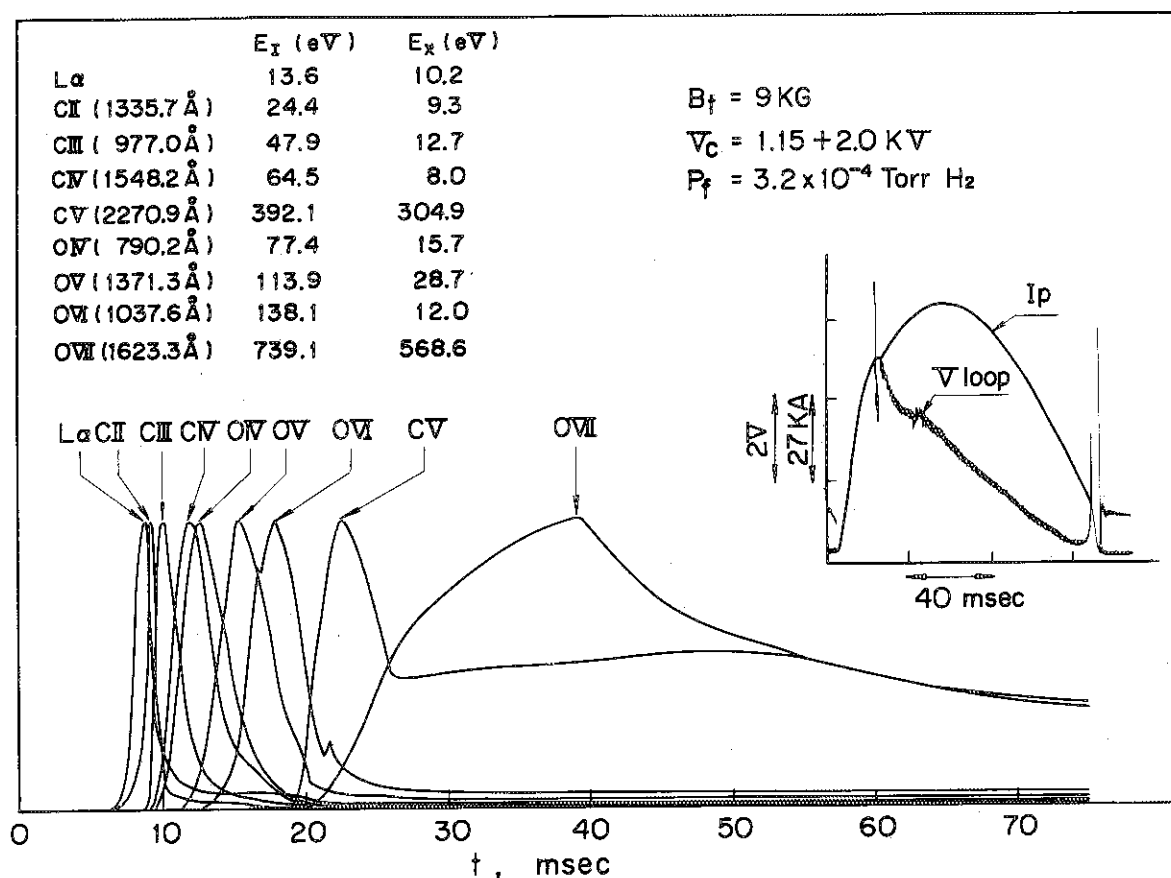


Fig. 7 Time-histories of  $L\alpha$  and impurity spectral lines radiated from the JFT-2 plasma.  $E_I$ : ionization potential,  $E_X$ : excitation potential. Traces of the plasma current  $I_p$  and the plasma loop voltage  $V_{loop}$  are also shown.

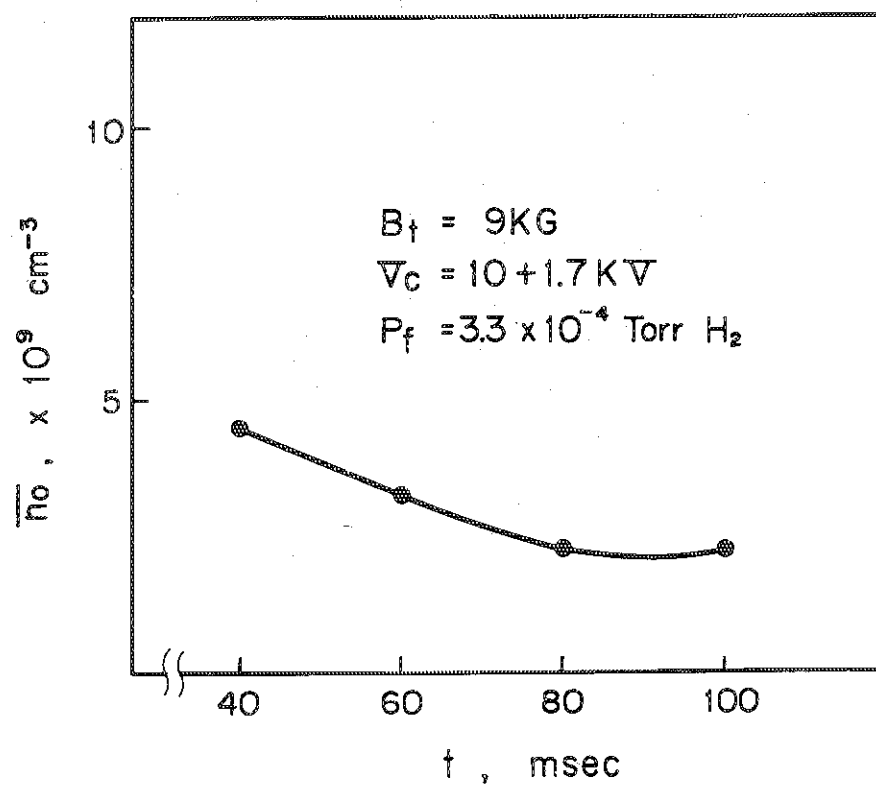


Fig. 8 Concentrations of the neutral hydrogen atoms averaged over the light path along the plasma center.

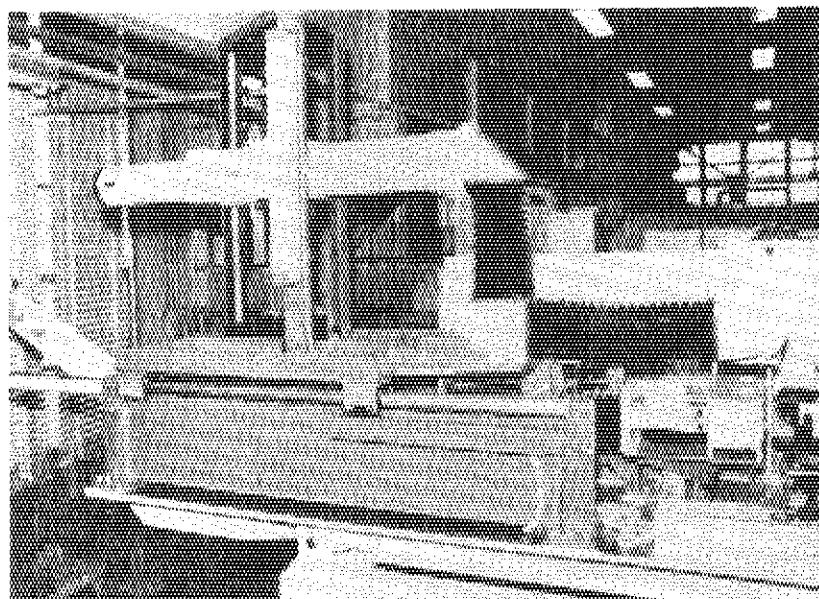
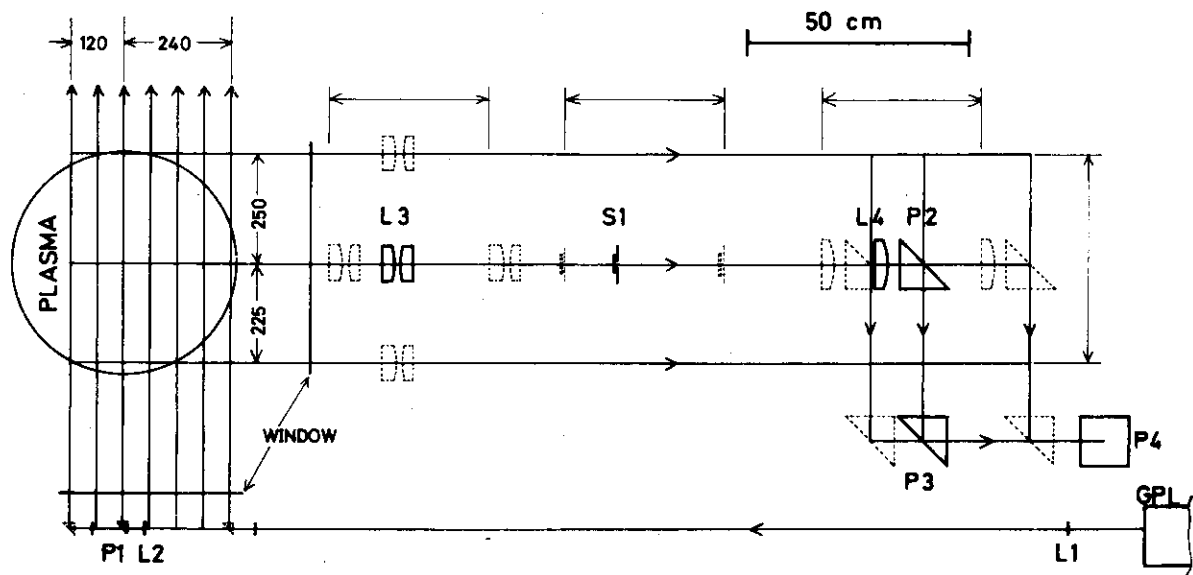
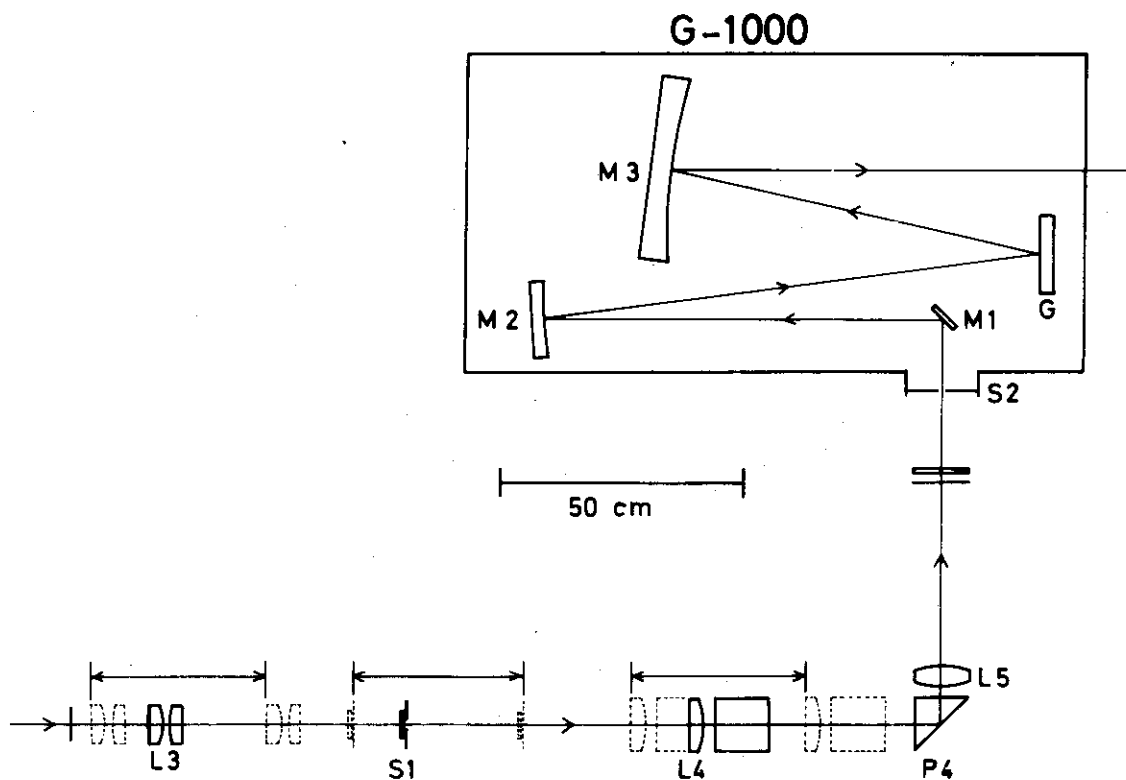


Fig. 9 General view of Thomson scattering apparatus



a)



b)

Fig. 10 The optical arrangement.

a) Side view. b) Plan view.

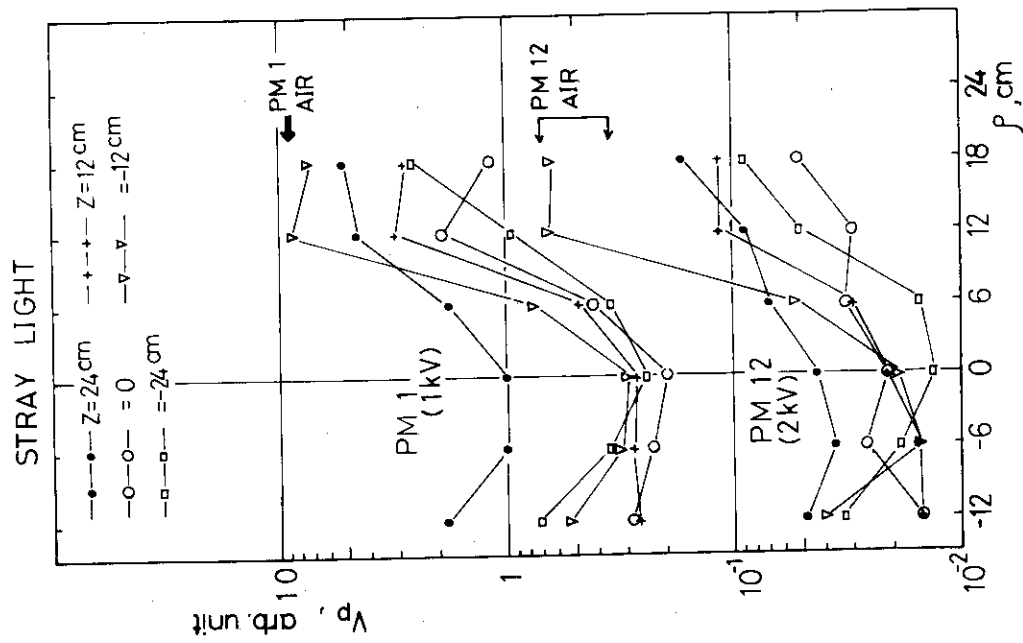


Fig. 12 Horizontal variation of stray light.

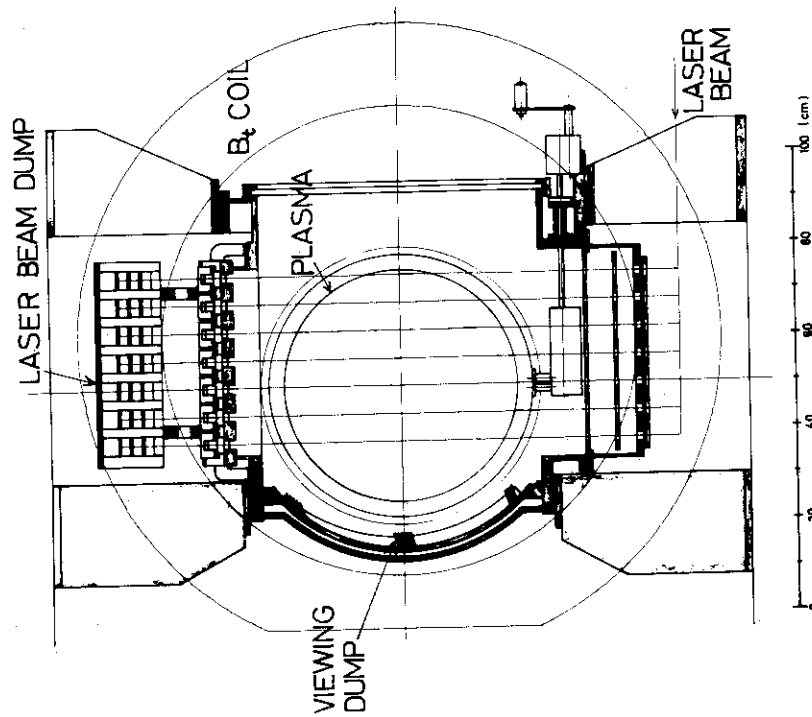


Fig. 11 The observation port.

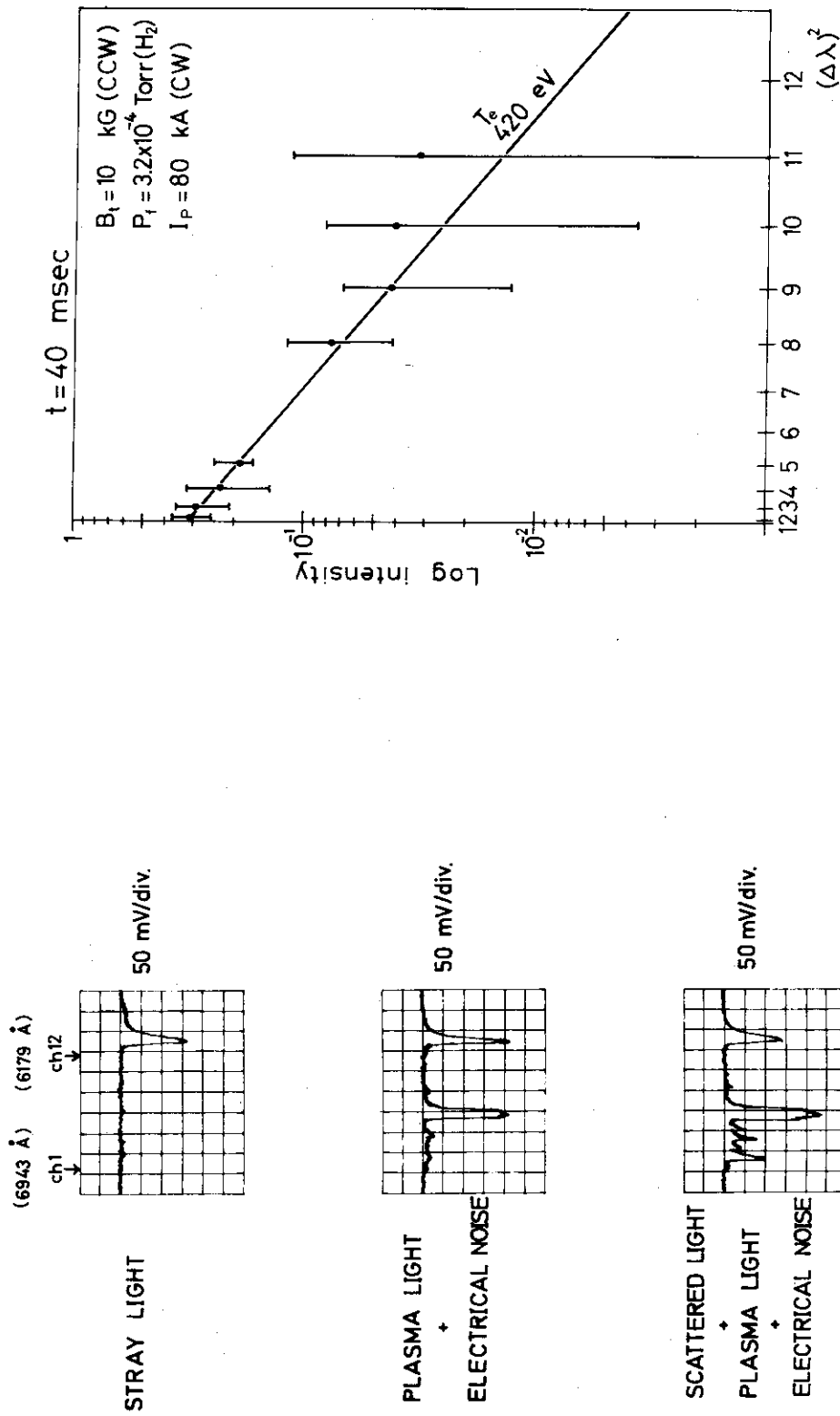


Fig. 13 Typical signals of sequenced output pulse.

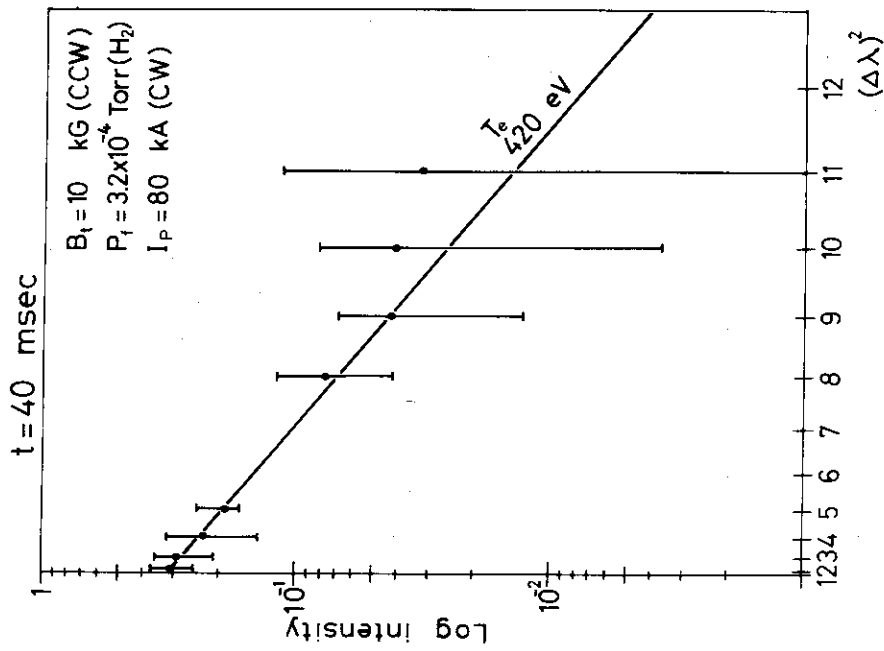


Fig. 14 Logarithm of the scattered intensity as a function of the square of the wave length shift.



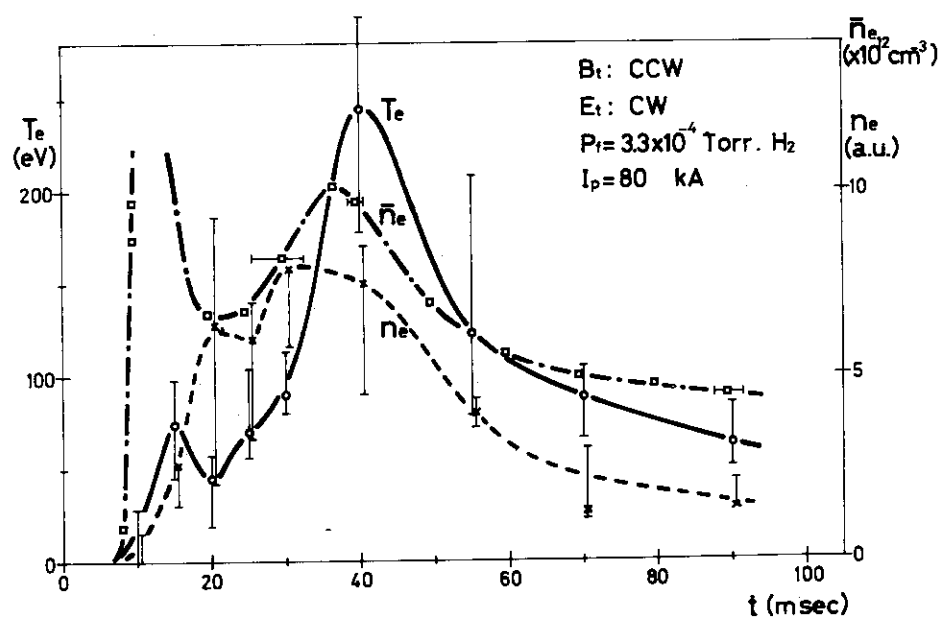


Fig. 15 Electron temperature and density as a function of time on axis.

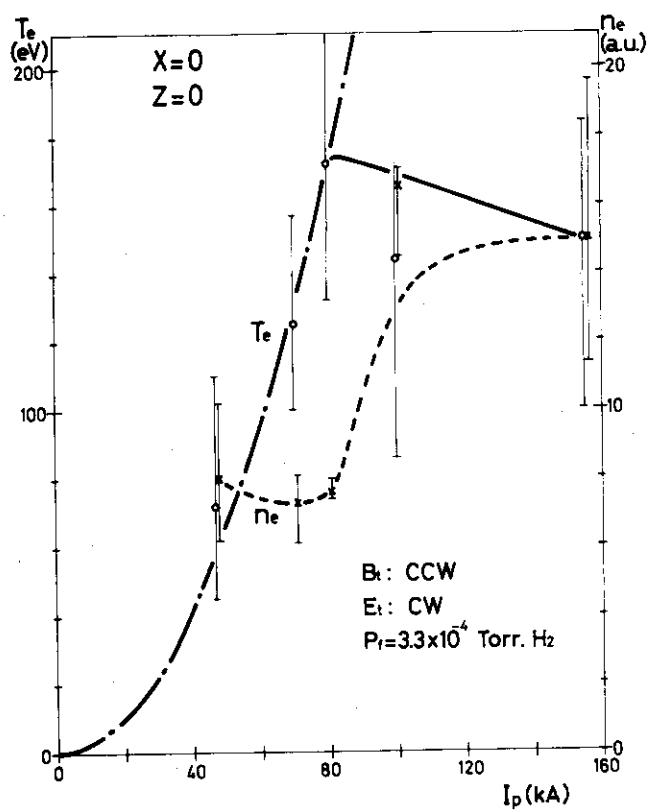


Fig. 16 Electron density and maximum temperature as a function of the peak plasma current.

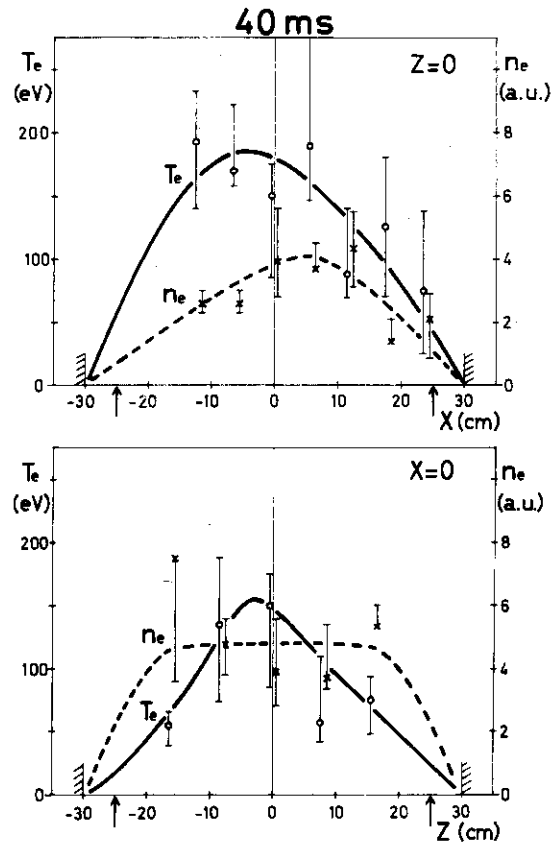


Fig. 17 The temperature and density profiles in the horizontal and vertical planes.

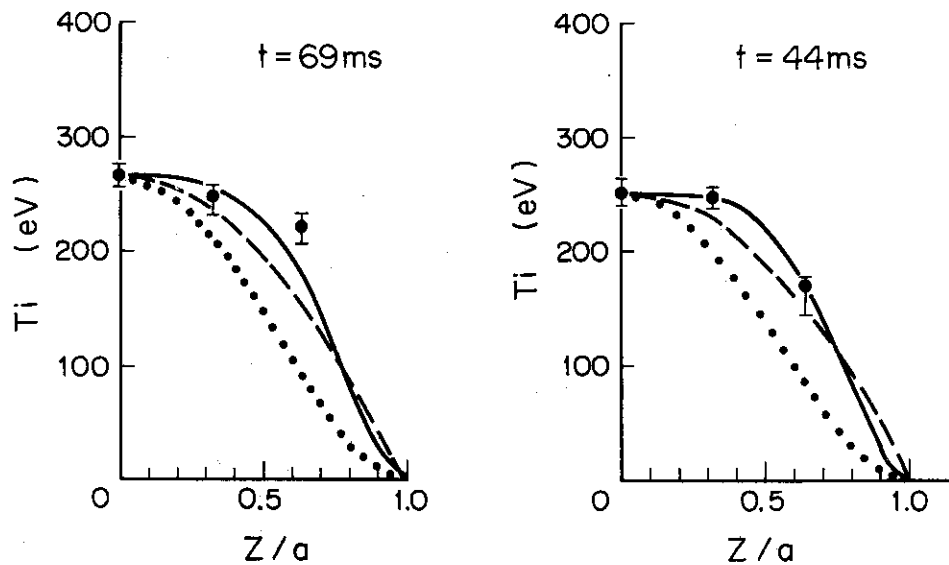


Fig. 18 Radial profiles of the ion temperature  $T_i$ .

— ;  $T_i \propto [1 - (\frac{Z}{a})^4]^2$  ,

--- ;  $T_i \propto [1 - (\frac{Z}{a})^2]$  ,

.... ;  $T_i \propto [1 - (\frac{Z}{a})^2]^2$  .

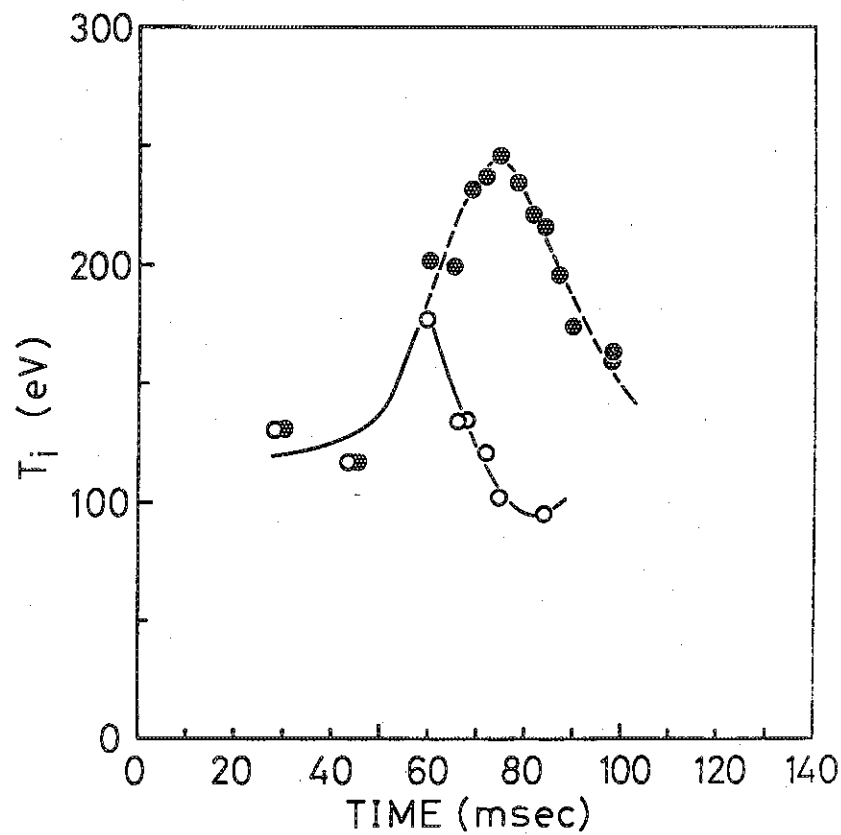


Fig. 19 Time-variation of the ion temperature under the dynamic limiter experiment.

●, closed-mode operation.

○, dynamic-mode operation.

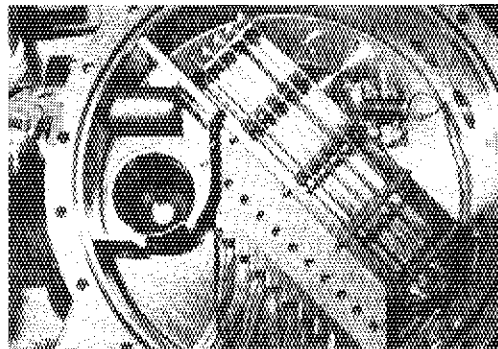


Fig. 20 Photograph of the ten-channel electrostatic analyzer.

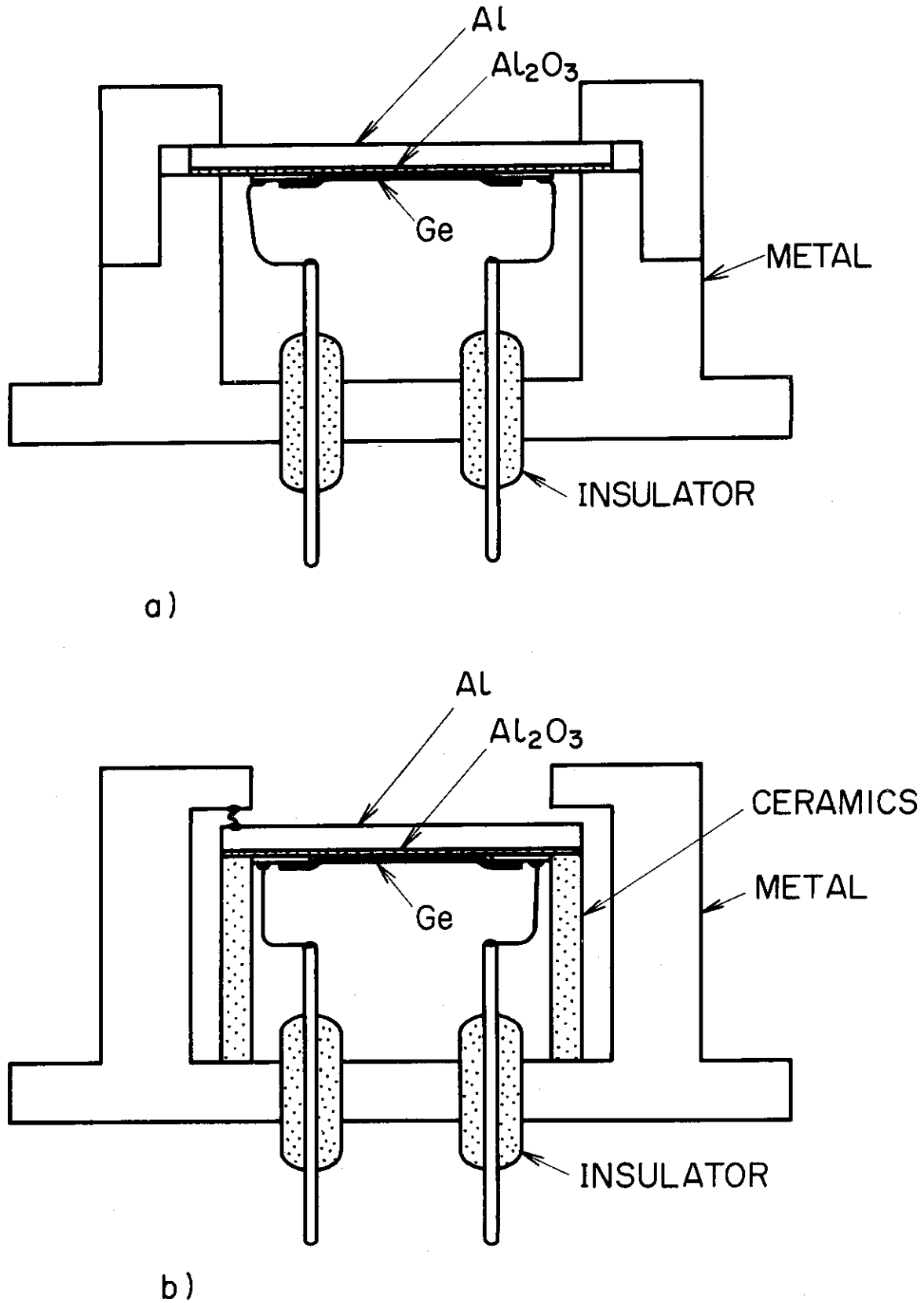


Fig. 21 Schematic cross sections of three thin layer thermistor bolometer.  
 a) The differential type. b) The integral type.

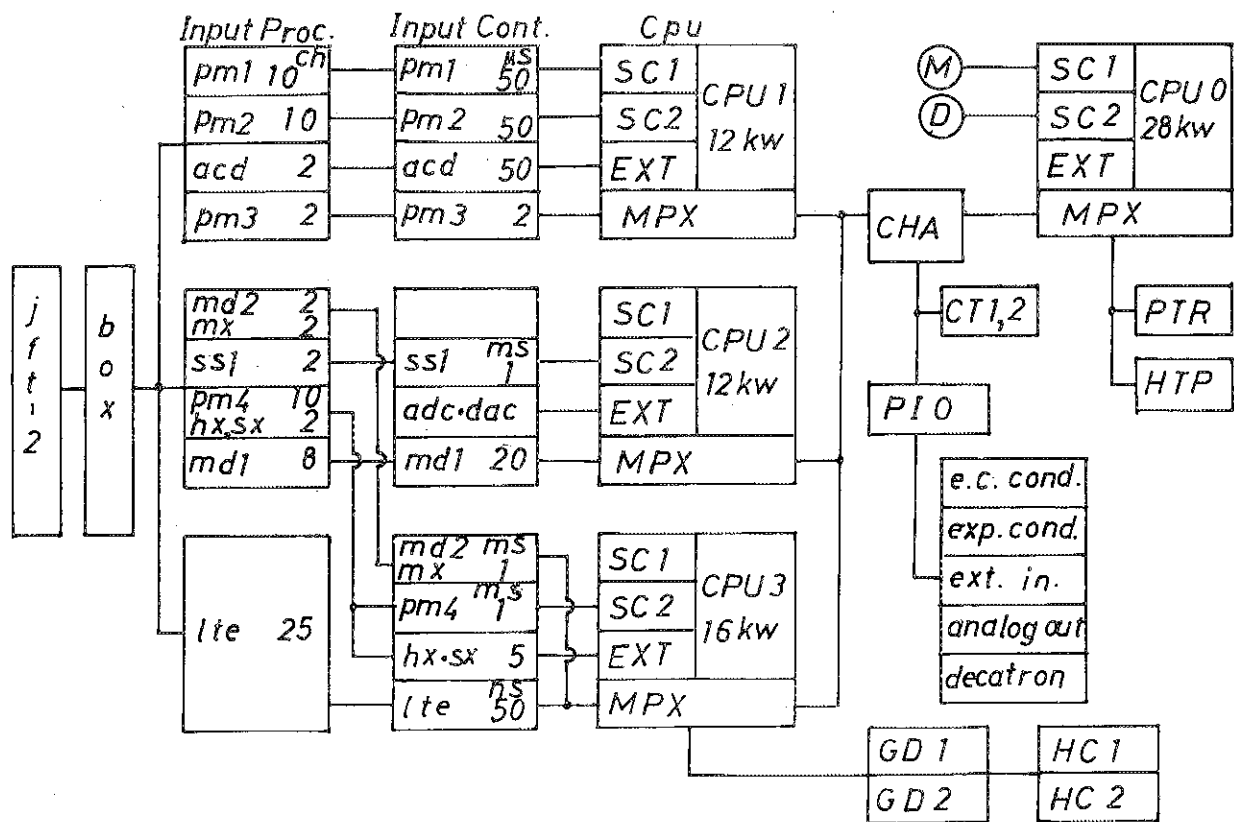
JFT 2 DATA PROCESSING SYSTEM

Fig. 22 Simplified block diagram of the data processing system.



Fig. 23 External aspect of the data processing system.

## 5. Operation and Technical Development

T. Arai, S. Kunieda, T. Ohga, T. Shiina,  
T. Tani, N. Toyoshima, K. Yokokura.

### 5.1 Introduction

The Group for Operation and Technical Development was formed in May 1973. The Group is responsible for the operation and maintenance of nuclear fusion devices and other associated equipments and the technical developments required in conducting research in the Thermonuclear Fusion Laboratory.

The major undertaking in the period 1973-1974 was to remodel the JFT-2 device to increase the toroidal magnetic field from the present 10 kG to 18 kG.

(S. Kunieda)

### 5.2 JFT-2

#### 1) Remodeling of JFT-2

In order to raise the toroidal magnetic field from 10 kG to 18 kG the following works were carried out by Hitachi, Ltd. and Division of Construction, JAERI. The Group took the responsibility of coordination and management to ensure proper execution of various works. Hitachi, Ltd. conducted under a contract the manufacture and installation of two new motor-generator sets, major modification of the existing motor-generator set, reinforcement of the toroidal field coil structures, and manufacture and installation of new d.c. vertical and horizontal field coils and a new vacuum chamber liner. The Division of Construction constructed a housing for the new motor-generator sets with Kajima Corporation as contractor.

Other works done in the present period in relation to JFT-2 include the installation of radiation shields to protect crew and researchers from X-ray radiation and of a one-turn coil to guard the d.c. vertical field coils from high spike-like voltages produced in the plasma.

## 2) Operation and Maintenance

In the present period more than 30,000 discharges were fired in the JFT-2 device. Figure 1 shows the number of shots in the period April 1972 - March 1974 and major technical events during the period.

### 5.3 JFT-2a (DIVA)

Construction of the device at Hitachi, Ltd. and development of other associated equipments were mainly handled by the JFT-2a Experimental Group and the Diagnostic Group. The Group for Operation and Technical Development worked in cooperation with those Groups to coordinate various tasks on both JFT-2 and JFT-2a being carried out at the same time and in the same experimental building.

The operation and maintenance and other developmental works on JFT-2a which is expected to come into operation in August 1974 will be managed by the Group.

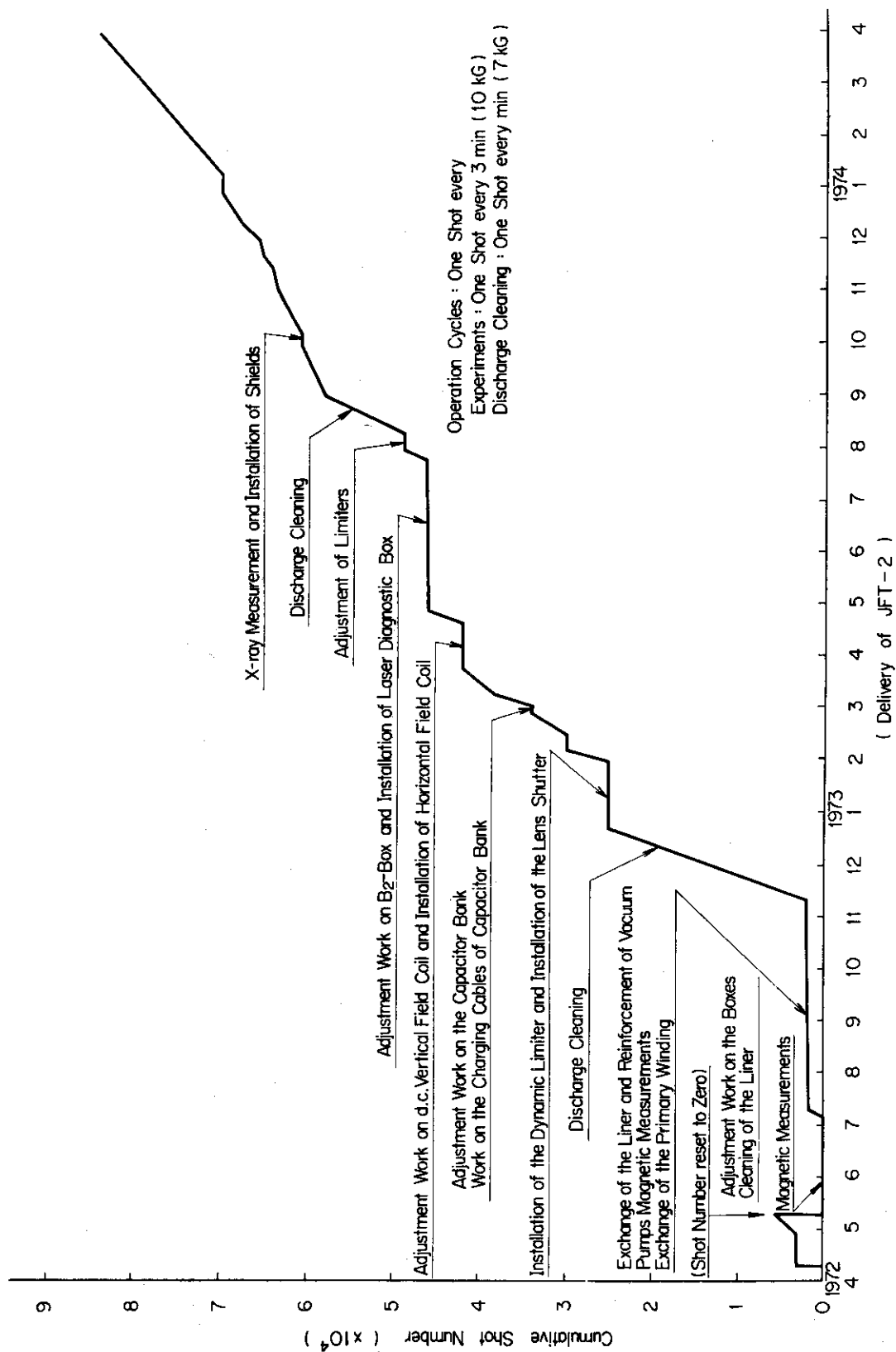


Fig. 1 Operation Log of JFT-2 Device



## II. DESIGN STUDY OF JT-60

N. Asami\*, A. Kameari\*, T. Kobayashi\*\*, M. Ohta,  
Y. Suzuki S. Tamura, H. Yamato\*\*\*, M. Yoshikawa

Considerable efforts were made in the preceeding years on the design of a large Tokamak device capable of producing plasmas with parameters close to the reactor plasma's. This year, in keeping response to the deliberations in Nuclear Fusion Research and Development Committee in AEC, a special study group was formed within Thermonuclear Fusion Laboratory to examine and redefine the scope of the experimental program. The Design Study Group, formally organized for the purpose, then undertook the job of further developing the basic concept and initiated plasma-physical studies of plasma confinement, heating, contamination, and other associated problems at or near the reactor plasma temperatures and densities. A reference design, the parameters of which are determined by an optimization study, was completed and put under more detailed physical as well as engineering investigation.

The present design study was carried out in many ways in cooperation with a number of people. Discussions with guest scientists and members of Committee on Nuclear Fusion Research of JAERI were greatly helpful. Works made in other Groups of Thermonuclear Fusion Laboratory were instrumental in conducting the study. In particular, industry made a valuable contribution to the study by providing technological assessments on required engineering and construction time-table and cost.

(M. Yoshikawa)

---

\* On leave from Engineering and Development Division, Mitsubishi Atomic Power Industries Inc.

\*\* On leave from Atomic Energy Research Laboratory, Hitachi, Ltd.

\*\*\* On leave from Research and Development Center, Tokyo Shibaura Electric Co. Ltd.

## III. Theory

M. Azumi, M. Tanaka, T. Tazima,  
T. Tuda, M. Wakatani

## 1. Introduction

We have continued theoretical studies concerning the tokamak confinement and heating in corporation with experimental groups. In the period under review the emphasis was placed on the hydromagnetic stability of a pinch, on the behaviour of impurity ions in a tokamak plasma as well as their influences on the plasma confinement, and finally on the heating of a tokamak plasma by, in particular, the neutral beam injection. They are described briefly in the following. Also we had made a survey on the theoretical problems crucial to the projected JT-60 tokamak device.

(M. Tanaka)

## 2. MHD Stability and Equilibrium

1) MHD stability of belt-pinch-type plasmas<sup>\*)</sup>

The stability of kink-like modes in a toroidal plasmas with hollow cylindrical geometry has been studied by means of their growth rate. The configurations simulate the tokamak with noncircular cross-section elongated vertically or the belt-pinch-type configuration. It is possible to increase the current in the toroidal plasmas of noncircular cross-section with large axial length. The stability properties, however, are similar to those in the cylindrical plasma column.

(M. Wakatani)

2) Nonlinear effect on the  $m = 1$  internal kink mode

The MHD stability theory shows that  $m = 1$  internal kink mode becomes unstable for  $q(0) < 1$  but  $q(a) > 1$  in tokamak plasmas. It is preferable to concentrate current density in the center of plasma column, as  $m \geq 2$  kink

---

<sup>\*)</sup> JAERI-M 5583 (1974)

modes become stable. However excessive concentration of current density makes the  $m = 1$  internal kink mode unstable.<sup>1)</sup>

We have studied the nonlinear effect on this mode by the use of perturbation theory, especially, the correction of its growth rate due to the mode coupling.

We expand the displacement  $\vec{\xi}$  as

$$\vec{\xi} = \vec{\xi}_1^{(0)} \exp[i(kz + \theta)] + \epsilon \{ \vec{\xi}_2^{(1)} \exp i(kz + 2\theta) + \vec{\xi}_0^{(1)} \exp ikz \} \quad (1)$$

$$+ \epsilon^2 \vec{\xi}_1^{(2)} \exp i(kz + \theta) + \dots,$$

where  $\epsilon$  is the small expansion parameter and  $\epsilon \approx ka < 1$  is assumed. Then the equation of motion in the cylindrical geometry is expanded as

$$(L^{(0)} + \epsilon L^{(1)}(\xi) + \epsilon^2 L^{(2)}(\xi^2)) \vec{\xi} = \rho (\omega_0 + \epsilon^2 \omega_1 + \dots)^2 \vec{\xi}, \quad (2)$$

where

$$L^{(0)} \xi_r = 0 \quad (3)$$

denotes the well-known Euler-Lagrange equation in the linear pinch.<sup>2)</sup>

For example, in the  $m = 1$  mode,  $L^{(1)}(\xi) \vec{\xi}$  means the  $m = 0$  mode or  $m = 2$  mode due to the growth of  $m = 1$  mode and  $L^{(2)}(\xi^2) \vec{\xi}$  means the mode coupling between  $m = 1$  mode and  $m = 2$  or between  $m = 1$  mode and  $m = 0$  mode. In (1), we have assumed that  $r$  component of  $\vec{\xi}_1^{(0)}$  is the solution of eq. (3), in order to satisfy the boundary condition  $\xi_r(a) = 0$ . In the order of  $\epsilon$ , we obtain the differential equations

$$\begin{cases} L^{(0)} \vec{\xi}_0^{(1)} = L^{(1)}(\xi_1^{(0)}) \vec{\xi}_1^{(0)}, \\ L^{(0)} \vec{\xi}_2^{(1)} = L^{(1)}(\xi_1^{(0)}) \vec{\xi}_1^{(0)}. \end{cases} \quad (4)$$

In the second order of  $\epsilon^2$ ,

$$(L^{(0)} - \rho \omega_0^2) \vec{\xi}_1^{(2)} = -L^{(1)}(\xi_1^{(0)}) \vec{\xi}_2^{(1)} - L^{(1)}(\xi_1^{(0)}) \vec{\xi}_0^{(1)} - L^{(2)}(\xi_1^{(0)2}) \vec{\xi}_1^{(0)} \\ + 2 \rho \omega_0 \omega_1 \vec{\xi}_1^{(0)} \quad (5)$$

is obtained. Multiplying  $\vec{\xi}_1^{(0)}$  and integrating eq. (5) in the plasma region, we find the correction of growth rate due to mode coupling,

$$\omega_1 = \frac{\int \{ (L^{(0)}(\xi_1^{(0)}) \vec{\xi}_2^{(1)} + L^{(1)}(\xi_1^{(0)}) \vec{\xi}_0^{(1)} + L^{(2)}(\xi_1^{(0)2}) \vec{\xi}_1^{(0)} ) \} \cdot \vec{\xi}_1^{(0)} d\vec{r}}{2\rho\omega_0 \int |\vec{\xi}_1^{(0)}|^2 d\vec{r}} \quad (6)$$

For the tokamak plasma of uniform current,  $\vec{\xi}_1^{(0)}$  can be written by the Bessel functions. We evaluate the magnitude of  $\omega_1$  by this  $\vec{\xi}_1^{(0)}$  using numerical integration.

(M. Wakatani)

### 3) Feedback stabilization of the high m kink mode<sup>\*</sup>)

In the cylindrical tokamak plasma of uniform current, the dispersion relation for high m kink modes is derived in the presence of a feedback magnetic field. The condition for stabilization of high m kink mode and the magnitude of feedback current in the helical windings are studied. Two methods of feedback stabilization are examined in detail. In the one the feedback current is driven proportional to the perturbed poloidal magnetic field, and in the other the feedback current is driven as a step function after the kink mode has grown up to some extent. Both methods may be available in tokamak experiments.

(M. Wakatani and M. Azumi)

### 4) Kink instability of a pinch in a slotted casing

We have examined the kink instability of a cylindrical pinch with uniform currents in a metallic casing having periodic gaps along the azimuthal direction. The casing is assumed to be infinitely thin and perfectly conducting.

The perturbed currents flowing on the casing are expanded into the Fourier series.

$$\vec{J} = (0, J_\theta, J_z),$$

$$J_{\theta,z} = \sum_m j_m^{(\theta,z)} e^{\omega t + im\theta + ikz},$$

which is nonvanishing only on the casing.

---

<sup>\*</sup>) JAERI-M 5703 (1974)

$$\frac{2\pi(n-1)}{N} - \theta_0 < \theta < \frac{2\pi(n-1)}{N} + \theta_0, \quad n = 1, 2, \dots, N.$$

The boundary conditions on the casing ( $r=r_s$ ) are obvious. The continuity of  $B_r$ , the jump conditions of  $B$ ,  $B_z$  yield relations between  $a_m$ ,  $b_m$ ,  $c_m$  and  $j_m = j_m^{(\theta)} = -\frac{m}{kr_s} j_m^{(z)}$ , where  $a_m$ ,  $b_m$ ,  $c_m$  are the Fourier coefficients of the vacuum magnetic fields. Further we should impose the following conditions, i.e.  $B_r = 0$  on the casing and  $J = 0$  at the gap. These yield the dual series equations in  $\theta$  (we can assume that  $k$  is constant. We make use of the boundary conditions at the plasma surface ( $r=a$ ) to obtain the dispersion relation, which leads in general the mode coupling between different  $m$  modes. The lowest approximation gives the following expression for the normalized growth rate of the  $m$ -th mode.

$$\Gamma^2 = 2(m+bka) \left[ 1 - \frac{m+bka}{1 - \left(\frac{a}{r_s}\right)^{2m} F(\theta_0)} \right], \quad (1)$$

$$F(\theta_0) = \frac{1}{\pi} \left( N\theta_0 - \frac{\sin 2mN\theta_0}{2m} \right),$$

where we have assumed long wavelength perturbations  $kr_s \ll 1$ . The pinch becomes unstable when

$$m - 1 + \left(\frac{a}{r_s}\right)^{2m} F(\theta_0) < nq < m.$$

It should be noted that  $F(\theta_0)$  is a monotonously increasing function of  $\theta_0$ . Eq. (1) is derived assuming  $B_r \propto \sin m\theta$  and  $j_\theta \propto \cos m\theta$ , while, when  $B_r \propto \cos m\theta$  and  $j_\theta \propto \sin m\theta$ , eq. (1) should be replaced by  $F(\theta_0) = \frac{1}{\pi} \left( N\theta_0 + \frac{\sin 2mN\theta_0}{2m} \right)$ . This is due to the phase difference between the perturbation and the position of the gap. The case of a thin resistive casing is also examined numerically.

(M. Azumi and M. Tanaka)

##### 5) An analysis of bifurcated helical equilibria of a pinch

A helical plasma equilibrium of finite amplitude may be established in a tokamak discharge as a consequence of the development of a high  $m$  kink mode, which has been investigated in detail by Rutherford et al.<sup>3)</sup> We have examined the same problem by different method, i.e. by using complex functions.

Starting from a cylindrical equilibrium with uniform currents in a strong longitudinal magnetic field, we can construct a long wavelength helical equilibrium of finite but small amplitude as follows. First we consider the equilibrium inside the plasma. Using the variables  $\rho$  and  $\sigma = m\theta - kz$ , where  $(\rho, \theta, z)$  are usual cylindrical coordinates, we can obtain the stream function of the magnetic field inside the plasma which describe small helical perturbations of the pinch.

$$\psi = A \left[ \rho^{\frac{2}{m}} + \frac{m\alpha_1^2}{4} \rho^{2-\frac{2}{m}} + \alpha_1 \rho \cos \sigma + \alpha_2 \rho^2 \cos 2\sigma + \dots \right],$$

where  $A = (2kB_z - mj_0)/4$  and  $\alpha_n$  are proportional to  $\epsilon^n$  ( $\epsilon$  is the expansion parameter). The polar equation of the plasma surface is given by

$$\rho_s = 1 + \frac{m(m-2)\alpha_1^2}{16} - \frac{m\alpha_1}{2} \cos \sigma - \left[ \frac{m(2-3m)\alpha_1^2}{16} + \frac{m\alpha_2}{2} \right] \cos 2\sigma + \dots$$

which, in the cartesian coordinate system  $(x, y)$ , can be rewritten as

$$W \equiv X + iY = \rho_s e^{i\sigma}.$$

The strength of the poloidal magnetic field on the plasma surface is given by

$$B = B_x + iB_y \\ = -iA \left[ \frac{2}{m} (WW^*)^{\frac{1}{m}-1} W + \alpha_1 + 2\alpha_2 W^* + \frac{(m-1)\alpha_1^2}{2} (WW^*)^{-\frac{1}{m}} W + \dots \right],$$

where the asterisk denotes complex conjugates.

Now we construct the vacuum magnetic field around the helical plasma equilibrium obtained above. The vacuum stream function satisfies

$$\frac{1}{\rho} \frac{\partial}{\partial \rho} \rho \frac{\partial \psi^e}{\partial \rho} + \frac{1}{\rho^2} \frac{\partial^2 \psi^e}{\partial \sigma^2} = \frac{4A^e}{m^2} \rho^{\frac{2}{m}-2}$$

with  $A^e = kB_z/2$ . Writing the solution as

$$\psi^e = A^e \left[ \rho^{\frac{2}{m}} + \psi_1 \right],$$

we find easily that  $\psi_1$  is harmonic. The vacuum magnetic field can be written as

$$B = -iA^e \left[ \frac{2}{m} (WW^*)^{\frac{1}{m}-1} W + \left( \frac{\partial \psi_1}{\partial x} + i \frac{\partial \psi_1}{\partial y} \right) \right]$$

with  $w = x + iy$ .

We consider a mapping defined by

$$w = W(\xi), \quad \xi = \sigma + i\tau.$$

The vacuum-plasma interface is mapped on the real axis of the  $(\sigma, \tau)$  plane  $\tau = 0$ , on which  $\partial\psi^e/\partial\sigma$  should vanish. Namely we have

$$\left. \frac{\partial\psi_1}{\partial\sigma} \right|_{\tau=0} = -\frac{2}{m}(WW^*)^{\frac{1}{m}-1} \operatorname{Re}(WW_\sigma^*) \equiv F(\sigma), \quad (1)$$

where  $W_\sigma = dW/d\sigma$ . On the other hand, using the continuity of the poloidal magnetic field, we have

$$\begin{aligned} \left. \frac{\partial\psi_1}{\partial\tau} \right|_{\tau=0} &= \operatorname{Im} \left\{ \left[ \frac{2}{m} \left( \frac{A}{A^e} - 1 \right) (WW^*)^{\frac{1}{m}-1} W + \frac{A}{A^e} (\alpha_1 + 2\alpha_2 W^*) \right. \right. \\ &\quad \left. \left. + \frac{A}{A^e} \frac{(m-1)\alpha_1^2}{2} (WW^*)^{-\frac{1}{m}} W \right] W_\sigma^* \right\} \equiv G(\sigma), \end{aligned} \quad (2)$$

where the Cauchy-Riemann relations have been used. Eqs. (1) and (2) are the boundary conditions at the plasma boundary on the complex potential defined by

$$\chi = \phi + i\psi_1.$$

Namely we have

$$\left. \frac{d\chi}{d\xi} \right|_{\tau=0} = G(\sigma) + iF(\sigma),$$

which can be continued analytically into the complex plane corresponding to the vacuum region. Finally we have the solution,

$$\chi = \int^\xi d\xi' [G(\xi') + iF(\xi')],$$

the imaginary part of which gives  $\psi_1$ . Thus we have completed the solution of a helical plasma equilibrium neighbouring a cylindrical one.

We now take account of the presence of a metallic casing of radius  $b (>1)$ . In the  $(\sigma, \tau)$  plane the surface of the casing can be represented by

$$\tau = \tau_b(\sigma) = \tau_0 + \tau_1 + \tau_2 + \dots,$$

where  $\tau_n = O(e^n)$ . The stream function  $\psi_1$  should be constant on the casing, which yields in the lowest approximation the following relation.

$$\alpha_1 \left[ \frac{A}{A^e} \operatorname{ch} \tau_0 + \frac{2}{m} \left( \frac{A}{A^e} - 1 \right) \operatorname{sh} \tau_0 - \frac{A}{A^e} \operatorname{sh} \tau_0 \right] = 0 .$$

A nonvanishing helical equilibrium exists only when the term inside the square brackets vanishes, i.e.

$$q = m - 1 + b^{-2m} ,$$

where  $q$  is the safety factor. Namely the neighbouring helical equilibrium becomes to exist just at the marginal stability of the pinch. The next approximation yields the relation between  $\alpha_1$  and  $\alpha_2$ , which can be written near the marginal stability as

$$\alpha_2 \approx \frac{m \alpha_1^2}{2(b^2 - 1)^2} .$$

(M. Tanaka, T. Tuda and M. Azumi)

#### 6) A computer code for the charged particle motion in toroidal magnetic fields

The containment of high temperature plasma may be realized by the use of suitably constructed toroidal magnetic fields. It is necessary to know orbits of charged particles in magnetic fields for understanding physics of rare collisional plasma in the toroidal system. To obtain charged particle orbits for any equilibrium configuration, we resort to numerical methods.

In slowly varying magnetic fields, a charged particle performs approximately helical motion about the field lines. In many applications, a knowledge of the precise particle orbit is not required. For example, when studying particle trapping in a magnetic mirror, we are interested in where points of reflection occur and how long the particle is trapped. The guiding center equations are applicable, when the local field seen by the particle changes slightly over a Larmor orbit. In this program, non-relativistic guiding center equations in time-independent magnetic fields



$$\frac{d\vec{r}}{dt} = v_{\parallel} \frac{\vec{B}}{B} + \frac{\vec{E} \times \vec{B}}{B^2} + \frac{1}{\Omega_j B} \left( \frac{\mu B}{m_j} + v_{\parallel}^2 \right) \frac{\vec{B}}{B} \times \vec{\nabla} B ,$$

$$\frac{dv_{\parallel}}{dt} = - \frac{1}{m_j} \frac{\vec{B}}{B} \cdot \vec{\nabla} (\mu B) + \frac{v_{\parallel}}{B} \frac{\vec{E} \times \vec{B}}{B^2} \cdot \vec{\nabla} B + \frac{1}{m_j} \frac{\vec{B}}{B} \cdot \vec{E} ,$$

$$\frac{d\mu}{dt} = 0$$

are used, where  $v_{\perp}^2 = 2\mu B/m_j$  and  $j = e$  or  $i$ . The predictor corrector method has applied to solve these equations in a cylindrical coordinates  $(x, \phi, z)$ , where  $\phi$  means the coordinate along the toroidal direction. Four equations are used, three describing the position of the guiding center and one the parallel velocity. The magnetic fields and its gradients are given by the subroutine in the program. We adopted the equilibrium with small aspect ratio for the test run shown in Fig. 1,<sup>4)</sup> where  $R/a = 3$ ,  $q(0) = 2$ . In this magnetic configuration, trapped particle orbits are shown in Fig. 2. A toroidal electric field driving toroidal current induces inward diffusion of banana trajectory,<sup>5)</sup> which is seen in Fig. 3. When the toroidal magnetic field has a small ripple, the particle orbit does not make a complete banana trajectory.<sup>6)</sup> This is shown in Fig. 4 where the magnitude of ripple field is 0.5 %.

In this program, we can solve the ion motion by the use of equation of motion with the Lorentz force on the particle,

$$m_i \frac{d\vec{v}}{dt} = e (\vec{E} + \vec{v} \times \vec{B}) .$$

Here the electromagnetic fields are also given by the subroutine. The particle motion in the magnetic field shown in Fig. 1 can be seen in Fig. 5.

This program will be developed to include the pitch angle scattering and to simulate the rare collisional plasmas.

(M. Wakatani)

### 3. Impurity Ions in a Tokamak Plasma

#### 1) The Pfirsch-Schluter diffusion in a multicomponent plasma<sup>\*)</sup>

The collisional cross-field particle transport in a toroidal plasma with multiple ion species is studied on the basis of a fluid model. The impurity flux across the magnetic field mainly determined by friction with protons tends to concentrate the impurity ions toward the center of the plasma. In the stationary state the conductivity of the plasma may be reduced to lead the inhibition of the current at the center, which may make the plasma kink unstable.

(T. Tuda and M. Tanaka)

#### 2) Impurity drift instability by trapped ions

Drift instability caused by the presence of impurity ions was found by Coppi et al.<sup>7)</sup> On the basis of the collisionless Vlasov equation they investigated the electrostatic perturbation of a inhomogeneous multi-species plasma in a uniform magnetic field, and found unstable modes excited by the ion Landau damping.

We have examined the low frequency electrostatic perturbations in a banana regime tokamak plasma by taking account of the effect of the collision of trapped ion. The unstable mode that we found is similar to the trapped electron mode by Kadomtsev and Pogutse<sup>8)</sup> but the growth rate is greater by a factor of the order of  $(m_i/m_e)^{\frac{1}{2}}$  than that of latter.

(T. Tuda and M. Tanaka)

#### 3) Impurity problems in tokamak devices

Plasma contamination by impurities, one of the serious problems in tokamak devices, is discussed from the following three points of view.

##### (i) Diffusion of impurity ions in a tokamak plasma

A numerical study is made on the density distributions of impurities, such as oxygen, carbon, and iron, by solving coupled equations for the densities  $n_k$  of the  $(k-1)$ -th ionized state ( $k=1,2, \dots, M$ ).

---

<sup>\*)</sup> JAERI-M 5376.

$$\frac{1}{r} \frac{d}{dr} \left( r D_k \frac{dn_k}{dr} \right) + n_e (\alpha_{k-1} n_{k-1} - \alpha_k n_k) - n_e (\beta_{k-1} n_k - \beta_k n_{k+1}) = 0 ,$$

where  $\alpha_k$  and  $\beta_k$  are ionization and recombination rates, respectively, and collisional diffusion coefficient  $D_k^{(9)}$  is used. More highly ionized impurity ions tend to accumulate closer to the center of the plasma column.<sup>10)</sup> Figure 6 shows an example of stationary-state distributions of oxygen ions in a typical Tokamak plasma.<sup>11)</sup>

### (ii) Energy losses caused by impurities

Energy losses caused by impurities, such as ionization  $P_I$ , bremsstrahlung  $P_{BR}$ , and excitation losses  $P_{EX}$  are calculated using the stationary distributions of impurity ions in the plasma column. It is pointed out that the permissible concentration of impurity ions to reach at fusion plasmas is rather low: of the order of  $10^{-2}$  for light elements and  $10^{-3}$  for heavy elements.

Fig. 7 shows the example of these energy losses compared with the neoclassical thermal conductive loss of ions  $P_I$ , the cyclotron radiation loss  $P_{CY}$ , and the joule heating power  $P_J$  in the case of JFT-60.

### (iii) Recycling processes of impurities

Influx of impurities may result from the boil-off of limiter materials, the sputtering of limiter and vacuum wall materials, and the desorption of impurity gases from the limiter and vacuum wall. These processes and other related processes are schematically shown in Fig. 8. The sputtering of wall materials by plasma ions and hot neutral particles generated through charge exchange process between plasma ions and cold neutral particles may cause a rapid increase in impurity concentration.

A simple model is used to estimate the impurity accumulation in the plasma

$$\frac{dN_Z}{dt} = \eta_1 (1 - \zeta_1) \frac{N_p}{\tau_p} + \eta_1 \left( \frac{r}{1-r} \right) \frac{N_p}{\tau_p} + \eta_2 (1 - \zeta_1) \frac{N_Z}{\tau_i} - \zeta_2 \frac{N_Z}{\tau_i} ,$$

where  $\eta_1$  and  $\eta_2$  are sputtering yields of plasma ions and impurity ions, respectively, and  $\zeta_1$  and  $\zeta_2$  are their respective divertor efficiencies.

$r$  is the number of hot neutral particles escaping from the plasma for each incident cold neutral particle. It can be shown that the impurity

concentration will reach the permissible level within a few  $\tau_i$  in conventional Tokamak devices (see Fig. 9 and 10).

(T. Tazima, K. Inoue, M. Tanaka,  
M. Azumi and M. Yoshikawa)

#### 4. Heating of a Tokamak plasma

##### 1) Efficiency of neutral injection heating in tokamak devices

One of the most promising methods of plasma heating applicable to tokamak devices is the injection of energetic neutrals and is currently of great interest from experimental and theoretical points of view. To obtain the optimum condition of the neutral injection heating in tokamak devices in JAERI (JFT-2 and JT-60), we have examined the behaviour of fast ions produced by the neutral beam with uniform flux and rectangular cross section, and the resulting space-time variations of plasma temperature. To avoid the appearance of singularities on the spatial distribution of fast ions, the width of the beam was taken to be finite but sufficiently small, and the divergence of the beam was neglected.

The motion of the fast ion was analyzed by using the drift approximation, and the fraction of fast ions lost to the metallic wall was evaluated. The banana orbits of the fast ions begin to exist from the outside of the torus as the injection approaches perpendicular to the magnetic field. The critical injection point for banana formation is  $R_I \sim \pm \sqrt{2a(R_0 + a)} - \rho_\theta/2$  ( $\rho_\theta$  is the larmor radius in the poloidal field) under the assumption of  $\rho_\theta/a, a/R_0 < 1$ . Figure 11 shows an example of efficiency of fast ions trapped in the plasma for various injection angles. The injection point giving the minimum efficiency is approximately  $R_I \sim -\sqrt{2a(R_0 + a)} + 3\rho_\theta/2$ . The beam particles lost to the wall as neutrals as well as fast ions not only decreases the efficiency of heating but also may cause the accumulation of the impurity in the plasma. This is one of the guideline selecting the injection angle.

To find the source profile of injection heating, the spatial density distributions of fast ions,  $S_r$ , were calculated under the assumption that the drift orbits of fast ions are concentric circles, neglecting the banana orbits. Figure 12 shows an example of  $S_r$  for various beam energies. To

obtain the effective injection of neutrals into the central part of plasma column, the beam energy should be  $E_B \geq 0.6 \times 10^{-15} n_0 A_B \sqrt{2aR_0} \alpha$  (where  $\alpha$  is the correction factor of density profile, and  $n_0$  is the peak plasma density), which corresponds to 100 keV for JT-60.

Using the 1-D tokamak simulation code,<sup>12)</sup> the space-time evolution of the plasma temperature under the neutral injection heating was calculated. The neo-classical transport coefficients were assumed and the effect of the loss due to the ripple of the toroidal field ( $\delta$ )<sup>13)</sup> was taken into account. Figure 13 shows the evolution of the average ion temperature in JT-60 for 10 MW parallel injection. For  $\delta = 0$ , the dependence on the beam energy is not apparent, but the plasma temperature has a peak near the periphery of the plasma column for lower beam energy. Taking account of the ripple diffusion, the efficiency of the heating decreases for lower beam energy.

The background neutrals in the plasma causes the fast ion loss through the charge-exchange process. For parallel injection and short mean free path ( $\lambda < \sqrt{aR_0}$ ), the fast ions stochastically escape by the successive processes of charge-exchange with neutral and with plasma ion. The diffusion coefficient of this process was calculated and the allowable density of background neutrals in the plasma was evaluated.

(M. Azumi, M. Tanaka)

## 2) Numerical calculation of the dispersion equation near the lower hybrid frequency

In addition to the neutral beam injection, another promising method of tokamak heating is the use of electromagnetic wave with lower hybrid resonance frequency. This wave is converted into the ion-Bernstein mode near the resonance density and is effectively absorbed by the plasma.<sup>14)</sup> To investigate the damping of the ion-Bernstein mode near the lower hybrid frequency a computer code solving the dispersion equation of this mode has been completed. The code is tested and preliminary results are obtained.

(M. Azumi)

## 5. Study of a Gas-Insulated Plasma

With a mind to apply the gas insulation to tokamak-like devices by using a neutral gas vortex, the pressure balance (Eq. (1)), the particle balance (Eq. (2)), and the energy losses caused by neutral gases are studied numerically.<sup>15)</sup>

$$\frac{d}{dr}(p_p + p_0) = j_z \cdot B_\theta, \quad (1)$$

$$\frac{1}{r} \frac{d}{dr} (r n_e v_p) = \alpha n_0 n_e - \beta n_e^2, \quad (2)$$

where  $n_p$  and  $n_0$  are the electron and neutral densities, respectively,  $j_z$  is the plasma current density,  $B_\theta$  is the poloidal magnetic field,  $\alpha$  and  $\beta$  are the ionization and recombination rates, respectively,  $p_p$  and  $p_0$  are the plasma and neutral gas pressures, respectively, and  $v_p$  is the diffusion velocity of the plasma.

Eq. (2) yields the possible maximum value of the neutral gas density at the plasma boundary, i.e.  $\max. n_0(a) \sim \{ [T_e(0) + T_i(0)] / T_0(a) \} \cdot n_e(0)$ , where  $T_e(0)$  and  $T_i(0)$  are the electron and ion temperatures at the plasma center, respectively. On the other hand, the maximum  $n_0(a)$  compatible with Eq. (2) is less than  $n_e(0)$  when we use the usual expression for  $v_p$  due to the collision between plasma ions and electrons in the magnetic field.

The diffusion velocity of the plasma is derived by taking account of the pressure gradient of the neutral gas and the collision between plasma ions and neutral particles. When this expression is used maximum  $n_0(a)$  can exceed  $n_e(0)$ . Further investigation is now underway.

(T. Tazima)

## References

- 1) T. Amano, M. Wakatani and M. Watanabe : J. Phys. Soc. Japan 33 (1972) 782.
- 2) W.A. Newcomb : Ann. Phys. 10 (1960) 232.
- 3) P.H. Rutherford et al., Plasma Physics and Controlled Nuclear Fusion Research (IAEA, Vienna, 1971) Vol. II 553.

- 4) T. Ohkawa : Kakuyugo-Kenkyu 22, 99 (1968).
- 5) A.A. Ware : Phys. Rev. Letters 25, 916 (1970).
- 6) T.E. Stringer : Nuclear Fusion 12, 689 (1972).
- 7) B. Coppi et al., Phys. Rev. Letters 17, 377 (1966).
- 8) B.B. Kadomtsev and O.P. Pogutse, Soviet Physics-Doklady 14,470 (1969).
- 9) T. Tuda and M. Tanaka : JAERI-M 5376 (1973).
- 10) V.A. Vershkov and S.V. Mirnov : IAE-2293 (1973).
- 11) T. Tazima, M. Tanaka, M. Yoshikawa and K. Inoue : to be published  
in Nucl. Fusion, M. Tanaka et al. JAERI-M 4961 (1972).
- 12) T. Tazima, et al. JAERI-M 4941 (1972).
- 13) T.E. Stringer, Nuclear Fusion 12,689 (1972).
- 14) T.M. Stix, Phys. Rev. Lett. 15,878 (1965).
- 15) T. Tazima : Proc. M.H.D. Symposium (1974) (in Japanese).

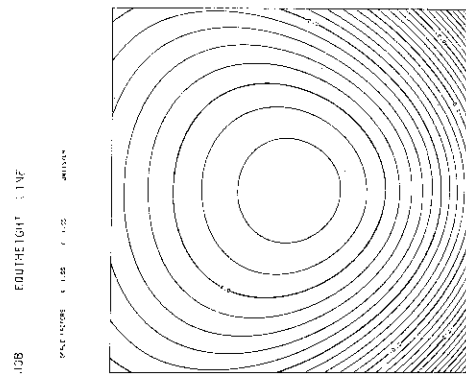


Fig.1 Equilibrium with small aspect ratio.

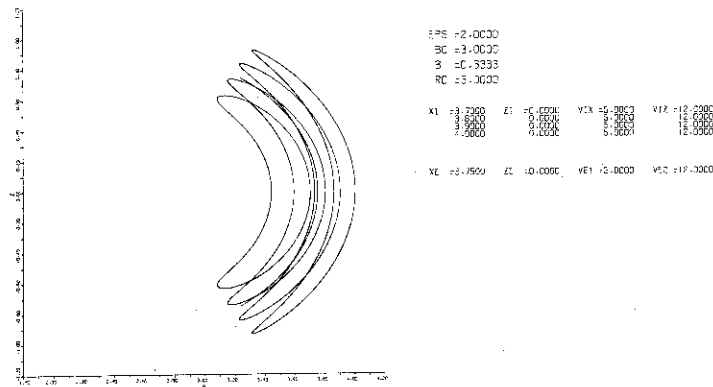


Fig.2 Banana trajectories.

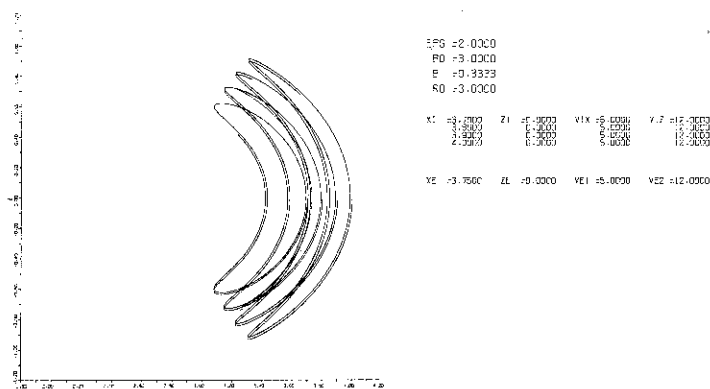


Fig.3 Banana trajectories with toroidal electric field.



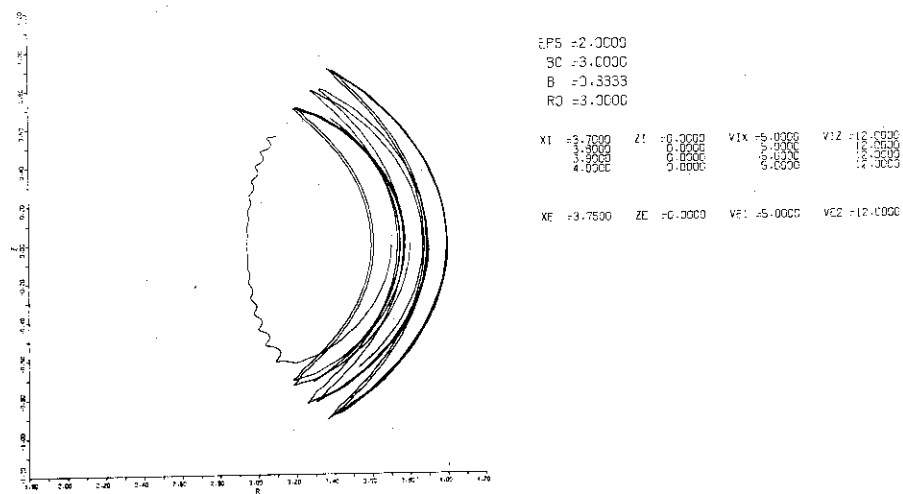


Fig. 4 Banana trajectories with the ripple field of 0.5%

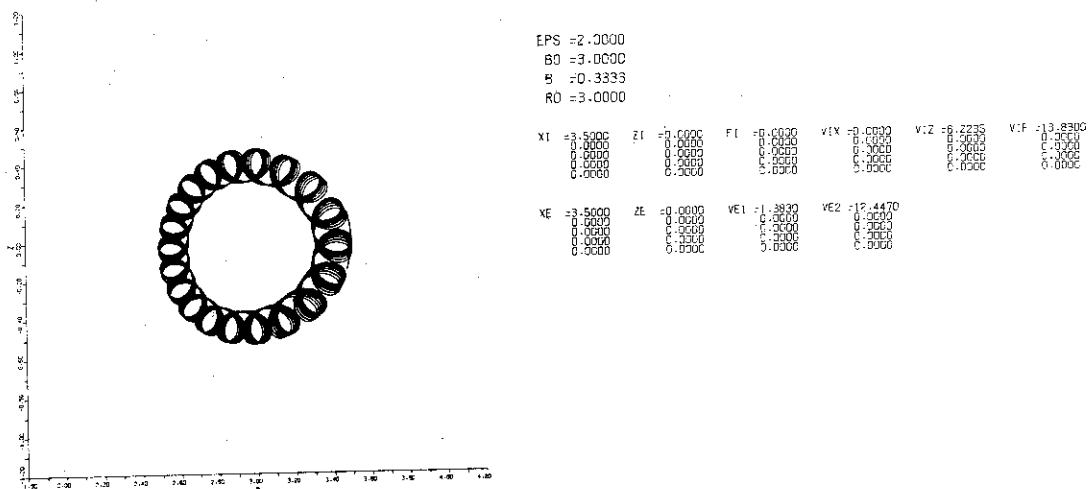


Fig. 5 Ion motion in the equilibrium shown in Fig. 1

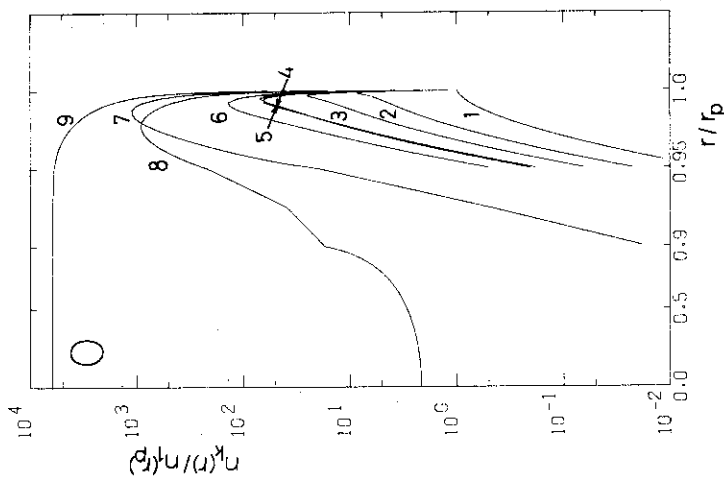


Fig. 6 An example of the stationary state distributions of oxygen ions in a typical tokamak plasma.

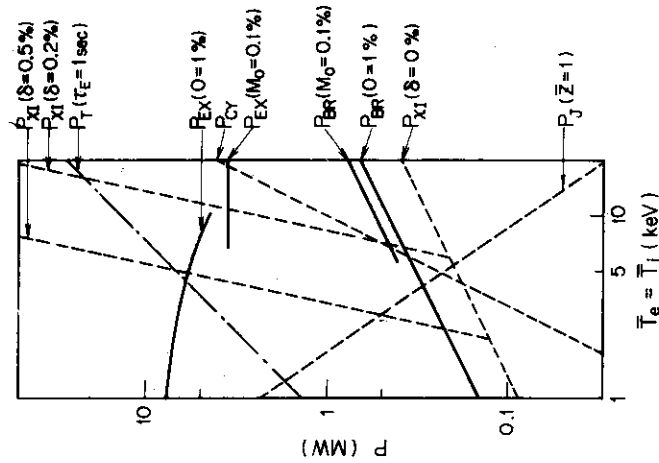


Fig. 7 Energy losses by impurities comparing to the neoclassical thermal conduction loss, the cyclotron radiation loss, and joule heating power in the case of JT-60 (torus radius is 3 m, plasma radius is 1 m, total plasma current is 3.3 MA, toroidal magnetic field is 5 Wb/m<sup>2</sup>, and mean plasma density is  $5 \times 10^{19}$  particles/m<sup>3</sup>).  $\delta$  is the ripple of the toroidal magnetic field.

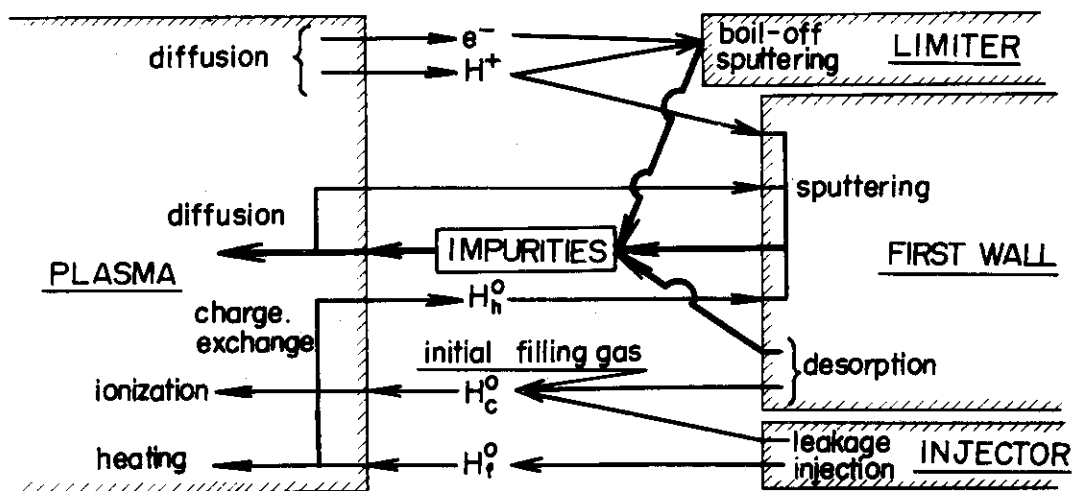


Fig. 8 Recycling processes of impurities.

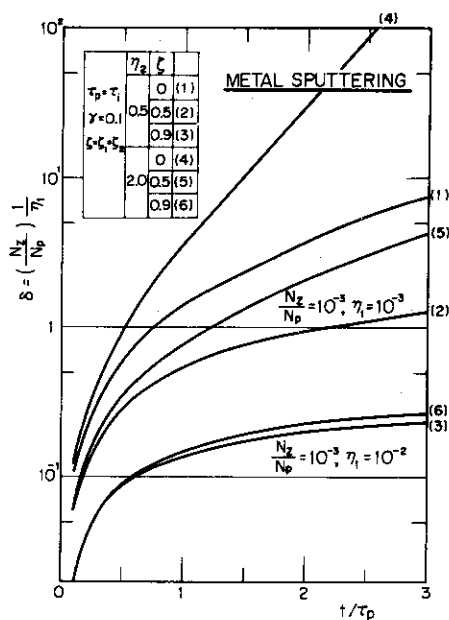


Fig. 9 Metallic impurity accumulation by sputtering.

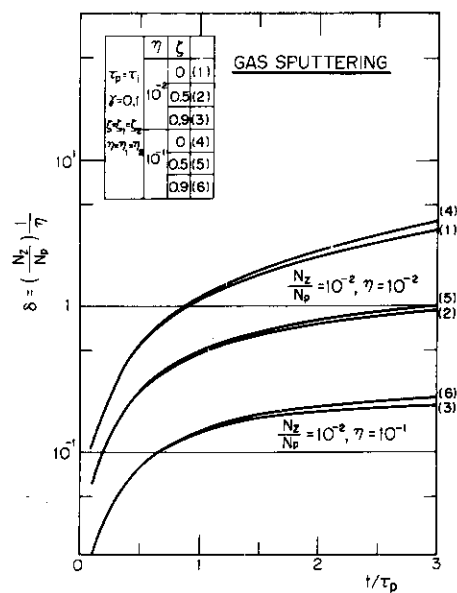


Fig. 10 Gas impurity accumulation by sputtering.

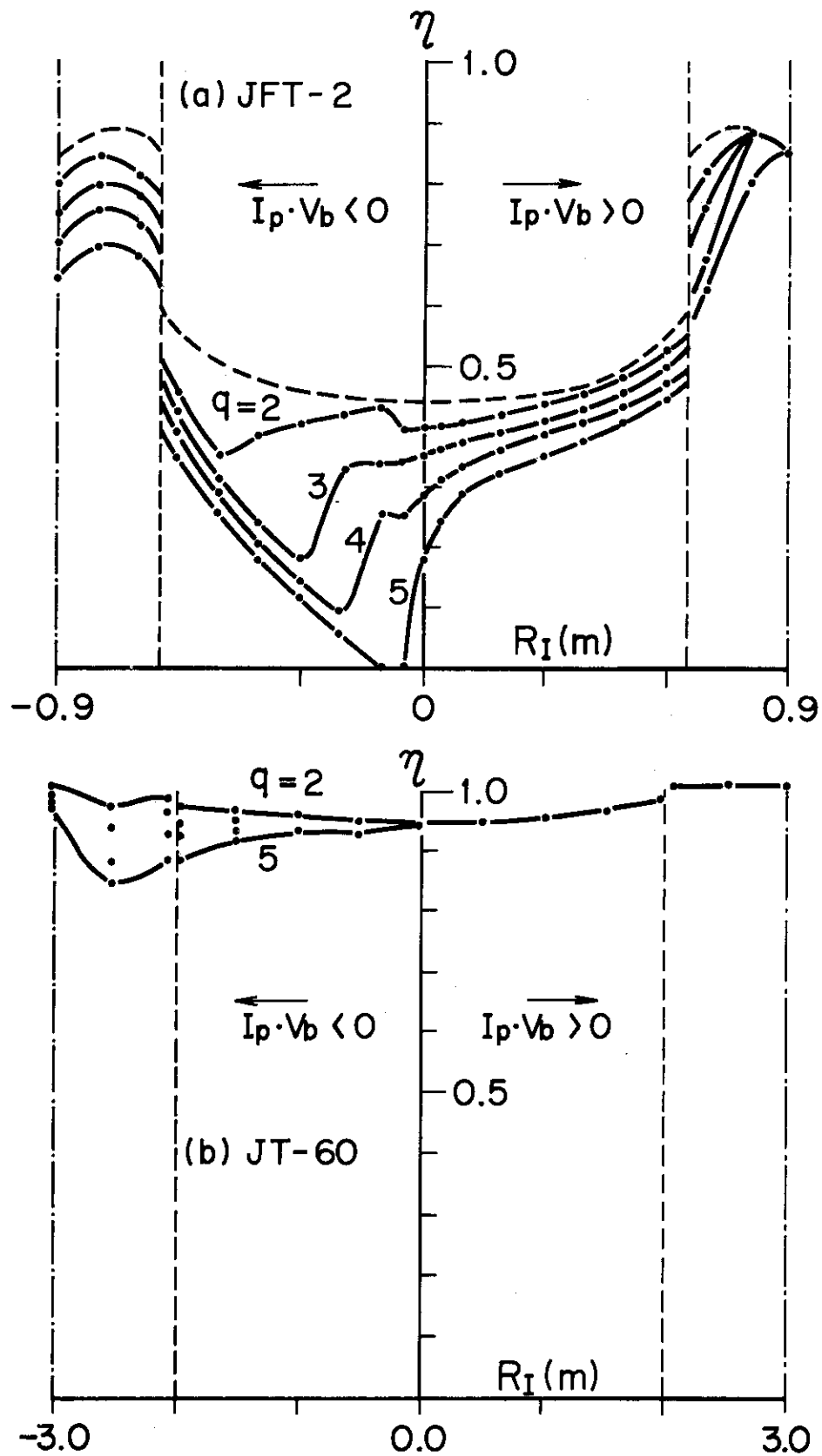
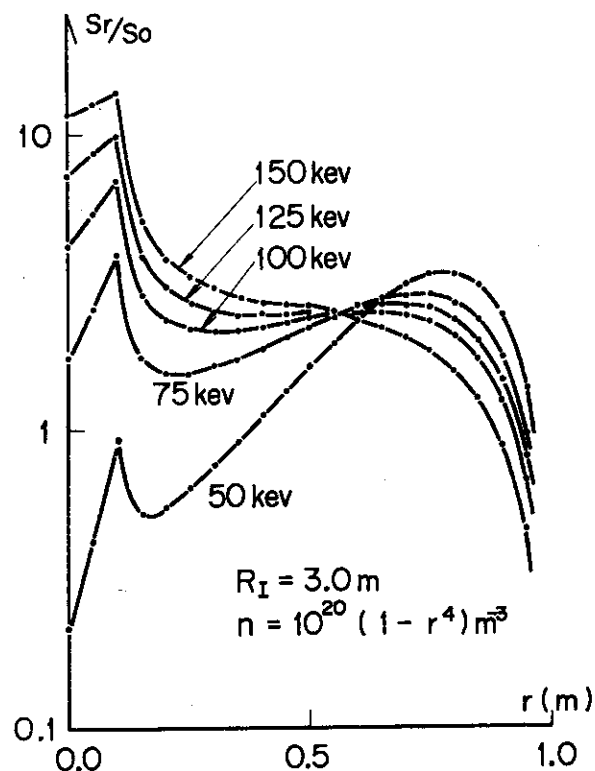


Fig. 11 Trapping efficiency of fast ions for a) 25 keV injection to JFT-2 and b) 100 keV injection to JT-60.



### FAST ION DENSITY DISTRIBUTION

Fig. 12 Density distribution of fast ions for parallel injection to JT-60.  $S_0$  is the injection rate of neutral particles averaged over the whole plasma volume.

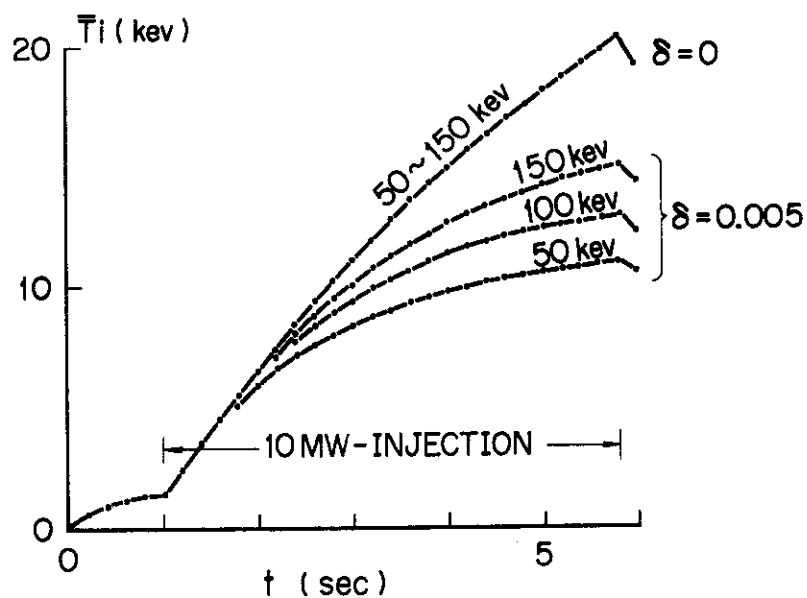


Fig. 13 Time evolution of the average ion temperature for 10 MW parallel injection into JT-60.  $\delta$  denotes the ripple of the toroidal magnetic field.

## IV. REACTOR DESIGN STUDY

N. Asami\*, M. Ohta, K. Sako, Y. Seki and H. Yamato\*\*

## 1. Introduction

The purposes of this design study are to clarify the problems on the fusion reactor development and to contribute to the effective progress of the R&D.

The relations of the reactor design study and R&D are shown in Fig. 1. The systematic reactor design study have been started in April 1973. We performed a conceptual design of a tokamak reactor and several design related studies which are described briefly in the following sections. From the experience of these preliminary design study, many problems were found and the necessity for more detailed design study was recognized.

(K. Sako)

2. Conceptual Design of a Gas Cooled Tokamak Reactor<sup>1,2)</sup>

A conceptual design of a helium cooled tokamak reactor has been carried out. Core plasma, reactor structure, blanket neutronics, material and magnet are evaluated.

The main design parameters of the reactor are as follows; reactor output 2000 MWt, first wall loading  $2 \text{ MW/m}^2$ , plasma major/minor radius 10/2m, average toroidal magnetic field 60 kG and reactor inlet/outlet coolant temperature 400/600°C.  $\text{Li}_2\text{O}$  pebble and Incoloy 800 are used for the blanket fertile material and the first wall material, respectively. More detailed design parameters are listed in Table 1 and overall view of the reactor is shown in Fig. 2.

In this design we discuss the following problems;

- (1) Core plasma; The plasma parameters were decided by assuming the circular cross sectional plasma and the plasma characteristics were analyzed for the steady state and transient state conditions. The

---

\* On leave from Mitsubishi Atomic Power Industries Inc., Omiya.

\*\* On leave from Tokyo Shibaura Electric Co. Ltd., Kawasaki.

- necessity of a divertor and its concept were also studied preliminarily.
- (2) Reactor structural design; A helium cooled reactor system which has the blanket of  $\text{Li}_2\text{O}$  pebbles and graphite balls was selected. This concept was selected to simplify the blanket structure. The thermal and mechanical evaluations were carried out.
  - (3) Blanket nuclear design; The heat generation and the tritium breeding in the blanket for the prescribed concept were evaluated.
  - (4) Material considerations; The first wall material of Incoloy 800 and the blanket fertile material of  $\text{Li}_2\text{O}$  were evaluated. Tritium recovery from the blanket was also studied.
  - (5) Magnet design; In consideration of the field intensity and its uniformity, configuration of SCM was decided. Characteristics of the toroidal field magnet were evaluated.

(K. Sako, M. Ohta, Y. Seki, H. Yamato,  
T. Hiraoka\*, K. Tanaka\*\*, N. Asami  
and S. Mori)

### 3. Design Related Study

#### 1) On the optimization of tokamak fusion reactor

We have investigated the optimum design of a tokamak reactor assuming that the optimum is given by the maximum power density at a fixed thermal power output of the reactor, maximum allowable stress of the toroidal coil, thickness of the blanket and radius of the transformer core.<sup>3,4)</sup> This optimization is compared with two other optimizations. In the first, the stored magnetic energy of the toroidal coils is minimized as cost of superconducting coil is roughly proportional to the stored energy due to the analysis of Lubell.<sup>5)</sup> In the second, the cost parameter introduced by Schmitter,<sup>6)</sup> which is the product of conductor length, field intensity and current in the coil, is minimized. The plasma temperature, the safety factor  $q$  and the poloidal  $\beta$  value are also fixed during optimizations. In this analysis, radius of the transformer is used as a variable and

---

\* Division of Reactor Engineering

\*\* Division of Radio Isotope Production

instead, field change in the core  $\Delta B_p$  is fixed. The designed values of a 2 GW reactor are listed in Table 2. The value  $f$  is the factor to determine the poloidal  $\beta$  by  $\beta_p = f R/a$ . Thus the maximum possible  $f$  is 1 from plasma equilibrium. The confinement time  $\tau_{op}$  is required confinement time in order to satisfy a self-sustain condition by  $\alpha$  heating and  $\tau_{ex}$  is empirical confinement time given by  $\tau_{ex} = 4a^2 B_p$  scaling. The result shows that the smallest aspect ratio and the highest toroidal field are obtained in the case 1 and the fattest reactor with lowest toroidal field is obtained in the case 3.

In Fig. 3, conditions for the maximum power density is plotted in the  $f$ ,  $q$  space, in which five lines correspond to different  $P_T$ . It is shown that the optimization is difficult in a reactor with small power output. For example, 5GW is almost the smallest possible optimized reactor, if  $f=0.3$ ,  $q=1.5$  and the power density  $P_D = 0.3 \text{ MW/m}^3$ .

(H. Yamato and M. Ohta)

## 2) Start-up and shutdown of a D-T tokamak reactor<sup>7,8)</sup>

The ignition and shutdown processes are discussed in a D-T tokamak reactor when the confinement time of the plasma is given by the pseudoclassical diffusion and the anomalous diffusion due to trapped ion instabilities or Neo-Bohm diffusion.

At the ignition phase it is desirable that the plasma density is initially fixed to be low at lower temperatures and gradually increases to a steady state at highest temperatures. The reason is that the required power of injected neutral beams can be considerably low by the help of powerful energy released to  $\alpha$ -particles.

At the shutdown of a reactor, smooth shutdown is desirable from the point of heat removal of the first wall and the divertor. Here the effect of increase and decrease of injection rate of fuel and also the effect of change in the mixing ratio of D-T fuels are examined. Numerical analyses show that it is not applicable for the shutdown of fusion plasma with charged particle heating and with classical type diffusion to stop the injection of fuel and is favorable to increase the injection rate. On the contrary, in Bohm type diffusion the effect of injected cold fuels on the shutdown phenomena of plasma is opposite to in classical type diffusion. In a reference reactor the following method is adopted that the injection of tritium is stopped and the injection rate of deuterium is doubled.

(M. Ohta and H. Yamato)



## 3) Fuel supply by neutral gas surrounding a core plasma

One of the best methods to supply fuel to a toroidal reactor is generally considered to be pellet injection. In this method, cold fuel can be injected into the center of the plasma and it may be possible to reduce charge-exchanged fast neutrals to hit the first wall.

Here we investigate an opposite extreme case, in which the fuel is supplied at the plasma surface by means of cold gas surrounding the hot core plasma.<sup>8)</sup> In this geometry, the fuel ionized at the surface diffuses into the plasma as the fuel is consumed by fusion reactions. A serious problem in this geometry may be sputtering of the first wall due to charge-exchanged fast neutrals and influx of impurities. It is expected, however, that the plasma and neutrals are mixed in a thin layer at the plasma surface and the plasma in this region is cooled down to temperatures as low as several 10eV, although there is small amount of neutrals which penetrate into the main plasma by successive charge-exchange processes. Thus it may be possible to reduce sputtering of the first wall because sputtering threshold is of the order of 10eV. The result of calculations of the plasma temperature and neutral density in the mixed region is shown in Fig. 4 when neutral density at the plasma surface  $n_{ns}$  is changed from  $10^{13}/\text{cm}^3$  to  $10^{15}/\text{cm}^3$  and the density of the main plasma is fixed to  $10^{14}/\text{cm}^3$ . In Fig. 5 number of charge-exchanged neutrals is plotted as a function of temperature. In this analysis, fast neutrals obtained after two or more charge-exchanges are not taken into account. Effect of these particles and thermal stability problem in this fueling geometry are now under investigation.

(H. Yamato and M. Ohta)

4) Tritium breeding in ceramic lithium-compound blanket<sup>9)</sup>

In a fusion reactor employing the deuterium-tritium reaction, the blanket surrounding the reacting plasma must breed tritium if the plant is to be selfsustaining in tritium cycle. Most of the blanket design concept so far published have as the tritium fertile material, lithium or lithium salt in liquid state. The blanket system containing ceramic lithium compound has been employed in the conceptual design of a helium cooled fusion reactor carried out in JAERI.<sup>1)</sup>

Four ceramic lithium-compounds are selected for their potentiality

for high tritium breeding. Tritium breeding ratio, material consistency in the blanket environment and tritium recovery methods for  $\text{LiD}$ ,  $\text{Li}_2\text{O}$ ,  $\text{Li}_3\text{N}$  and  $\text{Li}_2\text{C}_2$  are investigated. Physical and chemical properties of lithium metal and four ceramic lithium compounds are shown in Table 3. The calculated tritium breeding ratios of the blankets with each material are given in Table 4. Lithium Oxide ( $\text{Li}_2\text{O}$ ) appeared to be the most promising for the blanket material and was adopted in the conceptual design.<sup>1)</sup>

(Y. Seki)

#### 5) Nuclear heating calculation in fusion reactor blanket

Nuclear heating calculation code system called RADHEAT, is developed in JAERI.<sup>10)</sup> The calculation flow chart is shown in Fig. 6. Using the code system, neutron and gamma-ray coupled cross section-set including KERMA factors are developed for 20 nuclides of interest for the fusion reactor blanket and shield. The 20 nuclides are listed in Table 5. The 42 neutron energy group structure and 21 gamma-ray energy group structure are shown in Table 6 and Table 7, respectively. Legendre coefficients of up to  $P_5$  are included in the coupled cross section-set.

The nuclear heating rate distribution in the blanket of the fusion reactor designed in JAERI<sup>1)</sup> is calculated using the coupled cross section.  $P_5$ - $S_8$  approximations is employed in the calculation by ANISN.<sup>11)</sup> The results of the calculation are shown in Fig. 7.

(Y. Seki)

#### 6) Toroidal field magnet

The design study of toroidal field magnet was performed by the method of parametric study of coil dimensions, structure and arrangement. The lower limit of field uniformity is decided from ripple diffusion analysis. This limitation is one of the most basic requirements for the toroidal field magnet design.

In consideration of plasma parameters and the blanket structures, minimum inner radius of toroidal coil was decided to be 5 meters. Dependency of ripple on coil number and averaged radius was analyzed at the outermost point of plasma region. Fig. 8 shows the results of the analysis. Ripple resulted to be insensitive to conductor distribution in the coil. According to Tuda, ripple should be less than 0.2%. On the basis of the analysis, we selected 24 divisions and 5.5 meters average

radius for the reactor design.

The spatial distribution of ripple was shown in Fig. 9. Magnetic field distribution and leakage flux were also calculated. Maximum magnetic field in the coil conductor was computed to be 112.5 KG. Electromagnetic force and stored energy were calculated to be  $1.0 \times 10^6$  tons for centering force,  $3.6 \times 10^6$  tons for expansion force and 54 GJ respectively. As the superconducting material,  $\text{Nb}_3\text{Sn}$  was chosen because of its economic advantages over  $\text{V}_3\text{Ga}$ . Design parameters for toroidal field coil are summarized in Table 1.

(N. Asami)

#### References

- 1) K. Sako, M. Ohta, Y. Seki, H. Yamato, T. Hiraoka, K. Tanaka and S. Mori, JAERI-M 5502 (1973).
- 2) K. Sako, M. Ohta, Y. Seki, H. Yamato, T. Hiraoka, K. Tanaka and S. Mori, Proc. IAEA Workshop (Culham, 1974) to be published in Nucl. Fusion Suppl.
- 3) M. Ohta, H. Yamato, S. Mori, JAERI memo-4448 (1971), unpublished.
- 4) M. Ohta, H. Yamato, S. Mori, "Proc. of Int. Working Session on Fusion Reactor Tech." (Oak Ridge, 1971) p.350 Conf-710624 (USAEC).
- 5) M.S. Lubell, H.M. Long, S.N. Luton, Jr., and W.C.T. Stoddart, ORNL-TM-3927 (1972).
- 6) K.H. Schmitter, Course on the Stationary and Quasi-stationary Toroidal Reactor (Int. School Erice-Trapani 1972), p. 163, (1973, CID, Luxembourg).
- 7) M. Ohta, H. Yamato and T. Tazima, JAERI-M 5569 (1974).
- 8) H. Yamato and M. Ohta, Proc. of the First Topical Meeting on the Technology of Controlled Nuclear Fusion." (San Diego, 1974) p. 309 CONF-740402-P2 (USAEC)
- 9) Y. Seki, K. Sako, K. Tanaka and T. Hiraoka, *ibid.*, p. 77.
- 10) S. Miyasaka et al., "Code System for the Radiation-Heating Calculation on a Nuclear Reactor RADHEAT", JAERI-M 5794 (1974).
- 11) W.W. Engle Jr., "A Users Manual for ANISN: A One Dimensional Discrete Ordinate Transport Code With Anisotropic Scattering," K-1963 (1967).

Table 1 Design Parameters

<u>Power</u>	Reactor thermal output	2000MW
	Electrical output	800MW
<u>Dimensions</u>	Torus major radius	10m
	Plasma radius	2m
	First wall radius	2.5m
<u>Core Plasma</u>	Average plasma temperature	15keV
	Average plasma density	$1.1 \times 10^{14} \text{ cm}^{-3}$
	Energy confinement time	2.3 sec
	Toroidal magnetic field(Axis)	60kG
	Safety factor ( q )	1.5
	Poloidal $\beta$ value	2.0
	Plasma current	8MA
	Operation period	100min
<u>Blanket</u>	Fertile material	$\text{Li}_2\text{O}$ pebbles
	Reflector material	Graphite balls
	First wall neutron flux(Total)	$2.7 \times 10^{14} \text{ n cm}^{-2} \text{ s}^{-1}$
	Tritium breeding ratio	1.16
	Structural material	Incoloy 800
<u>Cooling System</u>	Reactor coolant, pressure	He, 20 ata
	Reactor inlet/outlet temperature	400/600°C
	Secondary system	Steam cycle
<u>Toroidal Magnet</u>	Number of coils	24
	Coil major radius	10.5 m
	Coil inner/outer radius	5/6 m
	Magnetic field(Max)	112.5kG
	Magnetomotive force	300MAT
	Stored energy	54GJ
	Electromagnetic force	
	Centering force	$1.6 \times 10^6 \text{ ton}$
	Expansion force	$3.6 \times 10^6 \text{ ton}$
	Average current density	$10\text{KA}/\text{cm}^2$
	Superconductor	$\text{Nb}_3\text{Sn}$
	Coil cross section	1m x 1m

Table 2. Optimum design parameters. The power density is maximized in 1 and the stored energy and the cost parameter of the toroidal coil are minimized in 2 and 3 respectively, where the thermal output of 2GW, the thickness of blanket of 2.5m (including the vacuum region between the plasma and first wall), maximum stress in the toroidal coil of 1 ton/cm<sup>2</sup> and the flux density in the transformer core of 1.5Wb/m<sup>2</sup> are assumed.

	1	2	3
Major Radius (m)	11.6	15.2	20.4
Plasma Radius (m)	2.0	4.9	8.6
Aspect Ratio	5.8	3.1	2.4
Core Radius (m)	5.2	7.0	8.7
Av. Radius of Toroidal Coil (m)	5.5	7.7	11.3
Toroidal Coil Thickness (m)	1.9	0.8	0.5
Axial Toroidal Field (T)	7.2	3.1	1.9
Maximum Toroidal Field (T)	11.7	6.1	4.2
Plasma Current (MA)	8.3	16.5	23.3
Power Density (MW/m <sup>3</sup> )	0.21	0.10	0.036
Stored Energy of Toroidal Coil(GJ)	152	73.1	80.6
Cost Parameter of Toroidal Coil(T.GA.m)	77.9	21.4	11.7
Wall Loading (MW/m <sup>2</sup> )	1.7	0.62	0.60
Required Confinement Time (sec)	2.2	6.1	12.3
Empirical Confinement Time (sec)	12.9	62.7	155
Plasma Density ( $\times 10^{14}$ /cm <sup>3</sup> )	0.98	0.35	0.17
Poloidal $\beta$	1.7	0.93	0.71
Toroidal $\beta$ (%)	2.3	4.3	5.6

Table 3 Some physical and chemical properties of the selected materials for the tritium breeding blanket

	Li metal	Li <sub>2</sub> O	LiD*	Li <sub>3</sub> N	Li <sub>2</sub> C <sub>2</sub>
Density (crystalline) (g·ml <sup>-1</sup> )	0.534	2.013	0.08826	1.38	1.65
Compressibility (10 <sup>-12</sup> ·cm <sup>2</sup> ·dyne <sup>-1</sup> )	11.3**		2.8		
Linear coefficient of thermal expansion (10 <sup>-5</sup> ·deg. <sup>-1</sup> )	6.0(180°C)		(3.6)		
Thermal conductivity(W·cm <sup>-1</sup> ·K <sup>-1</sup> )	0.394(466.8°C)	0.0173	(0.025)		
Electrical conductivity (Ω <sup>-1</sup> ·cm <sup>-1</sup> )	2.8 x 10 <sup>4</sup> **		0.001		
Heat of formation (kcal·mol <sup>-1</sup> )	0	-142.1	-21.6	-47.2	-14.2
Free energy of reaction (kcal·mol <sup>-1</sup> )	0		-16.72		
Entropy (cal·deg <sup>-1</sup> ·mol <sup>-1</sup> )	6.7	9.06	5.9		
Specific heat, C <sub>p</sub> (cal·deg <sup>-1</sup> ·mol <sup>-1</sup> )	5.95 6.91**	12.9	8.3	21.7	
Melting point (C)	180.54	1727	688	845	
Boiling point (C)	1342	2327	d.	d.	d.

\* Data are referred to LiH except density

\*\* The results at 600°C

d. decompose

Table 4. Tritium breeding ratio for ceramic lithium-compounds in the standard blanket configuration (43 cm fertile material region + 20 cm graphite reflector)

Ceramic Lithium- compounds	Lithium atom densities (10 <sup>24</sup> atoms/cm <sup>3</sup> )	T <sub>6</sub>	T <sub>7</sub>	T
LiD	0.04138	1.034	0.295	1.329
Li <sub>2</sub> O	0.05708	0.799	0.364	1.163
Li <sub>2</sub> C <sub>2</sub>	0.03670	0.767	0.260	1.027
Li <sub>3</sub> N	0.04648	0.686	0.375	1.061
Li*	0.03248	0.612	0.393	1.005

where

T<sub>6</sub> = <sup>6</sup>Li(n,α)T triton-producing reactionsT<sub>7</sub> = <sup>7</sup>Li(n, n'α)T triton-producing reactionsT = T<sub>6</sub> + T<sub>7</sub> = total tritons.

\* Liquid lithium used under the same configuration is shown for comparison.

Table 5 List of the Nuclides Included in  
the Neutron-Gamma Coupled Cross  
Section-Set

Nuclide No.	Tape Name	
	COUPLE-1	COUPLE-2
1	Li-6	H-1
2	Li-7	H-2
3	C-12	He-3
4	O-16	Be
5	He-4	B-10
6	Nb	N
7	Mo	Al
8	Cr	V
9	Fe	Cu
10	Ni	Pb

Table 6 Neutron Energy Group Structure

Group	Energy Limits	Mid-Point Energy
1	15.000 - 13.720 MeV	14.360 MeV
2	13.720 - 12.549	13.135
3	12.549 - 11.478	12.014
4	11.478 - 10.500	10.989
5	10.500 - 9.314	9.907
6	9.314 - 8.261	8.788
7	8.261 - 7.328	7.795
8	7.328 - 6.500	6.914
9	6.500 - 5.757	6.129
10	5.757 - 5.099	5.428
11	5.099 - 4.516	4.808
12	4.516 - 4.000	4.258
13	4.000 - 3.162	3.581
14	3.162 - 2.500	2.831
15	2.500 - 1.871	2.186
16	1.871 - 1.400	1.636
17	1.400 - 1.058	1.229
18	1.058 - 0.800	0.929
20	0.566 - 0.400	0.483
21	0.400 - 0.283	0.342
22	0.283 - 0.200	0.242
23	0.200 - 0.141	0.171
24	0.141 - 0.100	0.121
25	100.0 - 46.5 KeV	73.25 KeV
26	46.5 - 21.5	34.0
27	21.5 - 10.0	15.75
28	10.0 - 4.65	7.325
29	4.65 - 2.15	3.40
30	2.15 - 1.00	2.825
31	1.00 - 0.465	0.733
32	0.465 - 0.215	0.340
33	0.215 - 0.100	0.158
34	100.0 - 46.5 eV	73.25 eV
35	46.5 - 21.5	34.0
36	21.5 - 10.0	15.75
37	10.0 - 4.65	7.325
38	4.65 - 2.15	3.40
39	2.15 - 1.00	1.58
40	1.00 - 0.465	0.733
41	0.465 - 0.215	0.340
42	0.215 - 0.001	0.108

Table 7 Gamma-Ray Energy Group Structure

Group	Energy Limits(MeV)	Mid-Point Energy(MeV)
1	14.0 - 12.0	13.0
2	12.0 - 10.0	11.0
3	10.0 - 8.0	9.0
4	8.0 - 7.5	7.75
5	7.5 - 7.0	7.25
6	7.0 - 6.5	6.75
7	6.5 - 6.0	6.25
8	6.0 - 5.5	5.75
9	5.5 - 5.0	5.25
10	5.0 - 4.5	4.75
11	4.5 - 4.0	4.25
12	4.0 - 3.5	3.75
13	3.5 - 3.0	3.25
14	3.0 - 2.5	2.75
15	2.5 - 2.0	2.25
16	2.0 - 1.5	1.75
17	1.5 - 1.0	1.15
18	1.0 - 0.4	0.7
19	0.4 - 0.2	0.3
20	0.2 - 0.1	0.15
21	0.1 - 0.01	0.055

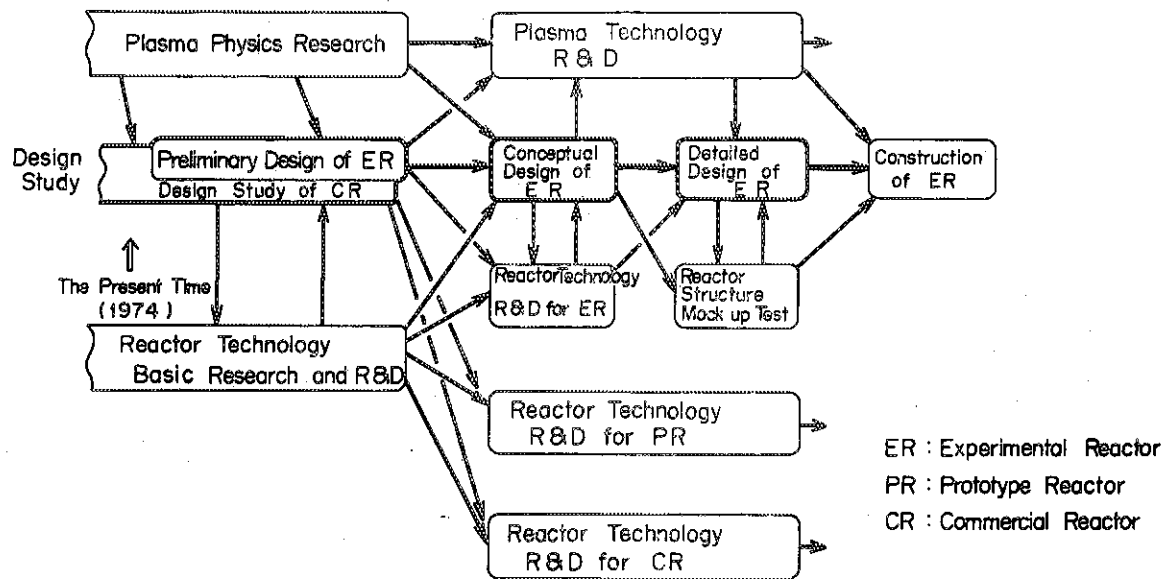


Fig.1 Design Study and R &amp; D

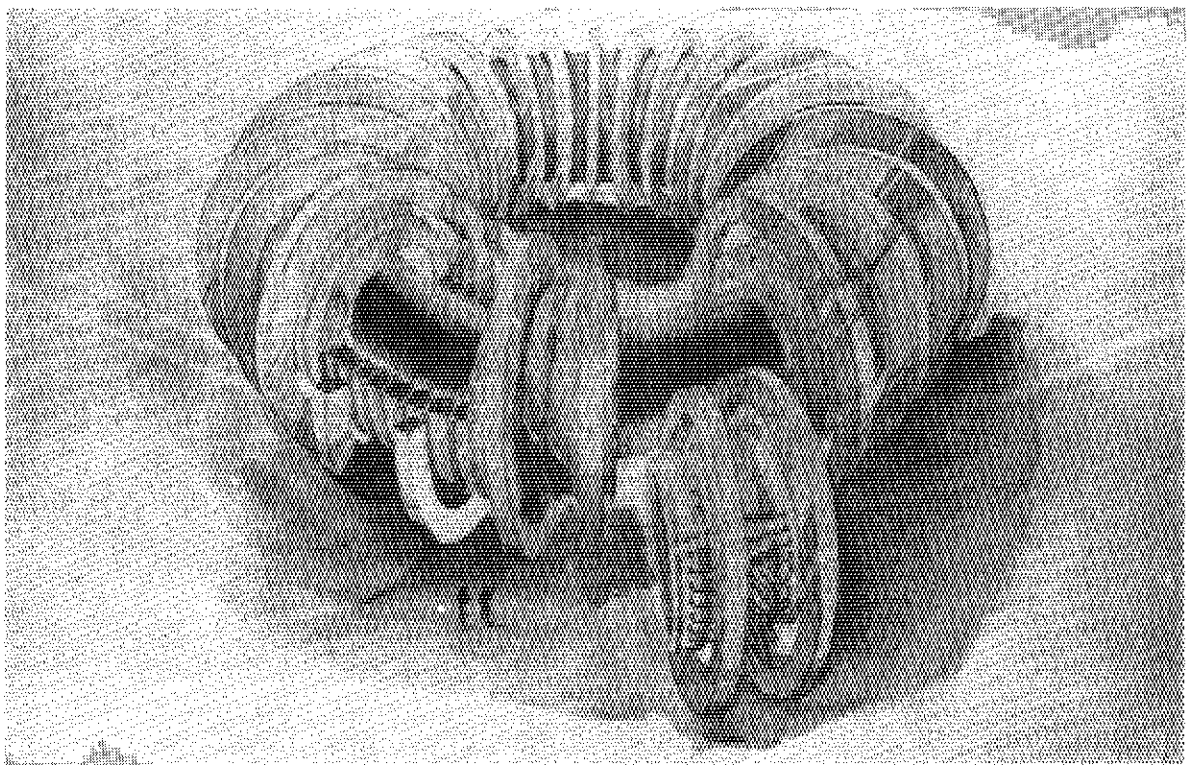


Fig.2 Overall view of the reactor



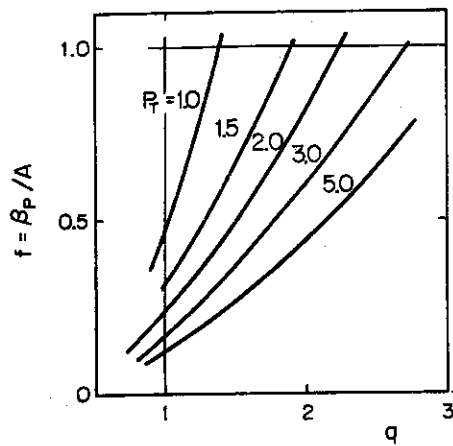


Fig. 3 Constant thermal power output  $P_T$  (GW) lines in the  $f$ - $q$  space, when the optimized power density  $P_D$  is fixed to  $0.3 \text{ GW/m}^2$ .

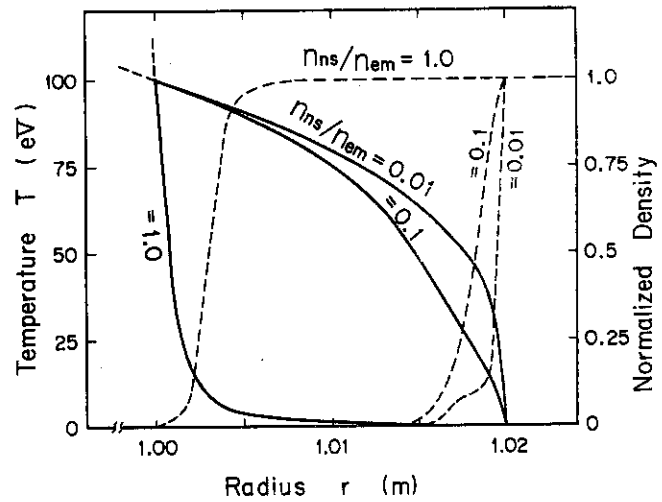


Fig. 4 Radial distributions of plasma temperature and neutral density in the mixed region of plasma and neutral gas. Solid line and dotted line indicate the temperature and density respectively where  $n_{ns}/n_{em}$  is the neutral density outside the plasma divided by the plasma density inside the main plasma.

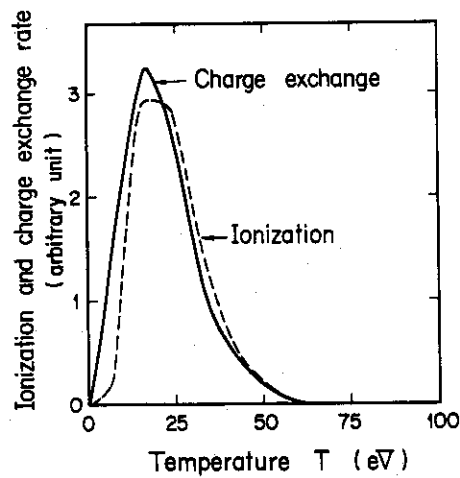


Fig. 5 Ionization and charge exchange rates vs. plasma temperatures of the positions where ionizations and charge-exchanges take place.

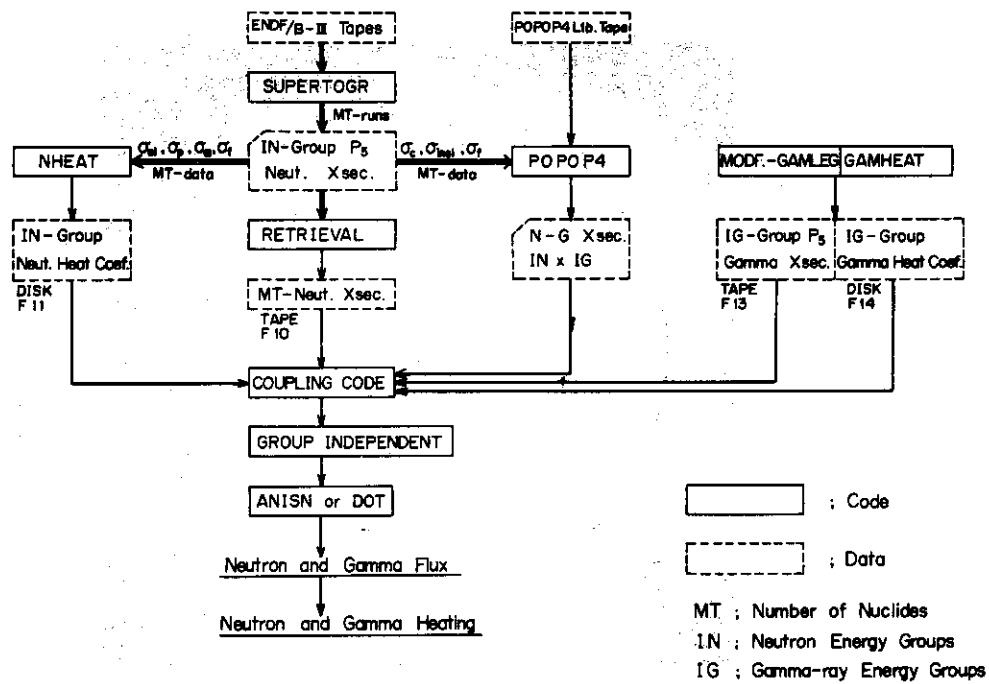


Fig. 6 Nuclear Heating Calculation Code System

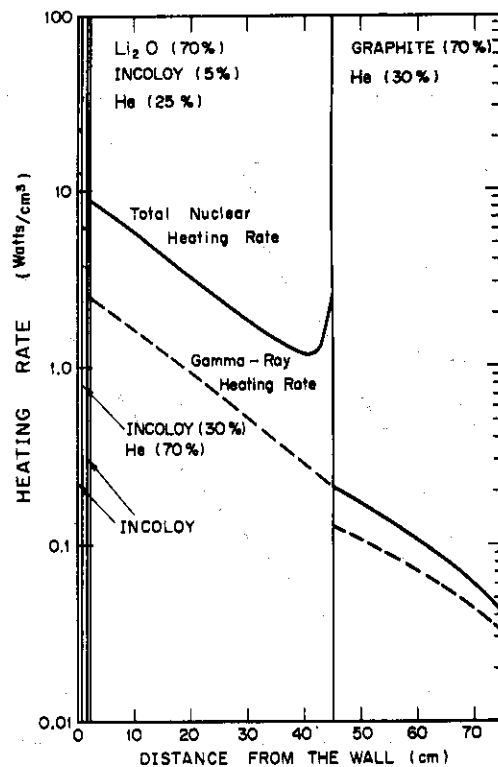


Fig. 7 The distribution of nuclear heating rate in the blanket.

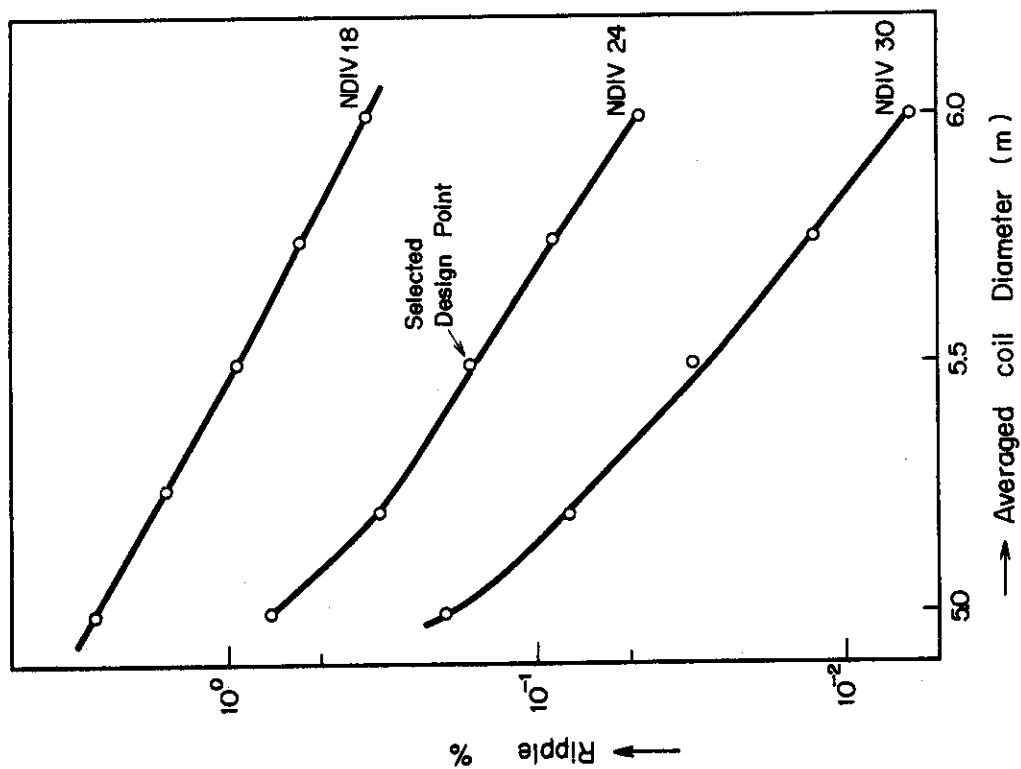


Fig. 8 Dependence of the Field Uniformity on Coil Diameter and Number of Toroidal Coils.

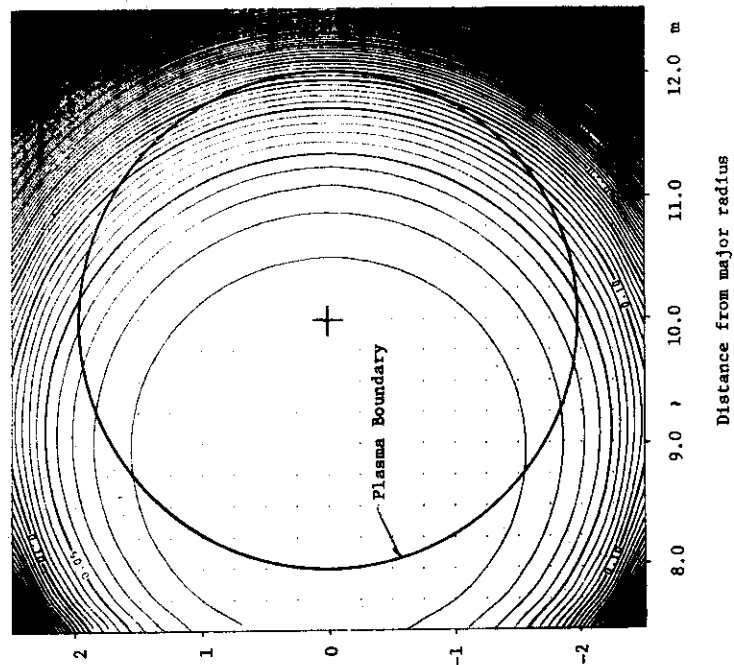


Fig. 9 Uniformity of Toroidal Field (Ripple %)

## APPENDICES

## 1. Publication List

Ariga, S\*, Matoba, T. and Miyamoto, K\*\* : Property of beryllium plasma produced by laser irradiation in a stellarator, Japan. J. Appl. Phys. 12 484-485 (1973).

(\* Kyoto University, \*\* Nagoya University)

Ohta, M., Itoh, S. and Fujisawa, N. : Analysis of magnetic field in inhomogeneous materials, Theoretical and Applied Mechanics, Vol. 21, 267-278 (1973) University of Tokyo Press.

Hayase, K\*, Toi, K\*\* and Okuda, T\* : Plasma production by Screw-pinch, J. Inst. Elec. Engrs. Japan 93-A, 127-132 (1973). (in Japanese).

(\* Nagoya University, \*\* Nagoya University, now at JAERI)

Tanaka, M. and Iwata, G\* : Singularities of the vacuum magnetic field around a noncircular plasma cylinder, Plasma Physics 15, 712-713 (1973).  
(\* Guest scientist on leave from Ochanomizu University)

Tanaka, M., Tuda, T. and Azumi, M. : Equilibrium vacuum magnetic field of an axisymmetric torus with an elliptical plasma cross-section, J. Phys. Soc. Japan 34, 1641-1644 (1973).

Tanaka, M., Azumi, M. and Tuda, T. : Long wavelength helical plasma equilibrium with a free boundary, J. Phys. Soc. Japan 34, 1645-1648 (1973).

Ohta, M., Yamato, H\* and Mori, S. : Thermal instability and control of inhomogeneous plasma in a D-T fusion reactor, J. Nucl. Sci. Technol. 10 (1973) 353.

(\* on leave from Tokyo Shibaura Electric Co., Ltd.)

Matsuda, S. : Measurement of the leakage magnetic field from the iron core in a tokamak device without shell, Japan. J. Appl. Phys. 12, 903-907 (1973)

Amano, T\*, Shimomura, Y.\*\* and Yamamoto, S.\*: Cyclotron instabilities in a finite pressure plasma, J. Phys. Soc. Japan 34, No. 6 (1973)  
(\* Osaka University, \*\* Osaka University, now at JAERI)

Nagashima, T., Tamura, S., Yamato\*, H., Arizono, S., Ohtsuka, H., Shiina, T., Yoshikawa, M. and Mori, S.: Observation of collisionless drift waves in a toroidal hexapole, Phys. Rev. Letters 31, 82-86 (1973).  
(\* on leave from Tokyo Shibaura Electric Co., Ltd.)

Matsui, T\*, Tanaka, Y.\*\* and Okuda, T.\*\* : Equilibrium of a plasma in translationally symmetric hybrid systems, Nuclear Fusion 13 671-675 (1973)  
(\* Nagoya University, now at JAERI, \*\* Nagoya University)

Shoji, T\*, Tanaka, T.\*\* and Okuda, T.\*\*: Theoretical and experimental examination of hybrid tokamak systems, J. Inst. Elec. Engrs. Japan 94-A 76-82 (1974). (in Japanese)  
(\* Nagoya University, now at JAERI, \*\* Nagoya University)

Yoshikawa, M., Shimomura, Y., Maeda, H. and Kitsunozaki, A.: An axisymmetric divertor in a tokamak with a tear drop-like cross section, in Proceedings of 6th European Conference on Controlled Fusion and Plasma Physics, Moscow, July 30 - August 3, 1973, p.173.

Sako, K., Ohta, M., Seki, Y., Yamato, H\*, Hiraoka, T.,\*\* Tanaka, K\*\*\*, Asami, N\*\*\*\* and Mori, S., Conceptual design of a gas cooled tokamak reactor, Proc. IAEA Workshop (Culham, Jan-Feb., 1974) to be published in Nuclear Fusion Suppl.

( \* on leave from Tokyo Shibaura Electric Co., Ltd.

\*\* Division of Nuclear Engineering

\*\*\* Division of Radio Isotope Production

\*\*\*\* on leave from Mitsubishi Atomic Power Industries, Inc.)

Tazima, T. : Equilibrium and energy balance of a gas-insulated plasma, Proc. of MHD Symposium (1973), 32-38 (1973) (in Japanese).

Komiya, S\*, Mizuno, M\*, Narusawa, T\*, Maeda, H. and Yoshikawa, M.: Composition profiles of several contaminated and cleaned surfaces of gold thick films on copper plates by auger electron and secondary ion mass spectroscopies, in Proceedings of 6th International Vacuum Congress, Kyoto, March 25-29, 1974.

Azumi, M., : Numerical calculation on the equilibrium and stability of a fat toroidal plasma, Kakuyugo Kenkyu 29, suppl. 7, 11-16 (1973) (Circular in Japanese).

Wakatani, M.: A Vlasov model for local helical instabilities, Kakuyugo Kenkyu 29, suppl. 7, 17-20 (1973) (Circular in Japanese).

Tanaka, M. and Tuda, T. : Drift-dissipative instabilities in a tokamak device, Kakuyugo Kenkyu 29, suppl. 7, 24-28 (1973) (Circular in Japanese).

Amano, T\*, Yoshii, A\* and Wakatani, M\*\* : On tokamak equilibrium, IPPJ-161 (February 1974) 30pp.

(\* Osaka University, \*\* Kyoto University, now at JAERI)

Fujisawa, N., Matoba, T., Sugawara, T\*, Kasai, S., Toi, K., Kunieda, S. and Itoh, S.: Leak test in JFT-2, JAERI-M 5226 (March, 1973) 17pp. (in Japanese) (\* on leave from Tokyo Shibaura Electric Co., Ltd.)

Nagashima, T., Yamato, H\*, Ohtsuka, H., Shiina, T., Tamura, S. and Arizono, S.: Experimental observation of collisionless drift waves in the JAERI toroidal hexapole (JFT-1), JAERI-M 5263 (May, 1973) 24 pp. (\* on leave from Tokyo Shibaura Electric Co., Ltd.)

Kitamura, A., Takahashi, K. and Yano, S. (Division of Physics) : Calibration of the neutral particle energy analyzer at the energies from 0.3 to 4.0 keV measurement of ion temperature of plasmas, JAERI-M 5275 (May, 1973) 26pp. (in Japanese).

Yano, S., Shirakata, H., Takahashi, K., Kitamura, A. and Makino, T. (Division of Physics) : Measurement of the ion temperature for the discharge condition Case 2 in JFT-2 (tokamak device), JAERI-M 5276 (May, 1973) 24pp. (in Japanese).

Fujisawa, N., Sugawara, T.<sup>\*</sup>, Toi, K., Matoba, T., Kasai, K. and Itoh, S.:  
Vacuum conditions in JFT-2, JAERI-M 5369 (August, 1973) 16pp.  
(\* on leave from Tokyo Shibaura Electric Co., Ltd.)

Tuda, T. and Tanaka, M. : Pfirsch-Schluter diffusion in a multi-component plasma, JAERI-M 5376 (August, 1973) 7 pp. (in Japanese).

Itoh, S., Fujisawa, N., Funahashi, A., Arai, T., Ohta, M., Kunieda, S., Takeda, T., Matoba, T., Yokokura, K., Matsuda, S., Kasai, S., Sugawara, T.<sup>\*</sup>, Toi, K., Mori, S., Ohga, T., Suzuki, N., Maeno, M. and Inoue, K.: First report on the JAERI Tokamak experiments, JAERI-M 5385 (September, 1973) 18pp.  
(\* on leave from Tokyo Shibaura Electric Co., Ltd.)

Kasai, S., Funahashi, A. and Inoue, K. : Early spectroscopic measurements in JFT-2 plasma, JAERI-M 5400 (Sept., 1973) 25pp. (in Japanese).

Fujisawa, N., Funahashi, A., Kasai, S. and Sugawara, T.<sup>\*</sup> : Ionization rates in tokamak plasma, JAERI-M 5431 (October, 1973) 16pp. (in Japanese).  
(\* on leave from Tokyo Shibaura Electric Co., Ltd.)

Ohta, M., Ohga, T., Kunieda, S., Yamamoto, M., Hamano, N. : Design and test of the driving mechanism for a dynamic limiter, JAERI-M 5433 (October, 1973) 17pp.

Toi, K. and Takeda, T.: Numerical data processing of the electromagnetic signals obtained in Tokamak Experiments by means of the method of least squares, JAERI-M 5437 (October, 1973) 36pp.

Maeda, H., Shimomura, Y., Kitsunezaki, A. and Yoshikawa, M.: Equilibrium configurations of a plasma column with external current-carrying conductors, JAERI-M 5462 (November, 1973) 7 pp. (in Japanese).

Sako, K., Ohta, M., Seki, Y., Yamato, H., Hiraoka, T. Tanaka, K., Asami, N. and Mori, S. : Conceptual design of a gas cooled tokamak reactor, JAERI-M 5502 (December, 1973) 17 pp.

Matoba, T., Funahashi, A. and Ando, K.\* : Thomson scattering apparatus for JFT-2, JAERI-M 5515 (Jan., 1974) 70pp. (in Japanese).

(\* Institute of Physical and Chemical Research)

Thermonuclear Fusion Laboratory: Annual Report of JAERI Thermonuclear Fusion Laboratory (covering the period April 1, 1972 - March, 1973) JAERI-M 5564 (February, 1974) 89 pp.

Ohta, M., Yamato, H., Tazima, T.: A consideration of ignition and shutdown of the JAERI tokamak reactor, JAERI-M 5569 (February, 1974) 14 pp.

Wakatani, M. : MHD stability of belt-type pinch, JAERI-M 5583 (February, 1974) 18 pp.

Kitsunezaki, A., Shimomura, Y., Maeda, H. and Yoshikawa, M. : Equilibrium and localized instability of JFT-2a. 1., JAERI-M 5612 (February, 1974) 38 pp. (in Japanese).

Shimomura, Y., Maeda, H., Kitsunezaki, A. and Yoshikawa, M.: Shaping of a plasma cross-section by external current-carrying conductors, JAERI-M 5621 (February, 1974) 9 pp. (in Japanese)

Ohtsuka, H., Tamura, S., Nagashima, T., Shiina, T., Yamato\*, H. and Arizono, S.: Anomalous plasma loss in the JAERI toroidal hexapole, JAERI-M 5649 (February, 1974) 12 pp.

(\* on leave from Tokyo Shibaura Electric Co., Ltd.)



## 2. Budget and Personnel

## Budget of the Laboratory

(in unit of million yen)

	(1) FY 1970	FY 1971	FY 1972	FY 1973	FY 1974
Scientific program (excluding staff & administration cost)	(550.) <sup>(2)</sup> 170.25 <sup>(3)</sup>	305.12 <sup>(3)</sup>	408.696 <sup>(3)</sup>	(658.9) <sup>(6)</sup> 433.946 <sup>(3)</sup>	790.213 <sup>(3)</sup>
Building & Establishment	(273.) <sup>(4)</sup> 82. <sup>(5)</sup>	90. <sup>(5)</sup>	101. <sup>(5)</sup>	26.369	—

- (1) From April to next March ,
- (2) Financial obligation from FY 1970 to 1972 to construct JFT-2 including a DC power supply,
- (3) Including cash of the financial obligation for each year,
- (4) Financial obligation from FY 1970 to 1972 for JFT-2 building,
- (5) Cash of the financial obligation for the building,
- (6) Financial obligation from FY 1973 to 1974 to construct JFT-2a and to remodel JFT-2 to increase the toroidal magnetic field from the present 10 KG to 18 KG.

## Number of Staffs of the Laboratory

	FY 1970	FY 1971	FY 1972	FY 1973	FY 1974 <sup>(4)</sup>
Regular staff <sup>(1)</sup>	21	27	32	42	52
Staff on loan	2	1	2	4	7 <sup>(2)</sup>
Guest scientist	1	2	2	3	3 <sup>(3)</sup>

- (1) Including scientists, technicians, secretaries and managers.  
Numbers in the table are at the end of each fiscal year.
- (2) Three from the Tokyo Shibaura Electric Co., Ltd; One from the Hitachi Ltd.; Two from the Mitsubishi Atomic Power Industries. Inc.; One from the Fuji Electric Co., Ltd.
- (3) From the Tokyo Univ., the Ochanomizu Univ. and the Kanazawa Univ.